Abstract

Title: **THE EFFECT OF IRREGULARITIES ON SOIL-AIR INTERFACE RESPONSE DUE TO A BURIED CHARGE**

Scott Austin Yamada, Master of Science 2010

Directed By: **Professor W.L. Fourney, Department of Mechanical Engineering**

Previous studies have shown that pressure loading on a target by a buried explosive is not smoothly distributed. Studies were done to explore the mechanisms that cause this uneven pressure distribution, primarily the surface instabilities caused by the explosive shockwave acting upon surface perturbations between saturated sand and air media. Small-scale tests using conical, hemispherical, and cylindrical shaped surface indentations in sand with a buried explosive were conducted to identify trends in the velocity and form of the instabilities. The velocity trends in the cones and hemispheres with regards to size are reversed, and the cylindrical imperfections cause jet velocities that are up to 200% of the cone velocities and 500% of the hemisphere velocities. Tests were conducted using sand with diminishing moisture content and larger grains, and additional tests were conducted with surfactant in the water. Lower moisture content results in the instabilities not forming, while the effects of the larger grain sand and the surfactant on the jet and dome velocities do not seem noticeable.

THE EFFECT OF IRREGULARITIES ON SOIL-AIR INTERFACE RESPONSE DUE TO A BURIED CHARGE

By

Scott Austin Yamada

Thesis submitted to the Faculty of the Graduate School of the
University of Maryland, College Park, in partial fulfillment
of the requirements for the degree of
Master of Science
2010

Advisory Committee:
Professor William Fourney, Chair
Professor James Duncan
Assistant Professor Santiago Solares
Assistant Professor Teng Li

Acknowledgements

I would like to acknowledge the many people who have helped throughout the development of this thesis and my higher education. I was extremely fortunate to be able to study under Dr. William Fourney, who provided the opportunity and environment for this research, as well as personal learning and growth. Without his patience, counsel and guidance, none of this would have been possible.

I also owe thanks to the other members of my thesis committee, Dr. Santiago Solares, Dr. Teng Li and Dr. James Duncan. Their encouragement and advice contributed greatly to this thesis and my education.

Next I would like to thank and recognize all of the help from Uli Leiste and Les Taylor, who were always there to advise me in the lab. Their experience was always there to lend me a hand.

I am also thankful for the help from Robert Benedetti, Dana Colegrove and Christine Ikeda. They were instrumental in my start at the lab and helping me along entire journey.

My education was managed expertly by Dr. Sami Ainane and Terry Island, who were there to advise me as an undergrad and encourage me to pursue a graduate degree. My graduate experience was managed by Amarildo Damata and Fitzgerald Walker. Both were extremely accommodating and always there to make sure I was on track.

Throughout my research, I often had to visit the Aerospace machine shop where Howie Grossenbacher was tremendously helpful in showing me how to machine whatever I needed. Without him, I would not have had the equipment I needed (or all of my fingers for that matter).

Last but not least I want to thank my friends and family for all of their encouragement and support in everything I do.

Dedication

This work is dedicated to all of the people in my life who helped me reach this achievement. This includes all of the people in the acknowledgements section, as well as the people who serve our nation and ensure our freedom to make all of this possible.

Table of Contents

List of Figures

List of Tables

Chapter 1: Introduction and Background

This thesis describes research conducted at the Dynamic Effects Laboratory at the University of Maryland's A. James Clark School of Engineering, College Park campus. When a target experiences loading from an explosive, the resulting pressure is dependent on the mass of the media which is impacting the target, as well as that mass's velocity. Previous works studying small-scale buried explosives in saturated sand have measured these pressures, and have found that they are not smoothly distributed on the area of the target[1]. The scope of the present research is to explore the reasons for the differences in pressure by analyzing the peak vertical positions of critical points of the blasts. The positions are then analyzed further to estimate velocity, and then compared to determine trends.

An explosion is caused by the detonation of an energetic material and is comprised of two significant events – the shockwave and the rapidly expanding high pressure gases. Unless a target is in contact with the surface of the soil, the shockwave does not play a significant role in loading the target[2, 3]. However, it is theorized that the surface instabilities are Richtmyer-Meshkov Instabilities (RMIs). A RMI is an event which occurs when an incident shock accelerates an interface between two fluids of different densities and amplifies any initial perturbation on the surface[4]. Conditions needed for RMIs are present in small-scale buried explosive tests in saturated sand. The detonation of an explosive buried in saturated sand provides a shockwave, while the two fluids of different densities are the saturated sand and the air above the surface. The incident shockwave causes a RMI at the interface of the saturated soil and air, which is described

in this thesis as a "jet." Aiding in propulsion of the jet is the high pressure gas that is travelling outward from the charge. The jet has a higher velocity than the resulting "dome" of sand-water mixture and expanding gases, and is the primary focus of this thesis.

The experiments conducted in this work were done using small-scale buried explosives in saturated sand. The charge is buried, the surface of the sand is smoothed, but a small imperfection is added to the surface to cause a jet in the resulting explosion. Tests are conducted using cone shaped imperfections, sphere shaped imperfections and cylinder shaped imperfections. Additionally, the depth of the imperfection, the grain size of the sand, the moisture content of the sand and the surface tension of the water are all varied in subsequent test series. Conclusions are drawn about the predicted load of the imperfection on a target that would hypothetically exist at a distance of approximately 16 in above the sand.

The research in this report relates to real world uses of buried explosives, such as land mines or improvised explosive devices (IEDs). It is a fact that most of the casualties in Operation Enduring Freedom and Iraqi Freedom are by a large margin from buried or concealed explosive devices such as IEDs and mines. The United States recorded 8,179 IED attacks in Afghanistan in 2009, with 3,867 and 2,677 recorded in 2008 and 2007 respectively[5]. The results of this paper allow for better understanding of the intricacies of explosive loading.

1.1 Introduction to Scaling

Small-scale tests are commonly employed due to lower cost, quicker execution, and increased accessibility. The explosive tests done for the work in this thesis are no exception. The Dynamic Effects Lab primarily uses cube-root scaling to correlate the small-scale results with the full-scale scenario[6, 7]. The scaling is done with respect to the energy of the charge. Since the energy of an explosion is directly related to its energy density, the explosion is "characterized by a mass dimension"[8].

$$SF = \left(\frac{mass_{full-scale}}{mass_{small-scale}} \right)^{1/3} = \frac{length_{full-scale}}{length_{small-scale}}$$

$$SF = \left(\frac{10lbs}{0.5g} \right)^{1/3} = \frac{length_{full-scale}}{1.19in}$$

$$SF = 20.86$$

This scaling factor length is multiplied by the small-scale parameters to yield full scale parameters. A small-scale target height of 0.75in was chosen to correlate to a full scale height of target (HOT).

$$HOT_{full-scale} = 15.64in$$

There are several reasons why these parameters are used to scale the tests. The first is for the easy comparison to the work in [9]. Since the same size charge and depth of burial (DOB) are used, there is no need to scale the results for comparison. Secondly, [9] shows that the presence of jets depends on the depth of burial of the charge and the mass of the

charge. Using the same parameters that induced a jet in previous tests ensures that the subsequent tests done in this thesis also produce jets. Finally, these parameters were selected by the United States Army. The full scale amounts of a 10 lb charge and a target height of approximately 16 in correspond to a realistically sized explosive mass and the stand off distance of the bottom of a vehicle.

Using this scaling factor, the parameters are listed below in Table 1.1. Note that the velocity is not included in the chart because it is invariant with respect to scaling. This is due to the similar scaling of both the length and time dimensions.

	Full-scale Dimension	Small-scale Dimension
Depth of Burial (DOB)	24.82 in	1.19 in
Charge Mass	10 lb	0.5 g
Distance to Target	15.64 in	0.75 in
Imperfection Diameters	2.61, 5.22, and 10.43 in	0.125, 0.25 and 0.5 in

Table 1.1: Sample Full-scale and Small-scale Values

Chapter 2: Research Equipment

2.1 Explosive Charge

The research was conducted using an assortment of materials and pieces of equipment. A typical experiment requires components to make a charge, a testing tank, tools for charge assembly and burial, the phantom high speed camera system and a remote firing set.

The charges used for all the experiments are made by coupling a precision secondary explosive detonator with a malleable sheet explosive. The detonator is an RP-87 Exploding Bridge Wire (EBW) Detonator manufactured by Teledyne RISI. The EBW detonators contain a small wire that is vaporized when electricity is suddenly discharged through it, which initiates a secondary explosive. It consists of 26 mg PETN initiating explosive, and 43 mg RDX output explosive, as shown in Figure 2.1

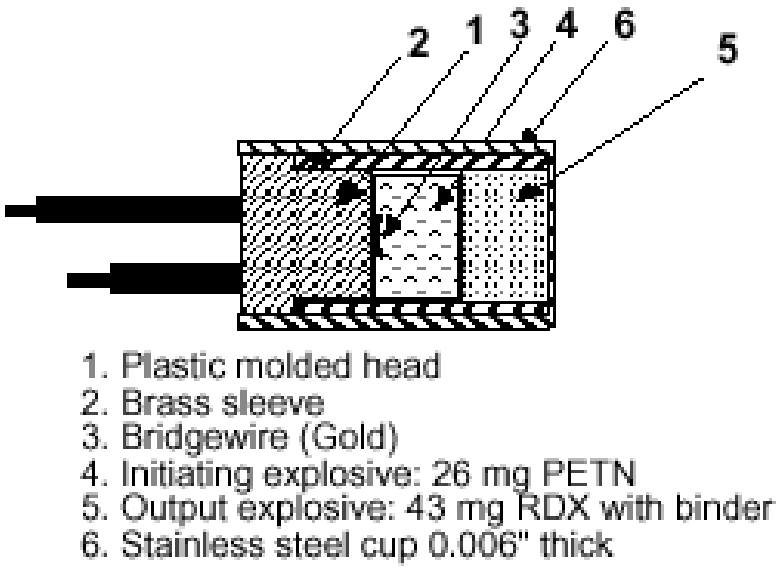

Figure 2.1 RP-87 Schematic

PETN stands for pentaerythritol tetranitrate, a powerful high explosive. RDX is cyclotrimethylenetrinitramine, a common military high explosive also known as cyclonite. The dimensions are shown in Figure 2.2.

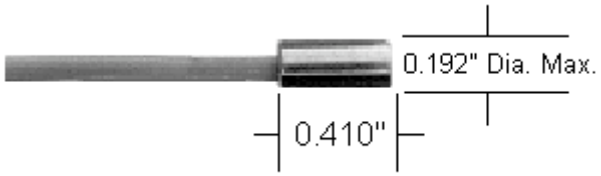

Figure 2.2 And RP-87 EBW

Threshold Burst Current	210 amps
Threshold Voltage	Approx. 500 volts
Threshold Voltage Std. Deviation	75 volts maximum
Function Time	1.95 µsec typical
Function Time Simultaneity Standard Deviation	0.125 µsec maximum

Table 2.1: RP-87 Firing Parameters

The cylindrical charge casings pictured in Figure 2.3 are made of Delrin and are used to house the malleable sheet explosive with the RP-87 detonator. The sheet explosive is a product called Deta Sheet, and is 63% PETN by mass, with the rest of the mass acting as a plasticizer to give it its malleable form. The dimensions of the charge casing are listed in Table 2.2.

Charge Casing Dimension	Length [in]
Outer Diameter	0.43
Wall Thickness	0.025
Length of Casing	0.45

Table 2.2: Charge Casing Dimensions

The charge is assembled by inserting the detonator into the center of the cylindrical Deta Sheet 1/16 in. The RP-87 is then secured in place by epoxy.

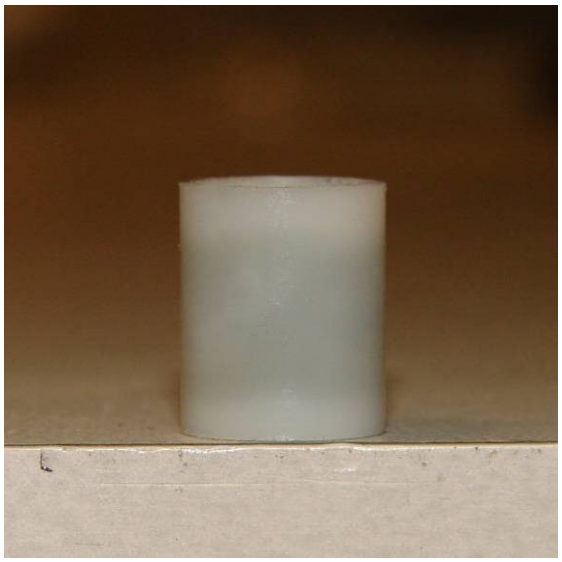

Figure 2.3: The Charge Casing Containing Deta Sheet

The mass of Deta Sheet used is 0.68g. The mass of the plasticizer is deducted from the mass of the Deta Sheet, and adding to that the mass of the explosive contained within the RP-87 equates to 0.50g of explosive. The completed charge is pictured in Figure 2.4

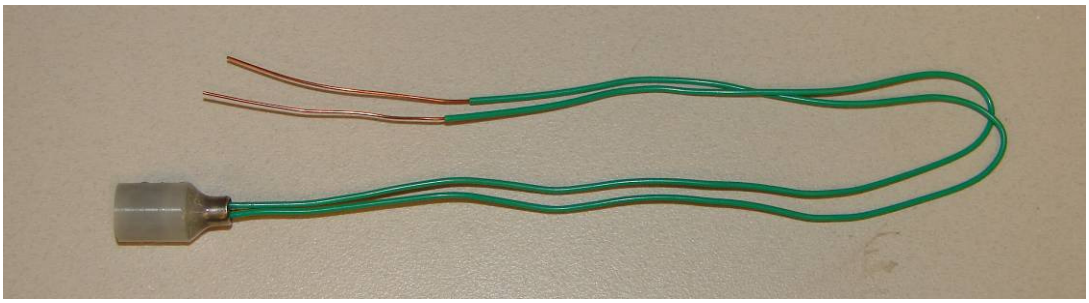

Figure 2.4: A Completed Charge

2.2 FS-17 Firing System

The charge is detonated remotely using a device known as a firing system. The particular firing system used is the FS-17 by Reynolds Industries Inc. The system consists of a control unit and a firing module[10]. The control works by sending a 4 kV signal to the detonator and a much smaller signal to another external device of the user's choice, which in this case is the high speed camera. These pieces of equipment are shown below in Figure 2.5.

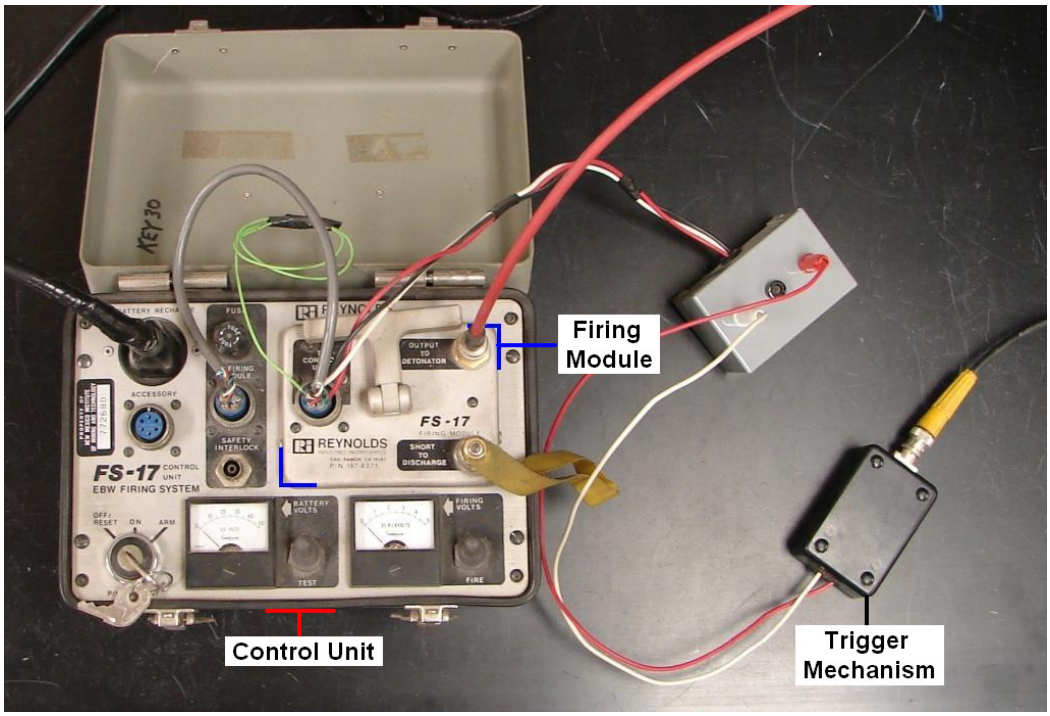

Figure 2.5: The FS-17 Firing System

The Trigger Mechanism is an optical switch, which communicates a signal to the Phantom High Speed Camera. This allows for the user to trigger the detonation remotely while simultaneously triggering the recording of the camera.

2.3 Dummy Charge

Due to the hazardous nature of the detonation, a device called a dummy charge is used to check the communication between the firing system, the camera, and the charge. The dummy charge is not a charge, but instead is comprised of two parallel wires running through a graphite block inside of an aluminum cylinder. If connected to the firing system, the electrical pulse from the system will cause an electrical arc to travel across the wires once the system is triggered. The arc is loud and is indicative that the firing box and all of its connections are functioning properly. Furthermore, the signal still triggers the camera, so it also ensures that the camera is properly connected.

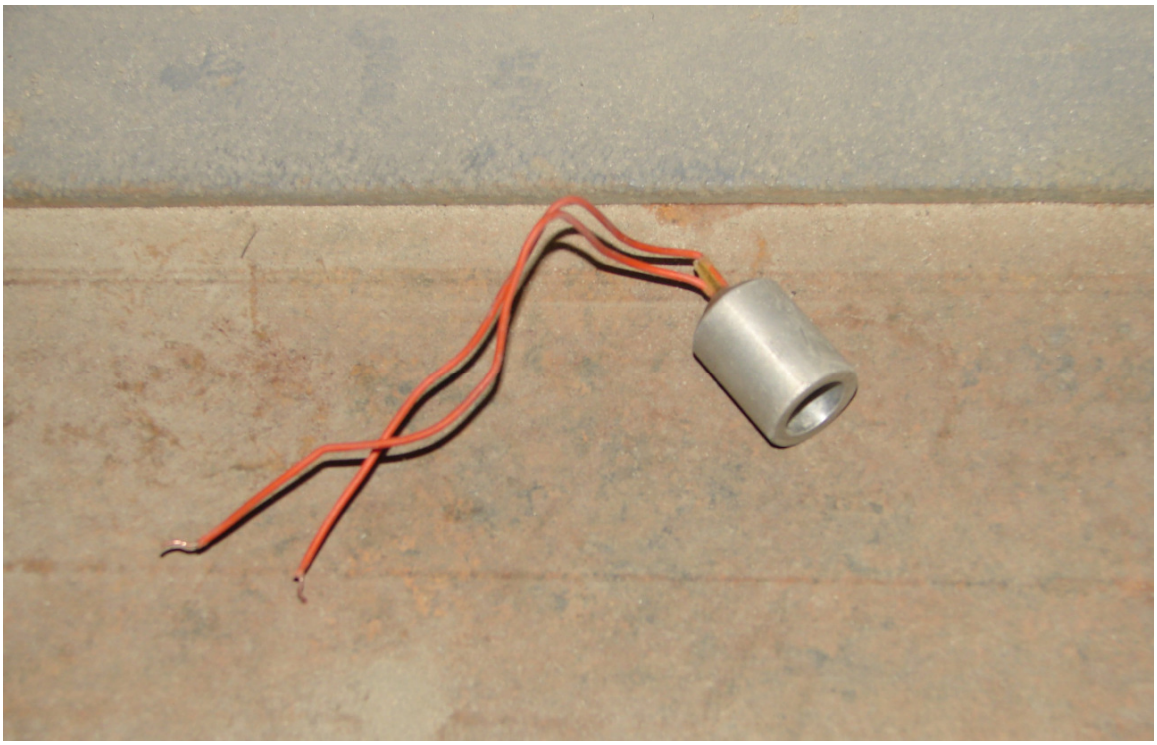

Figure 2.6: Dummy Charge

2.4 The 2-D Blasting Tank

The explosive tests are conducted in the 2-D Blasting Tank, which is located in a chamber refashioned from an old industrial oil drum. The tank's overall dimensions are in Table 2.3.

Tank Length	36 in
Tank Thickness	6 in
Tank Height	20 in
Thick Acrylic Sheet Thickness	0.75 in
Sacrificial Acrylic Sheet Thickness	0.125 in

Table 2.3: 2-D Blasting Tank Dimensions

The tank is assembled from 3 thick acrylic pieces which are bolted to an aluminum frame. The inside faces of the acrylic are covered with additional thin pieces of acrylic which are used sacrificially. The tank is also sealed with silicone rubber gaskets and caulked to make it water tight. The tank is called 2-D because the thickness dimension is relatively small. The tank is pictured in Figure 2.7.

Figure 2.7 Assembled 2-D Blasting Tank

The tank houses two different types of sand in the subsequent series of tests. The first and most frequently used sand is Berkeley Springs Sand. This sand is known for its white color and fine grain. The second type is recreational sand, and has a wider distribution of grain size sieved to include only larger grains.

2.5 Surface Imperfection Tools

Various geometric shapes are used to create surface imperfections of specific geometries. The first of which are cones with a half angle of 45 degrees as shown in Figure 2.8. They are made out of steel and thus can easily be taken out of the sand with a magnet.

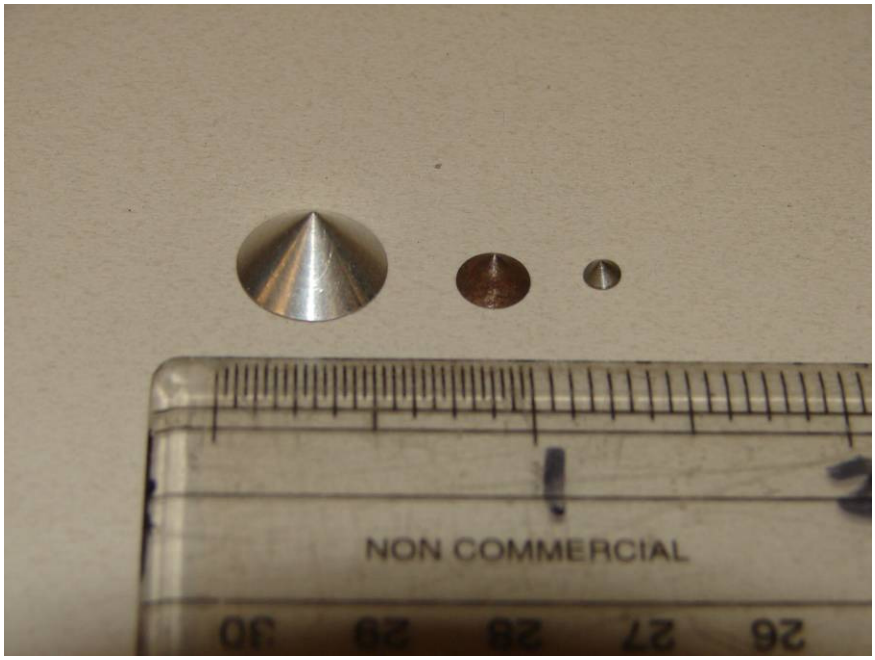

Figure 2.8: 0.5, 0.25 and 0.125 in Diameter Cones Used to Make Conical Imperfections

The second series of tests uses hardened steel ball bearings shown in Figure 2.9 to make hemispherical impressions in the sand.

Figure 2.9: 0.5, 0.25 and 0.125 in Diameter Ball Bearings Used to Make Hemispherical Imperfections

Finally, the tools pictured in Figure 2.10 are used to make cylindrical indentations in the sand, while the tape on the rods is used to ensure that they are inserted to the correct depth.

Figure 2.10: 0.5, 0.25 and 0.125 in Diameter Cylinder Tools Used to Make Cylindrical Imperfections

2.6 Phantom v12.1 High Speed Camera

The Phantom v12.1 High Speed Camera is the primary data acquisition tool. The Phantom is capable of recording at speeds of up to 1,000,000 pictures per second. The speed affects highly the resolution and available exposure time[11].

Figure 2.11: The Phantom v12.1 High Speed Camera[12]

All of the experiments use uniform settings in the Phantom Camera, which are in the table below. Note the relatively slow resolution. This effectively limits the spatial precision of the measurements significantly, but allows for better temporal resolution.

Resolution	128 x 128 pixels
Frame rate	180,000 fps
Exposure Time	4.82 μs
Image Interval	5.55 μs

Table 2.4: Camera Test Settings

2.7 Lighting

The Phantom High Speed Camera requires an intensive light source in order to record clearly visible movies at such high speeds. To accommodate this, two North Star halogen lamps operating at 250W are clamped around the blasting tank and light the region above the buried charge.

Figure 2.12: A 250W North Star Halogen Lamp [13]

Chapter 3: General Experimental Procedures

The tests are conducted using a repeatable routine with the equipment described in the previous chapter. A schematic of the test setup is shown below in Figure 3.1.

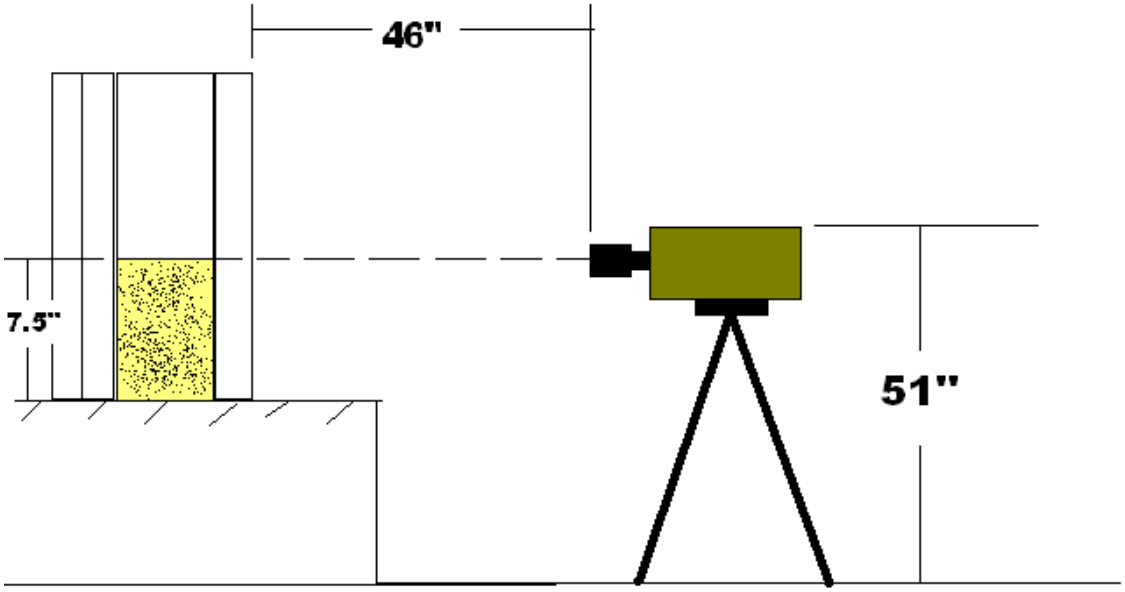

Figure 3.1: Schematic of the Testing Camera

The tests are considered two dimensional due to the small thickness of the tank sand bed. Additionally, effects of the position of the camera that might affect the vertical displacement measurements are ignored because only small angles are involved.

3.1 Tank and Sand Bed Preparation

Once the test charge is assembled, setup begins with the preparation of the sand bed. The sand is first compacted everywhere to ensure similar sand density for each test. The surface of the sand is then scraped using a tool to plane the surface of the sand at a specific height. A portion of the surface is selected where the sacrificial glass is the least scratched for the burial of the charge. Finally, both the inside and outside surface of the tank are cleaned with glass cleaner to aid in viewing. The finished surface region can be seen in Figure 3.2

Figure 3.2: 2-D Blasting Tank in the Test Chamber

3.2 Charge Burial and Surface Alteration

With the surface of the sand prepared and the glass cleaned, the tank is ready for the charge. The burial location is always centered between the two walls of the tank to minimize wall effects on the resulting blast. This is done through the use of a simple template paper that has the same height as the width of the chamber. The paper shown in Figure 3.3 contains 4 small holes and a cutout at the bottom to assist in burying the charge.

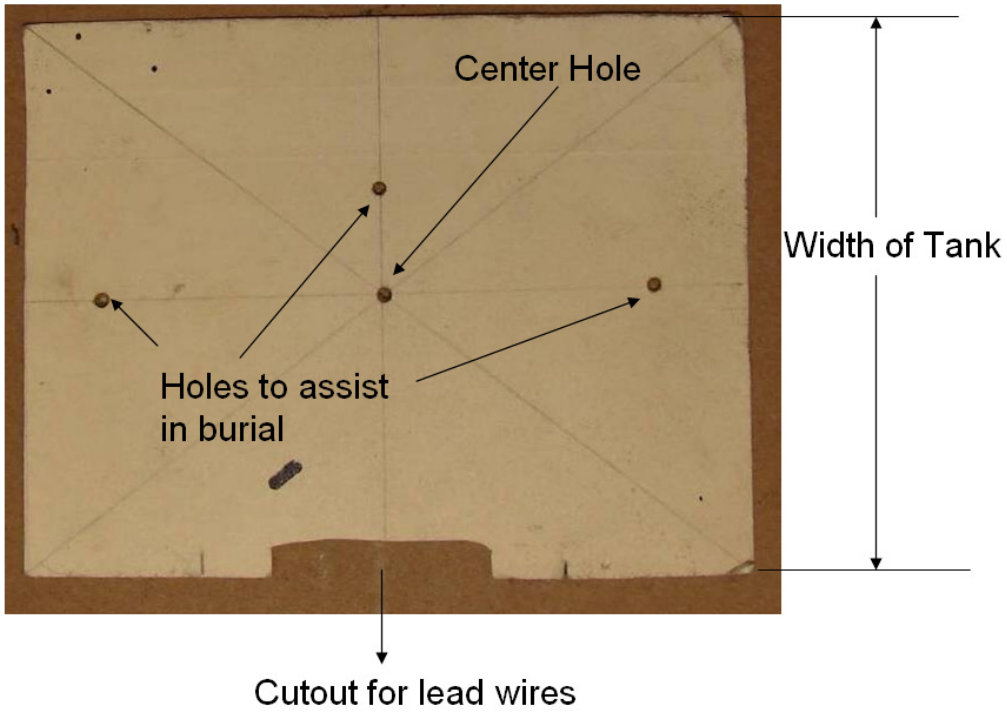

Figure 3.3: Burial Paper

The center hole allows the user to mark the location of the burial hole while the two side and top holes help the user keep the charge centered once the center has been dug out. Figure 3.4 shows the paper in the tank prior to the burial process.

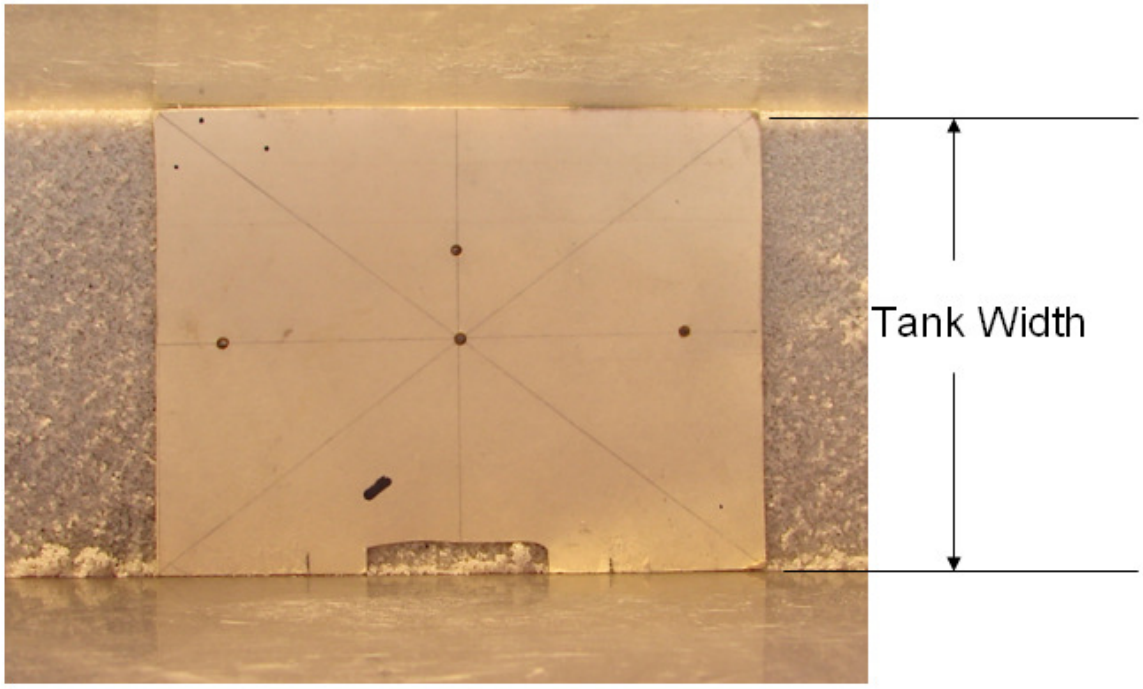

Figure 3.4: Burial Paper Inside of the Tank

Using the paper to mark a location for burial, a screwdriver is inserted into the marked center hole location to hollow out a cavity in the sand. The screwdriver is then removed and tools are used to remove sand from in front of the hole with minimal effect on the surface of the sand. The charge is then inserted into the hole with the lead wires towards the bottom at a right angle so that they can be taped to the back of the tank.

The precise depth of burial of the charge is ensured by the use of calipers and a block of aluminum with a hole as shown in Figure 3.5. The block provides a stable, smooth surface from which to measure the depth of the charge. The calipers are extended through the hole to measure the depth from the surface of the sand to the top of the charge.

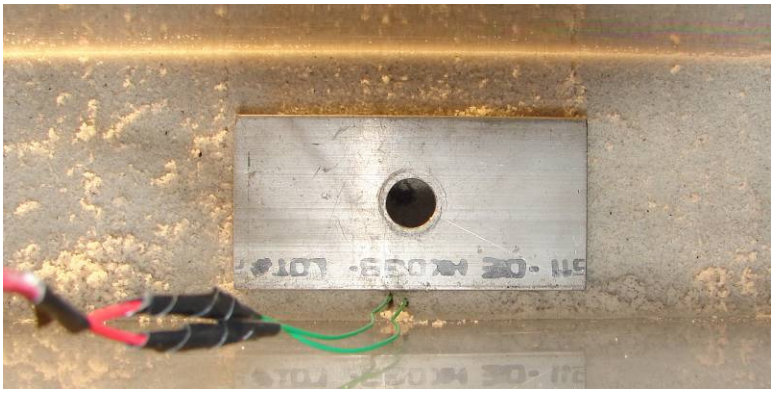

Figure 3.5: An Aluminum Plate to Assist in Burying the Charge

Once the correct burial depth is achieved, the aluminum block is removed and the hole is then filled with sand back to the level surface. The sand is carefully compacted to once again homogenize the density of the sand. Using the marks made prior to burying the charge, the center location is then marked again to aid the focusing of the camera and to locate the surface imperfection. The final result is pictured in Figure 3.6.

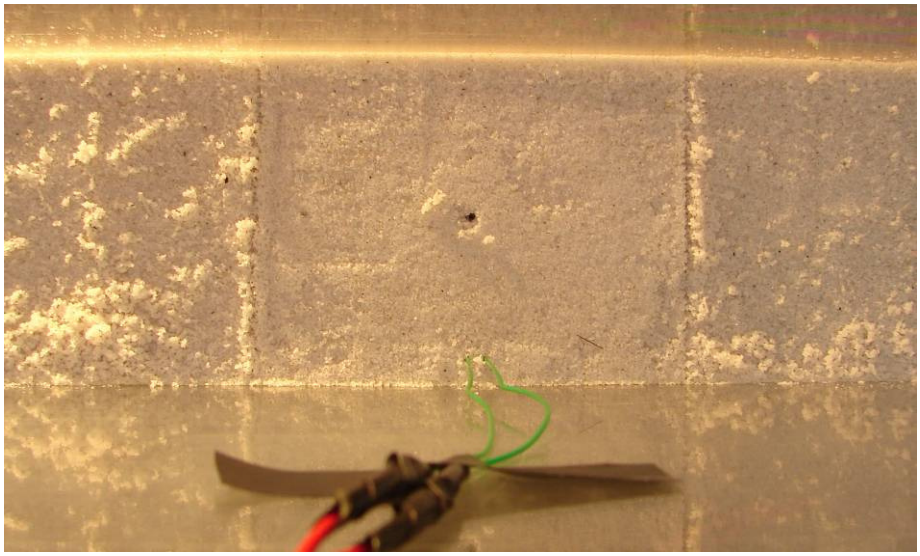

Figure 3.6: A Successfully Buried Charge with Marking to Indicate Position

3.2.1 Procedure for Cone or Hemisphere Imperfections

The sand surface is altered by inserting an object with the desired shape into the surface of the sand. In order to make a cone shaped imperfection, the appropriate size cone is inserted directly over the center of the charge into the surface of the sand. This is made possible by the marks created earlier when burying the charge. The cone (or ball bearing) is carefully inserted all of the way into the surface of the sand while ensuring the surrounding surface remains planar and unaltered. A similar procedure is used for inserting spherical ball bearings into the sand to create hemisphere impressions. The objects remain in the sand to aid in the camera setup, but are removed with minimal surface irritation with a bar magnet before detonation. The finished setup shown in Figure 3.7.

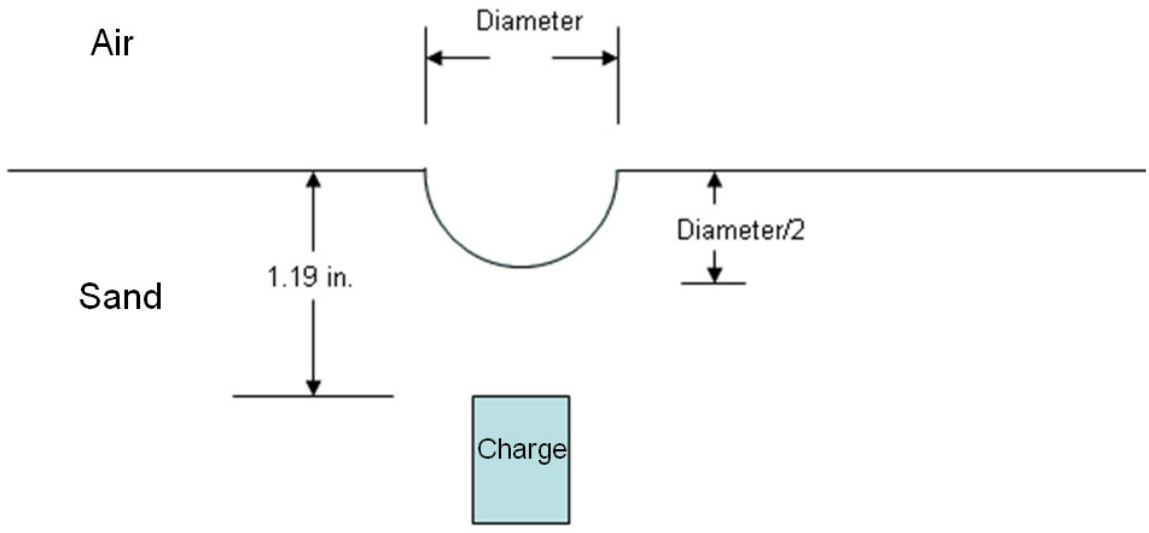

Figure 3.7: Hemispherical Imperfection Schematic

3.2.2 Procedure for Cylinder Imperfections

The implementation of the imperfection is slightly different if a cylindrical imperfection is desired. Since there are an abundant amount of objects that can make cylindrical impressions, rods of diameters 0.5, 0.25 and 0.125 in are inserted into the sand to the appropriate depths. The disadvantage to this is that the cylinder cannot remain in the hole to aid in camera setup. An example cylindrical imperfection is shown in Figure 3.8.

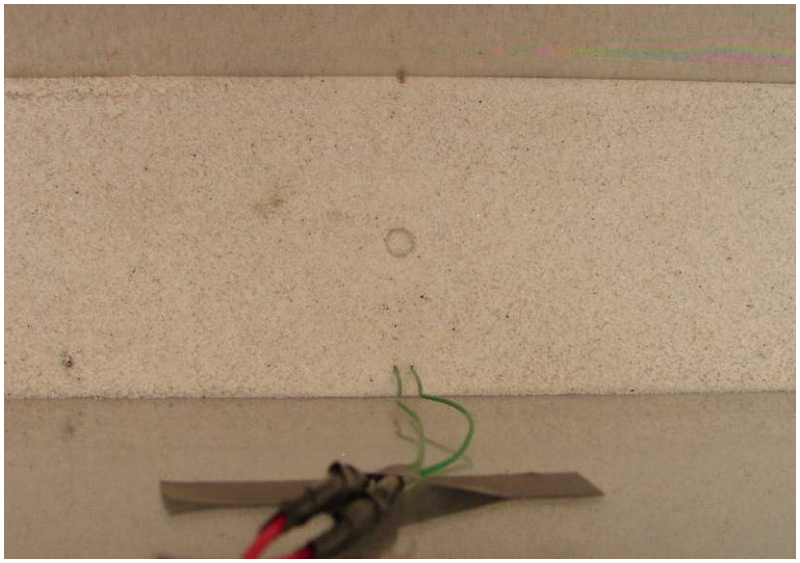

Figure 3.8: A Successfully Buried Charge with Cylindrical Surface Imperfection

3.2.3 Camera Setup

With the charge buried and the surface imperfection made, the camera is then prepared to capture the detonation. The camera is set to a standard position and angle to match the standard height of the sand. The camera is set to the settings previously tabulated in Table 2.4.

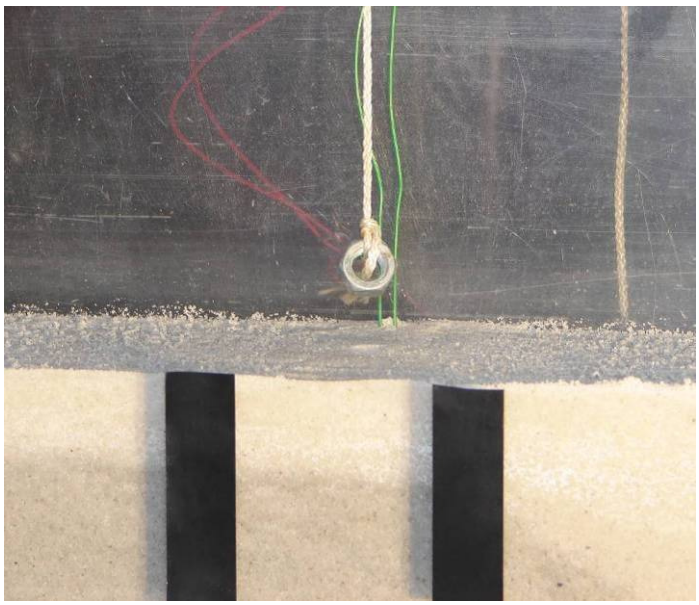

Figure 3.9: Using a Nut to Focus and Center the Camera

The camera is then focused by hanging a nut above the charge (Figure 3.9). Note the two parallel pieces of electrical tape. These pieces of tape are positioned precisely 2.0 in away from one another to provide a length scale when reviewing the resulting photos. The pieces of tape are placed 1.0 in to the left and right from the center of the imperfection.

3.3 Saturation, Detonation and Data Recording

Before detonation, the sand is saturated with water. This is done to create RMIs by making the sand act more like a fluid. The tank is irrigated through a spout at the bottom rear of the tank by way of siphon. This is shown in Figure 3.10.

Figure 3.10: Siphoning Water into the 2-D Tank

The water level is carefully monitored to ensure that the imperfection is undisturbed. The sand is deemed saturated when the water level is within 0.25 in of the top of the sand because full saturation would collapse the imperfection.

Next, the dummy charge is connected to the firing box to test the setup. The firing box is charged, and then triggered. If everything is connected properly, the dummy charge will emit a loud sound, and the camera will trigger with the desired settings. This is repeated at least once to ensure that the setup is reliable. The finished setup can be seen in Figure 3.11.

Figure 3.11: Camera Set For Viewing the Imminent Experiment

The final step is to detonate the charge. The area is alerted to the imminent test while the user puts on ear protection. The countdown is initiated after the firing box capacitors are charged. At the end of the countdown, the signal is sent and the charge detonates as the camera begins recording.

3.4 Data Acquisition and Analysis

3.4.1 Collecting and Tracking Points in Phantom Software

Once the test has been run, the data are retrieved in the form of a .cine file from the camera. The cine file is a movie file that can be analyzed and edited frame by frame with the Phantom Camera software. The movie is trimmed of irrelevant footage to make the analysis easier and the .cine file is opened and prepared for analysis.

The data in the tests consist of the position of the top of the instability (jet), and the position of the top of the smooth sand domes. The user tracks the location of the dome and the jet in each frame by scaling the image with a gauge distance, assigning a datum axis, and simply using the mouse to click the topmost point on the dome and the jet through each recorded image. A screenshot of point tracking in the Phantom Software can be seen in Figure 3.12.

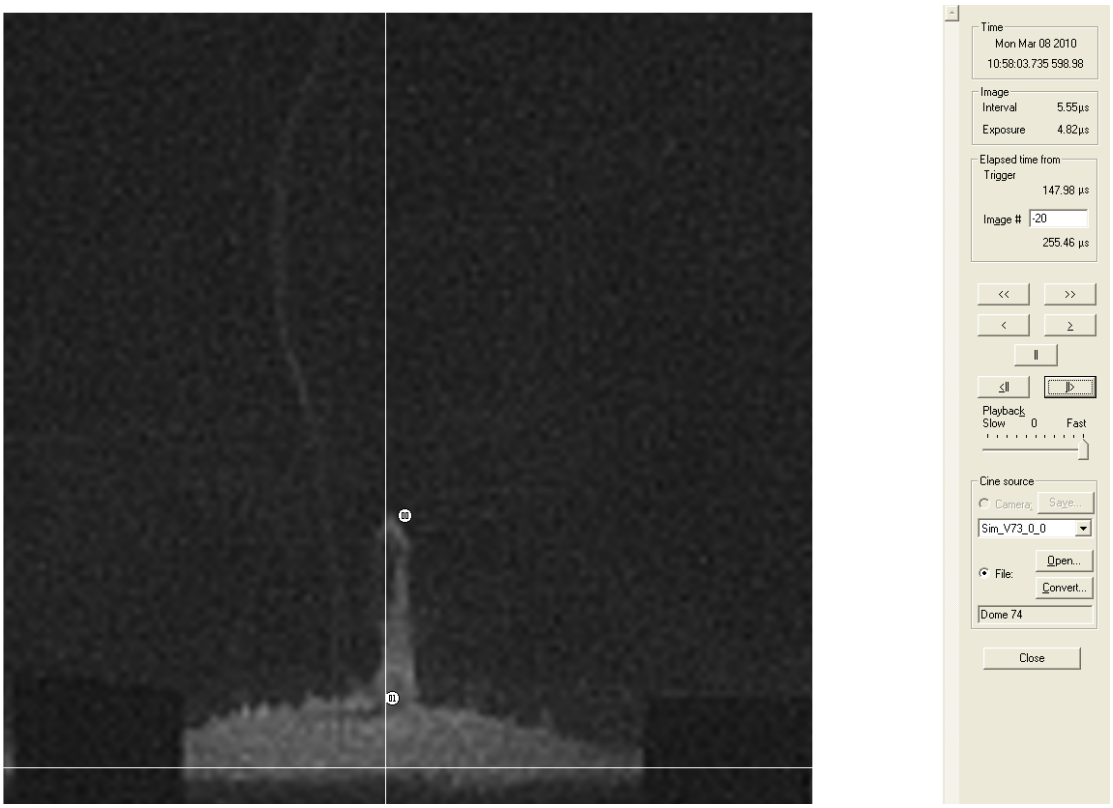

Figure 3.12: Tracking Points on the Jet and Dome

The circles are the points that mark the vertical position of the top of the dome and the jet. This system of tracking points is relatively simple, but it has limitations that can lead to artifacts in the resulting position vs. time data. The main shortcoming is the fact that the user must decide which points to track on the dome and the jet in addition to being hindered by the low spatial resolution. In this thesis, the top most point of the jet and the top of the crest of the dome are tracked. However, this method encounters difficulty when the top of the jet or dome is not clearly defined or changes throughout the video. For example, often there are regions of the jet containing "fingers" that move with a velocity higher than the rest of the jet. Worse yet, these fingers often appear then

disappear, giving the resulting position vs. time curve spikes in displacement. An example of fingers can be seen in Figure 3.13.

Figure 3.13: Example of Fingers in Jet 47

This effect can be seen and addressed when analyzing the data simultaneously with the video, but it is not an *error*. Though the fingers may posses a velocity that is not representative of the jet as a whole, it still exists, and therefore, must be noted since the pressure caused by one of these jets impacting a target is dependent on velocity. The data from the image tracking process are stored in a text file as coordinates of time and vertical distance. The coordinates are then read into Excel and the data sorted into columns and visualized in scatter plots.

3.4.2 Curve Fitting and Velocity Calculations

The data from image tracking provide insight into the positions and velocities of the jets and domes relative to one another, but they do not quantify the velocity. To quantify the velocities, a curve fitting operation is performed on a specific region of the data and is differentiated to yield velocity as a function of time.

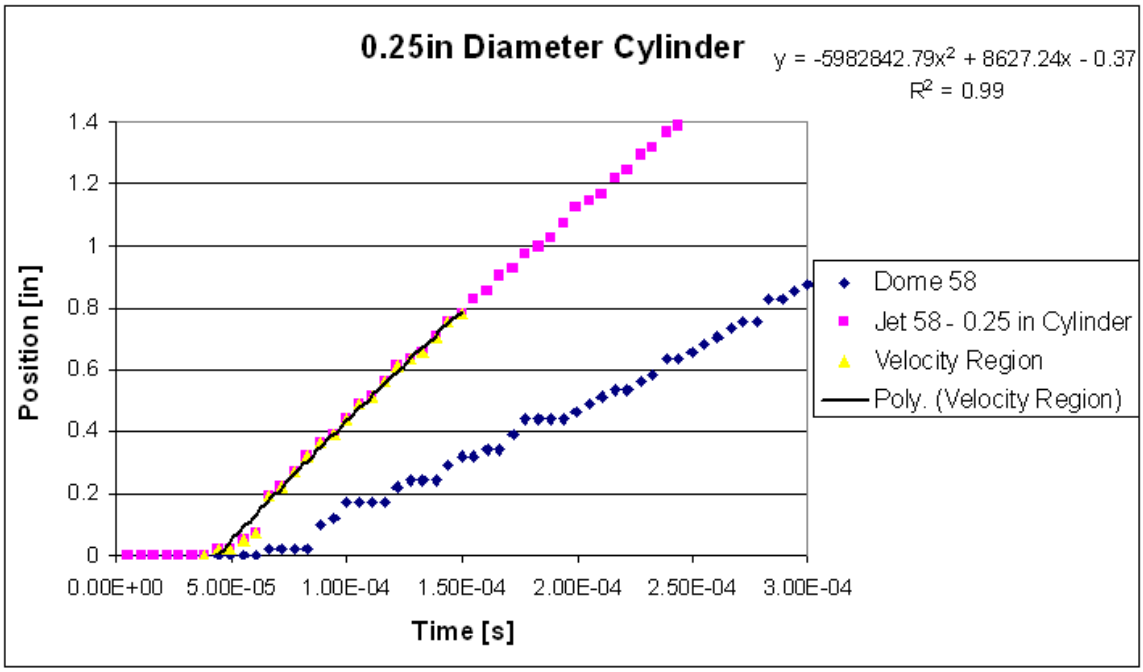

Figure 3.14: Example Position vs. Time Curve on Selected Region

Figure 3.14 shows an example plot of the position and time data of a jet and dome from a test. The yellow Velocity Region is the set of data that is used to generate the fitted function. The function y in the upper right hand corner is a second order polynomial fit of the position vs. time data. This mathematical form is chosen because of its ability to accurately recreate the slight concavity of the jet and dome plots.

Once the function y is differentiated with respect to x (time), the velocity is then evaluated at a time at which the jet or dome would be reaching a target that is at a small-scale height 0.75 in above the surface of the sand. This is where the 16 in stand-off of the bottom of a vehicle would be. This time is slightly different for each test, but is obtained from the position vs. time data acquired from image tracking.

Chapter 4: Results

From the data analysis, sets of position and time pairs and velocity values are obtained. The data are then plotted in sets to compare the different test series to see how a certain variable affects the resulting velocities of the dome and jet. In addition to the velocities, any trends in velocity or interesting characteristics of the explosion are noted.

The test series are presented in the following order:

- Cone Imperfection Series
- Hemisphere Imperfection Series
    - Hemisphere Imperfection Series with 1.19 in DOB
    - Hemisphere Imperfection Series with Reduced 0.69 in DOB
- Cylinder Imperfection Series
    - Cylinder Imperfection Series with Constant Depth to Diameter Ratio
    - Cylinder Imperfection Series with Constant Imperfection Depth
    - Cylinder Imperfection Series with Constant Imperfection Geometry
- Moist Sand Test Series
- Surfactant Test Series
- Coarse Grain Test Series

All of the tests containing cones were conducted prior to the work in this thesis and are the focus of the work in [9].

4.1 Cone Imperfection Series Results

A graph containing the position and time data for the jets from 0.125, 0.25 and 0.5 in diameter cones with constant charge mass and depth of burial (DOB) is shown in Figure 4.1. The DOB of the charge is 1.19 in and the charge mass is 0.5 g.

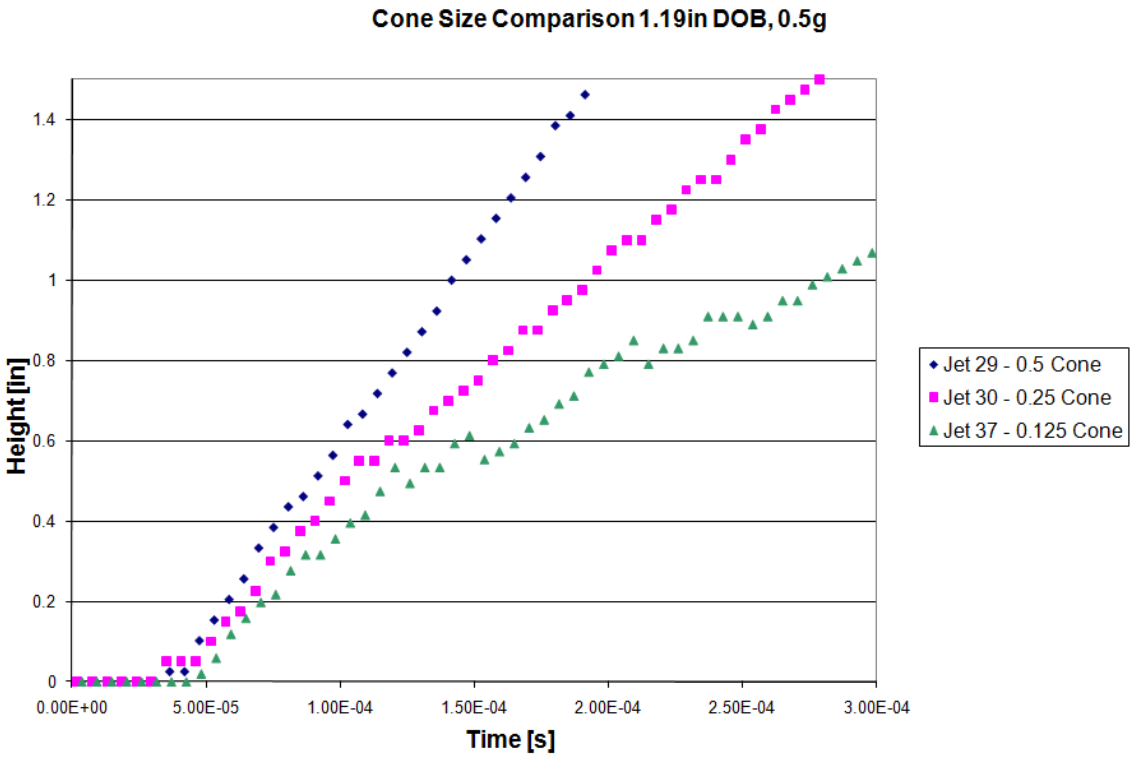

Figure 4.1: Position vs. Time Data for the Cone Imperfection Test Series Using 0.5, 0.25 and 0.125 in Diameter Imperfections

The results from the cone series of test are important in the development of the work in this thesis. One important characteristic is that the jets are clearly defined using the 1.19 in DOB. Another aspect is the trend in the position time data. From Figure 4.1 it can be seen that the velocity at the time that the jet reaches the target height of 0.75 in increases

with increasing cone diameter. The domes from the tests all behave very similarly because their velocity is a function of the DOB rather than the surface imperfection.

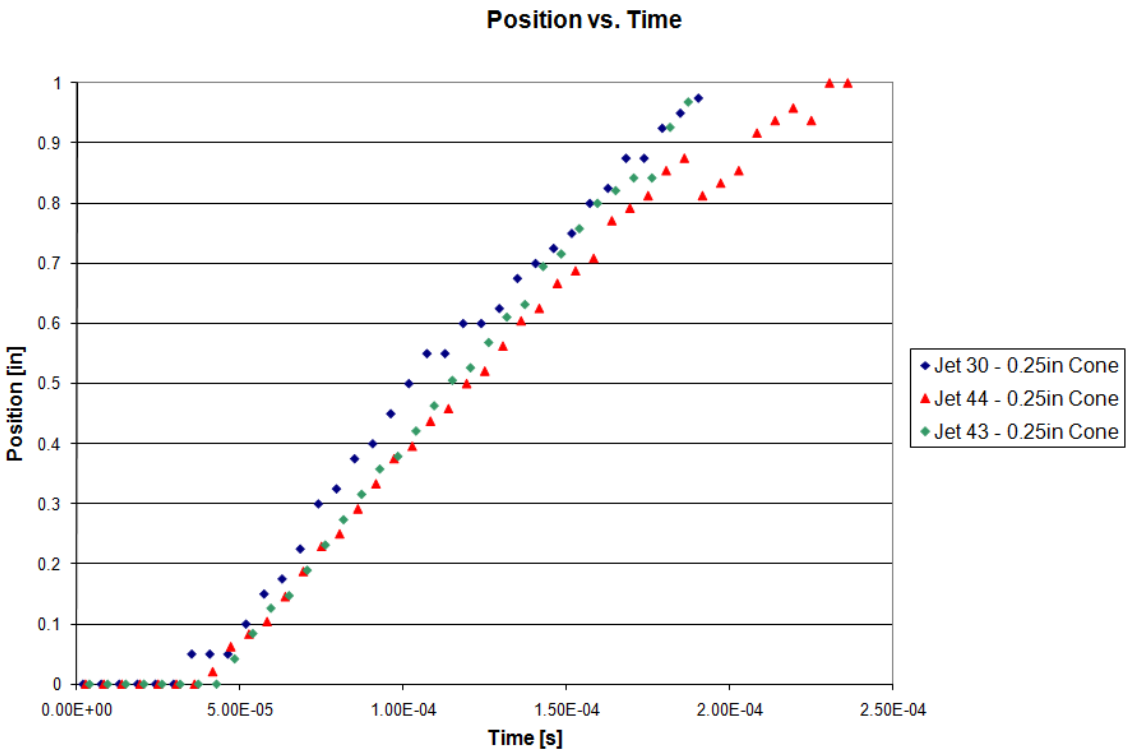

Figure 4.2: Position and Time Data for Repeated 0.25 in Diameter Cone Tests

Figure 4.2 exemplifies that the cone series results contain some repeatability. All three tests in Figure 4.2 were done using the same conditions with 0.25 in diameter cones and 1.19in DOB. Though the results in this case look promising, the small-scale nature, combined with the randomness of sand and the detonation process combine to make perfect repeatability out of reach. The results from this series show that with a carefully controlled procedure, the *trends* are often repeatable.

The results of the cone test are also compared to a 2-D computational simulation with density contours in Figure 4.3. The simulation is also able to produce a jet, and was completed by Drew Wardlaw, ATR Corporation[14]. Each picture contains results of a test without imperfections, and results of a test with an imperfection. The left sides of the images contain no imperfection while the right sides contain a cone shaped imperfection.

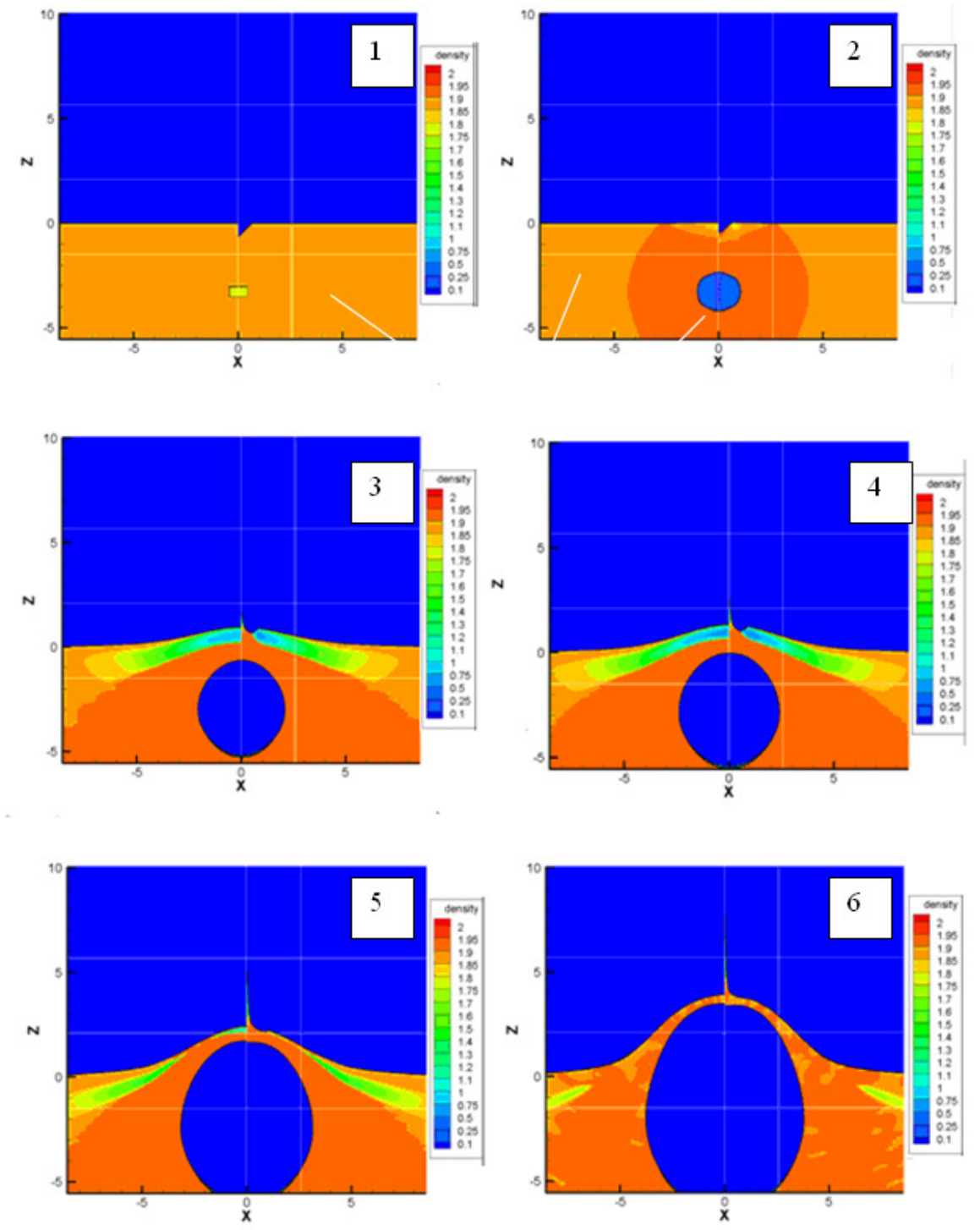

Figure 4.3: Computational Simulation with Density Contours of a Control Test and a Test with a Cone Imperfection

4.2 Hemisphere Imperfection Series

Continuing the work from the cone series of tests, two sets of tests were conducted using ball bearings to make hemispherical surface imperfections. The first used three different size ball bearings to make hemispherical imperfections in the sand containing a buried explosive with a DOB of 1.19 in. The second series was done with the same sized ball bearing, but with a reduced DOB of 0.69 in.

4.2.1 Hemisphere Imperfection Series with 1.19 Depth of Burial

The first series of tests were done to observe the effect of the change in the size of the hemispherical surface imperfection on the resulting jet due to an explosion in saturated sand. The test numbers start at number 45; all prior tests were conducted using cones. There are three sized ball bearings – from largest to smallest they are 0.5, 0.25 and 0.125 in diameter steel ball bearings. The ball bearings are inserted halfway into the sand to ensure easy removal and no overhangs in the sand surface. Because of their geometry, the hemispheres and cones have a constant imperfection depth to imperfection diameter ratio for every test in the series. The position vs. time data for the jets in the Hemisphere Imperfection Series with 1.19 in DOB are shown in Figure 4.4.

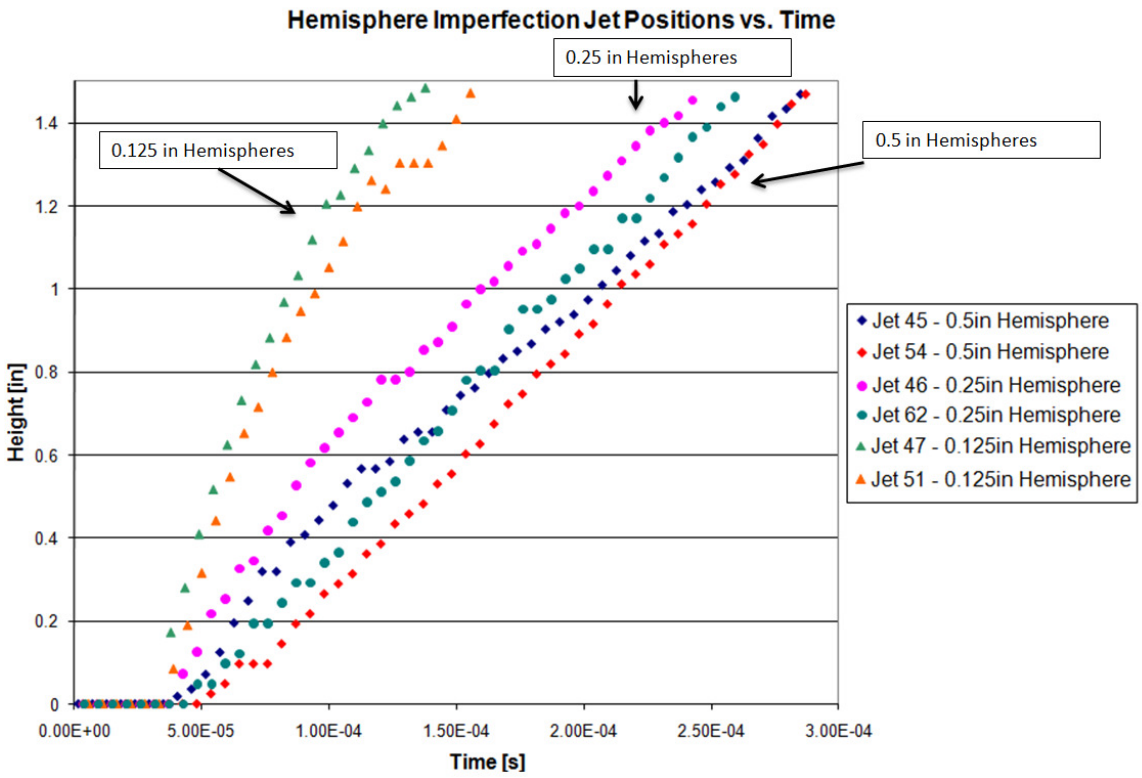

Figure 4.4: Position vs. Time Data for the Hemisphere Imperfection Test Series with 1.19 in DOB Using 0.5, 0.25 and 0.125 in Diameter Imperfections

Figure 4.4 indicates that velocity increases monotonically with decreasing hemisphere diameter. Also, it is evident that the velocities of the jets in the 0.125 in hemisphere diameter tests are remarkably higher than those seen in the 0.25 and 0.5 in hemisphere diameter tests. The difference can be seen clearly in the .cine files recorded from the camera.

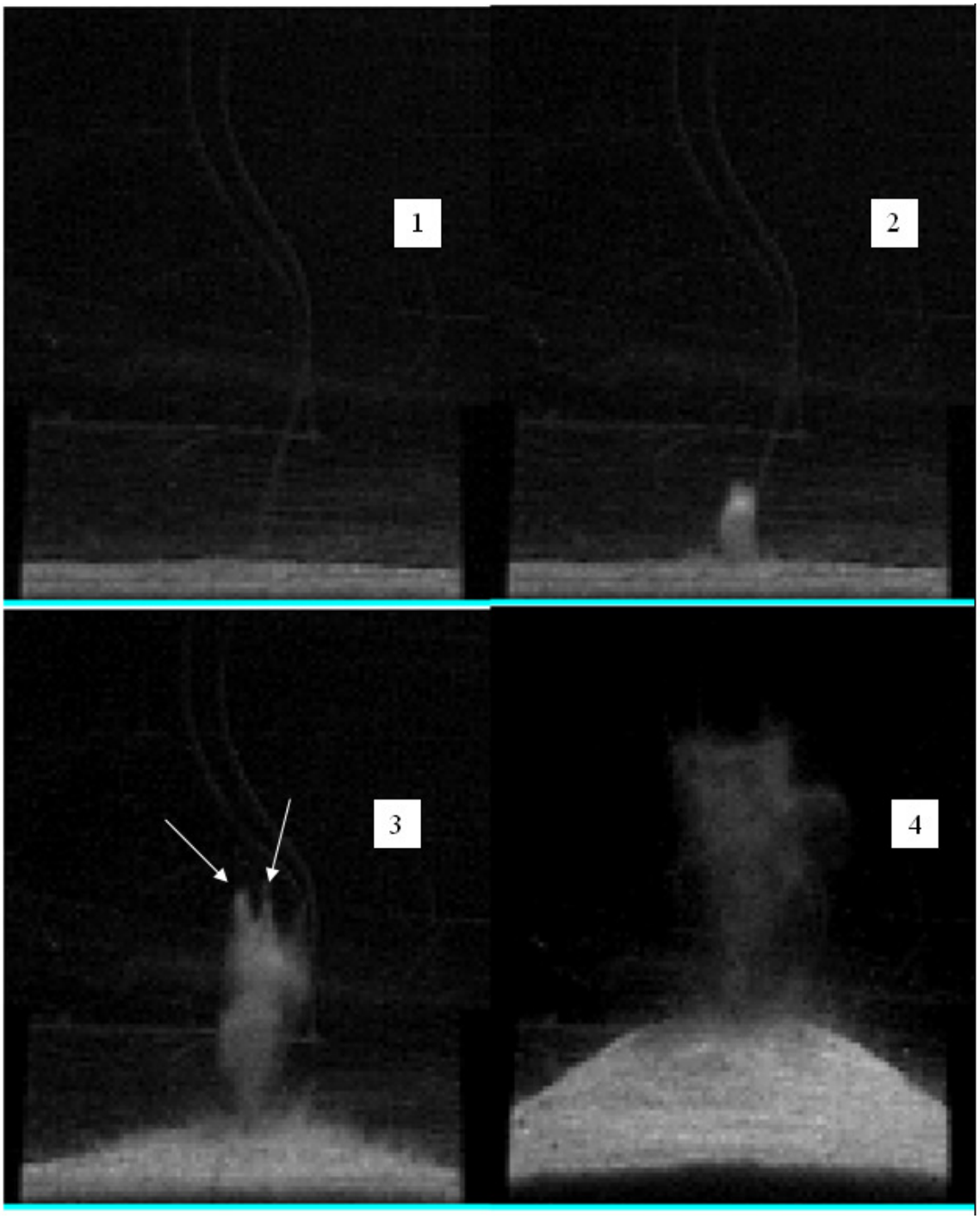

Figure 4.5: Jet from a 0.125in Diameter Hemisphere Imperfection

Figure 4.5 contains images from the cine file for Test 47, which used the 0.125 in diameter ball to make an imperfection. The jet emerges clearly and quickly, but it is

evident by image 3 that the jet contains regions of higher velocity than the rest of the jet. These "fingers" are noted by the white arrows on the figure. However by image 4, the jet begins to slow down, widen, and through volumetric dissipation begins to drop in density. Though no quantitative data were obtained to quantify this drop in density, it is apparent because of the reduced opacity of the jet. The jet dissipation does not occur until after the jet has reached the hypothetical target at 0.75in above the sand. Therefore, the high speed fingers of the jet were used in calculation of the velocity, and hence, the velocities of the jets in Tests 47 and 51 seen in Table 4.1 are quite high.

Test Number	Hemisphere Diameter [in]	DOB [in]	Mass [g]	Depth/Diameter	Jet Velocity [in/s]	Dome Velocity [in/s]
45	0.5	1.19	0.5	0.5	3872	3545
46	0.25	1.19	0.5	0.5	6488	3027
47	0.125	1.19	0.5	0.5	15373	3742
51	0.125	1.19	0.5	0.5	15253	2827
54	0.5	1.19	0.5	0.5	7204	3918
62	0.25	1.19	0.5	0.5	8041	3140
64	NA	1.19	0.5	NA	NA	3250

Table 4.1: Hemisphere Series Data For 1.19 DOB Tests

Another interesting observation is the jet velocity as a function of imperfection size trend is reversed from that of the cone series. That is to say, the largest diameter cone caused the fastest jet, but the largest diameter hemisphere caused the slowest jet.

Another computational simulation was run to compare with the experimental results. Figure 4.6 shows a side by side comparison of a simulation of a buried charge in sand,

and one with a semi-circle removed from the surface of saturated sand. It is important to note that the simulation also produces a jet. The simulations were completed by Drew Wardlaw, ATR Corporation[14]. The left halves of the images contain no surface imperfections while the right halves contain a hemispherical imperfection.

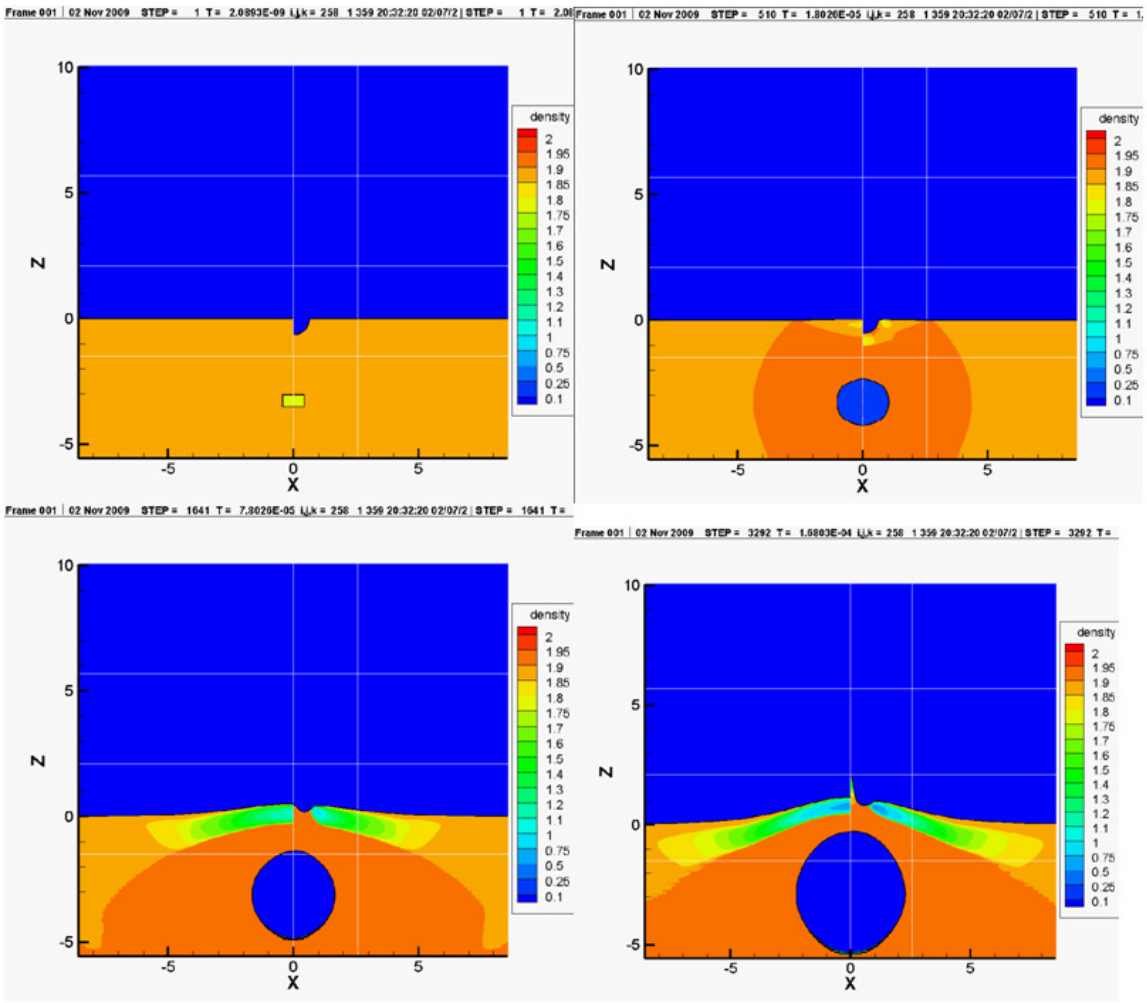

Figure 4.6: Computational Simulation with Density Contours of a Control Test and a Test with a Hemisphere Imperfection

4.2.2 Hemisphere Imperfection Series with Reduced 0.69 in Depth of Burial

An investigation into the effect of depth of burial (DOB) on the jet was conducted in the shallow depth series with hemisphere imperfections. This was achieved by reducing the DOB from 1.19 in to 0.69 in. This DOB was chosen because it would expand upon the work done in [9] where tests are conducted with DOBs of 2.38 in, 1.19 in and 0.595 in. The 0.595 in DOB proved to be too shallow to get a smooth dome and clear jet, yet the 1.19in depth of burial is quite deep relative to a charge of mass 0.5 g, equating to about 24.8 in full scale. Therefore, tests were conducted to see if there are any changes in the jet characteristics at this distance between the shallow 0.595 in depth and the deep 1.19 in depth.

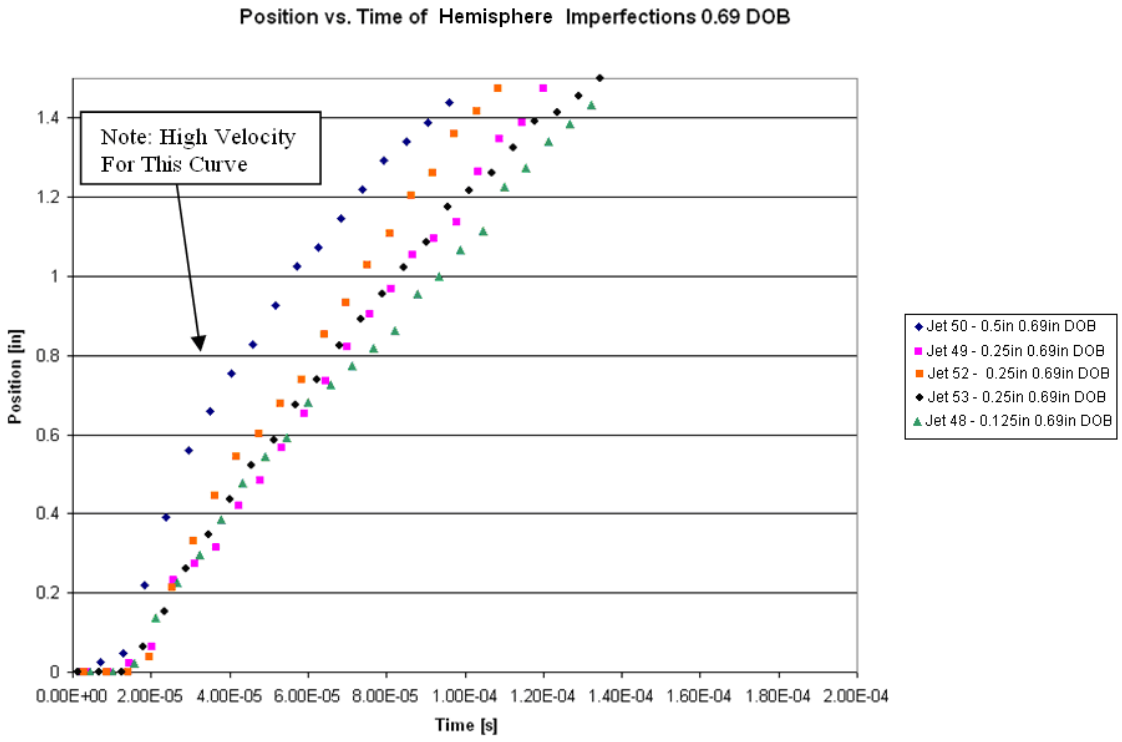

Figure 4.7: Position vs. Time Data for the Hemispheres Series with 0.69 in Charge DOB Using 0.5, 0.25 and 0.125 in Diameter Imperfections

Test Number	Hemisphere Diameter [in]	DOB [in]	Mass [g]	Depth/Diameter	Jet Velocity [in/s]	Dome Velocity [in/s]
48	0.125	0.69	0.5	0.5	10225	10199
49	0.25	0.69	0.5	0.5	7739	8567
50	0.5	0.69	0.5	0.5	12409	NA
52	0.25	0.69	0.5	0.5	12632	6725
53	0.25	0.69	0.5	0.5	14294	11097

Table 4.2: Hemisphere Series with 0.69 in DOB Data

A quick glance of the .cine video files will show that the overall motion of the sand is more violent than the previous hemisphere series or the subsequent cylinder series. This is due to the reduced DOB of the charge. With the exception of the jet from Test 50, the plots in Figure 4.7 show little variation, especially in the first 0.75in. The increased velocity of Jet 50 is due to a finger of the jet accelerating faster than the rest of the jet.

The Jet velocity values in Table 4.2 vary significantly from one another, despite the similarity in the position vs. time graphs. Due to the faster velocities, shorter time intervals, and the more difficult to track jets and domes, the error in these calculations is likely to be quite high.

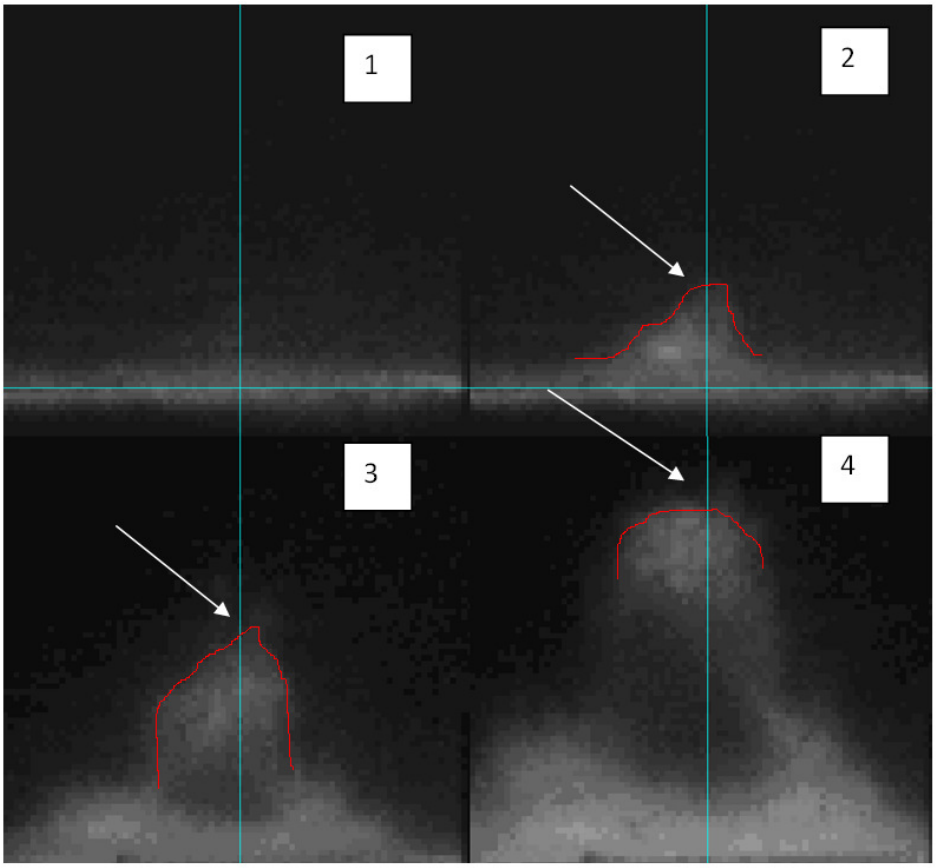

Figure 4.8: The Jet of Test 50

In Figure 4.8 the jet emerges with certain shape, but as it travels its shape changes to a rounded tip, as emphasized by the red contour. This is often noticeable in any given test, but is particularly prevalent in this series of reduced depth of burial tests. To remain consistent in tracking the jets, the topmost point of the jet is tracked and provides the position vs. time, and therefore, the velocity vs. time of the jet. Test 50 is an example of how the amorphous shape of the jet can affect the data and imply trends, such as a higher than normal velocity when it may not necessarily be representative of the jet as a whole. It is still important, however, to note that a part of the jet does possess a higher velocity than the rest of the jet, and could therefore affect the pressure resulting from this jet hitting a target.

This series is important in indicating that there is a distance in which one will not see a well defined jet and dome due to the violent motion in the explosion. The jet that appears is a function of the user-made imperfection, as well as the natural, random imperfections within the sand when charges are buried. One can create surface imperfections of a certain length scale, but as the depth of burial is more and more shallow, instabilities from smaller imperfections of a smaller length scale contribute to the jet. The small-scale instabilities are by definition random, and thus predicting their effect on a target becomes less direct. Because of these factors, the model of a separate jet and smooth dome breaks down when the depth of burial is reduced to certain distances. Conversely, there also exists a deep enough DOB at which one will not see a jet because the charge is too far away from the surface.

The results of this test are useful in that they further state the importance of the DOB on the formation of the jet. Despite the usefulness of the results, no further tests were conducted at this DOB. The focus of this work is to investigate the effect of different variables on the well defined jet and dome where the data are more reliable and consistent.

4.3 Cylinder Imperfection Series

The next sets of tests were done using rods to make cylindrical shaped imperfections in the sand. Unlike cones and ball bearings, the cylinders do not have geometries that limit their ability to be inserted in the sand. Because of this feature, additional series of tests of could be conducted in addition to the constant imperfection depth to imperfection diameter ratio tests done for the hemisphere series and the cone series. Therefore, three test series were done using cylinder shapes: The Cylinder Imperfection Series with Constant Depth to Diameter Ratio, the Cylinder Imperfection Series with Constant Imperfection Depth, and the Cylinder Imperfection Series with Constant Imperfection Geometry. Each of these test series are explained in detail in the following sections.

4.3.1 Cylinder Imperfection Series with Constant Depth to Diameter Ratio

The next step in the test series was to try a new shape for the imperfection and implement it in the same manner as the previous cone and hemisphere test series. Three rods of diameters 0.125 in, 0.25 in and 0.5 in were used to make the imperfections. Rods of appropriate diameter were inserted into the sand to a depth that was equal to half of the rod diameter. This was done to keep the distance from the charge to the bottom of the imperfection and the diameter of the imperfection comparable to the tests done using hemispheres and cones. An example of the setup can be seen in Figure 4.9.

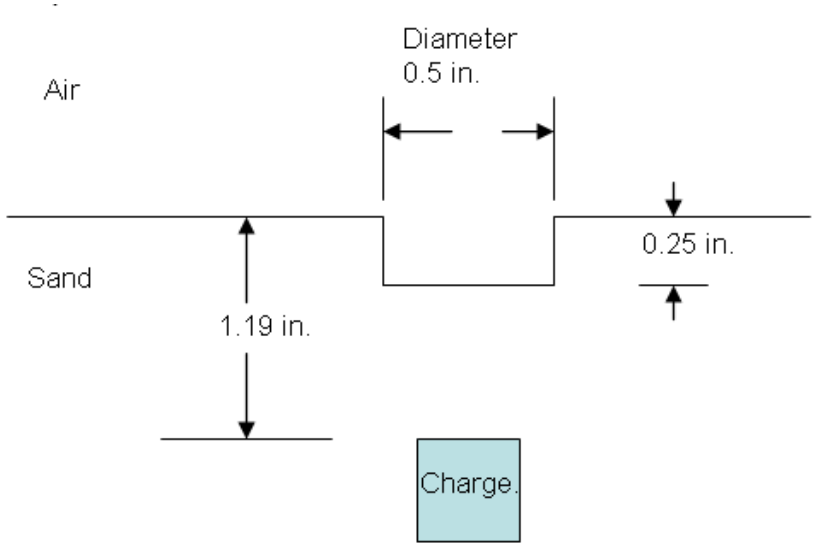

Figure 4.9: Schematic for the Cylinder Imperfection Test Series with Constant Depth to Diameter Ratio

The test procedure remained the same as the previous hemisphere and cone tests. The resulting data from this test series are plotted to produce Figure 4.10.

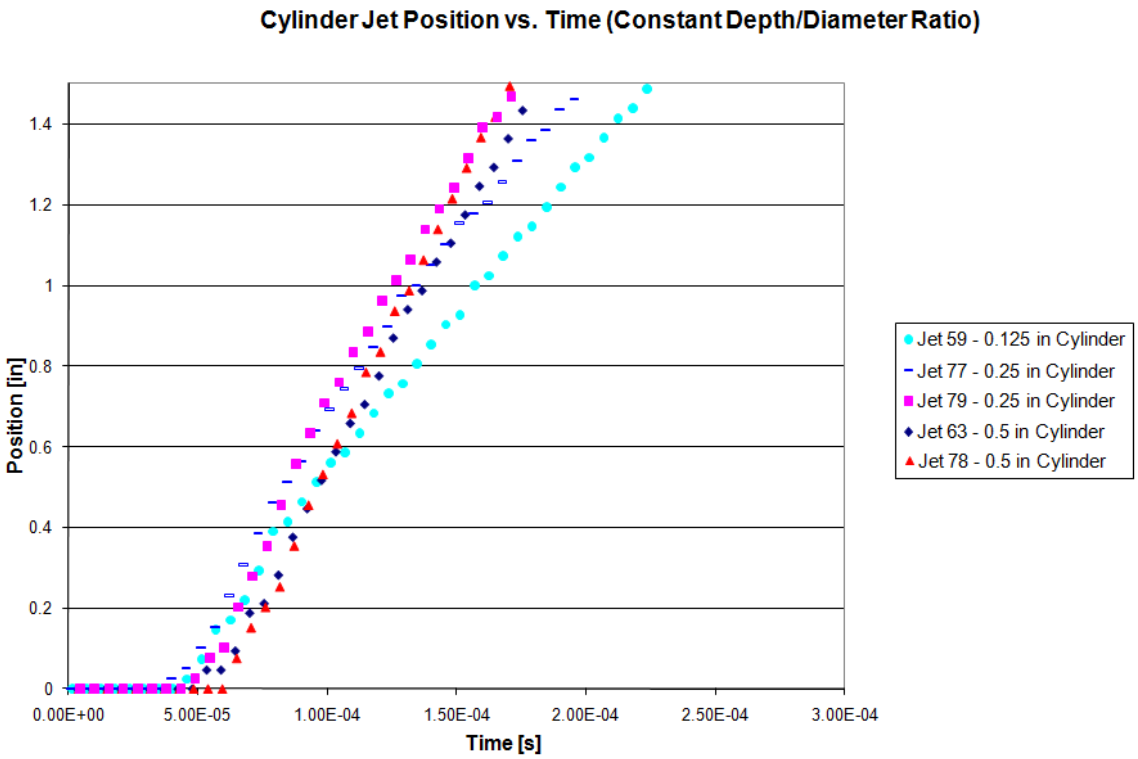

Figure 4.10: Position vs. Time Data for the Cylinder Imperfection Series with Constant Depth to Diameter Ratio Using 0.5, 0.25 and 0.125 in Diameter Imperfections

Test Number	Cylinder Diameter [in]	DOB [in]	Mass [g]	Depth/Diameter	Jet Velocity [in/s]	Dome Velocity [in/s]
57	0.5	1.19	0.5	0.5	10006	5177
58	0.25	1.19	0.5	0.5	6901	3817
59	0.125	1.19	0.5	0.5	7305	3312
63	0.5	1.19	0.5	0.5	14594	4488
64	NA	1.19	0.5	NA	NA	3250
77	0.25	1.19	0.5	0.5	9879	3442
78	0.5	1.19	0.5	0.5	15393	4024
79	0.25	1.19	0.5	0.5	12181	3154

Table 4.3: Cylinder Imperfection Series with Constant Depth to Diameter Ratio Data

The position vs. time results in Figure 4.10 show data that appear close to one another, especially compared to the 1.19in DOB cone and hemisphere series. The jet velocities are higher in this series, with velocities of 14,594 and 15,393 in/s for the 0.5 in cylinders compared to the 7204 in/s for the same size hemisphere. Also, note the decreasing velocity of Jet 59, which used a 0.125 in diameter cylinder. The velocity decreases once again due to the dissipation mechanism seen before in the 0.125 in diameter hemisphere tests at 1.19in diameter.

Please note that Tests 57, 58 and 64 do not appear on the graph. Test 64 was a control test and did not contain an imperfection, but was used to gather data on the dome velocity. Tests 57 and 58, however, were removed because the data in them are affected by a collapse of the imperfection. The collapse of the cylinder imperfection caused the data to fall significantly out of line with Tests 77, 78 and 79, which were repeated using the same conditions, and thus Tests 57 and 58 were removed from this graph. This removal will be described in more detail in a later section.

The data in this series indicate that the cylinders utilized with the same depth/diameter ratio as the cones and hemisphere cause jets that are faster than those made by the cone and sphere shapes. It is theorized that this is due to the shape of the cylinder. The cylinder provides a surface perturbation that has walls that are perpendicular to the surface of the sand, and thus maximize the amount of volume they displace relative to their diameter. Also, this imperfection creates a surface above the charge that has an

effectively reduced depth of burial, rather than a point in the case of the hemisphere and the cone shapes.

In the case of the jets for the hemisphere and conical imperfections, the imperfection depth is dependent on the imperfection diameter; a cone or sphere of a particular diameter can only be precisely inserted into the sand a distance equal to its radius. This is not the case with cylinders. It remains to be seen how the depth of the imperfection and the diameter of the imperfection affect the jet independently. This is investigated in the next series of tests.

4.3.2 Cylinder Imperfection Series with Constant Imperfection Depth

The Cylinder Imperfection Series with Constant Imperfection Depth was conducted to test the effect of varying only the diameter of the cylinder on the resulting jet. By varying just the diameter of the cylinder, the distance from the charge to the imperfection is kept constant.

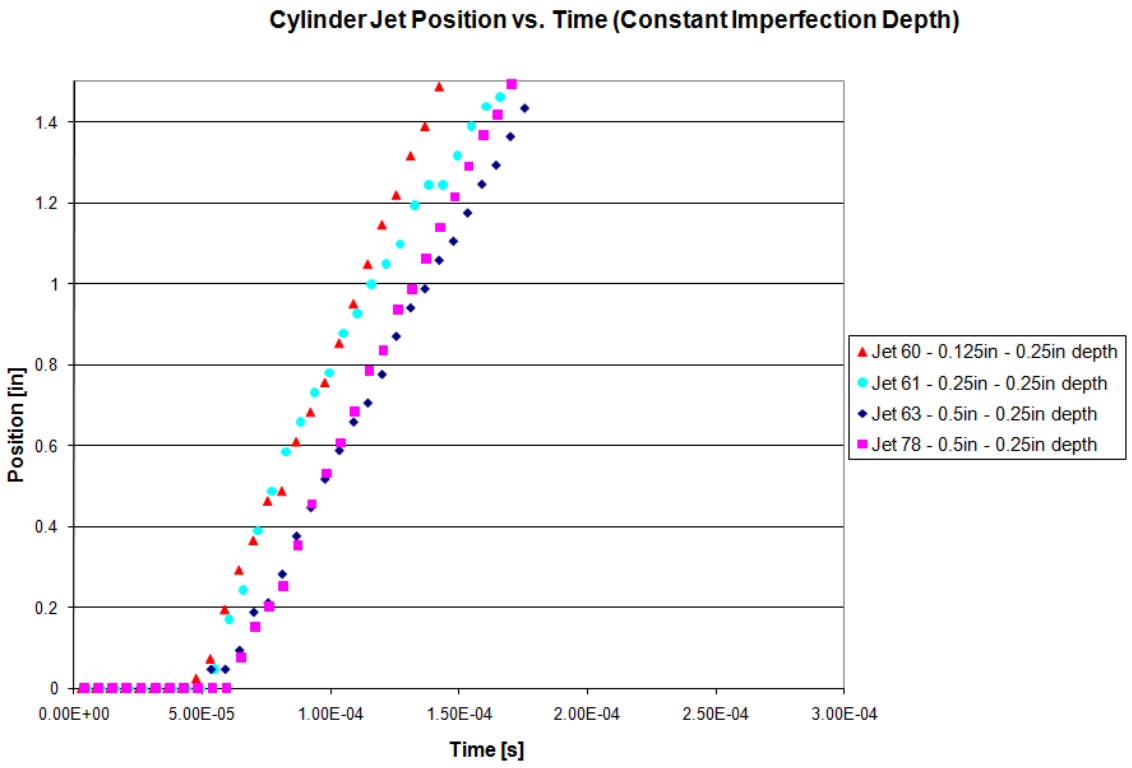

Figure 4.11: Position vs. Time Data for the Cylinder Imperfection Series with Constant Imperfection Depth Using 0.5, 0.25 and 0.125 in Diameter Imperfections

Test Number	Cylinder Diameter [in]	DOB [in]	Mass [g]	Depth/Diameter	Jet Velocity [in/s]	Dome Velocity [in/s]
60	0.125	1.19	0.5	2	15241	NA
61	0.25	1.19	0.5	1	13975	NA
63	0.5	1.19	0.5	0.5	14594	4488
78	0.5	1.19	0.5	0.5	15393	4024

Table 4.4: Cylinder Imperfection Series with Constant Imperfection Depth Data

The data in Figure 4.11 show that at a constant distance away from the charge, the imperfection diameter does not heavily affect the jet velocity. This trend is verified in Table 4.4 by comparing the velocities. It is now evident that imperfection diameter is less important than the depth to which the imperfection extends.

Since the distance from the charge to the imperfection is constant in every test, the time at which the jet first emerges should not change. From the graph, it is evident that the jet in some tests emerges later than expected. This indicates that there could be a finite amount of error in the camera trigger timing or in the charge detonation in some tests.

4.3.3 Cylinder Imperfection Series with Constant Imperfection Geometry

This test series was completed by varying the depth of an imperfection while holding the imperfection geometry constant. The same 0.25 in rod was used to make imperfections that extend to depths of 0.125 in, 0.25 in and 0.375 in. This test series is designed to observe the effect of the depth of the imperfection only.

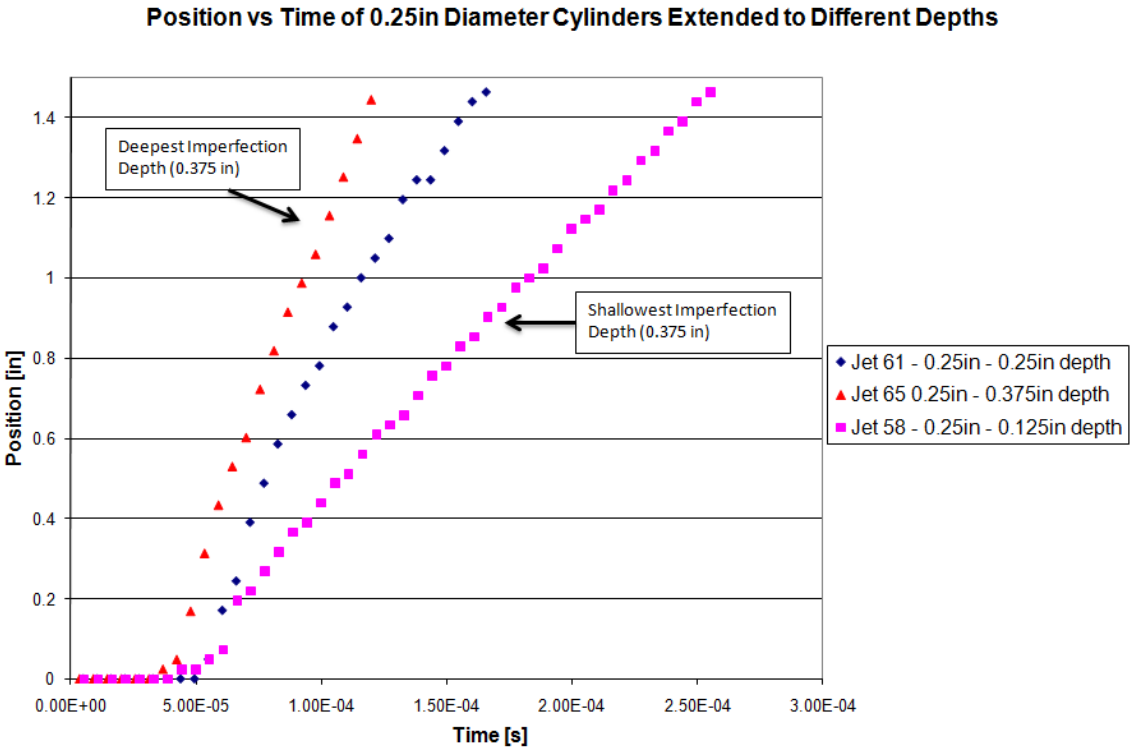

Figure 4.12: Position vs. Time Data for the Cylinder Imperfection Series with Constant Imperfection Geometry Test Using 0.25 in Diameter Imperfections

Test Number	Cylinder Diameter [in]	DOB [in]	Mass [g]	Depth/Diameter	Jet Velocity [in/s]	Dome Velocity [in/s]
58	0.25	1.19	0.5	0.5	6901	NA
61	0.25	1.19	0.5	1.0	13975	NA
65	0.25	1.19	0.5	1.5	16351	3154

Table 4.5: Cylinder Imperfection Series with Constant Imperfection Geometry Data

The results from this series in Figure 4.12 and Table 4.5 are somewhat intuitive. The results imply that the increasing depth of the imperfection causes a jet with higher velocity. This makes sense because as the imperfection is pressed further, it decreases the distance to the charge, which places the surface of the imperfection closer to the charge. Compared to the diameter of the imperfection, the depth to which the imperfection extends appears to be much more important to the peak jet velocity.

4.4 Moist Sand Test Series

Up until the Moist Sand Test Series, all tests were done using saturated Berkeley Springs Sand. The tests in the Moist Sand Tests Series were conducted to examine the effect of moisture content of the sand on the resulting dome and jet. Instead of detonating the charge in saturated sand, these tests were conducted a specified amount of time after the sand has been drained of excess water. Tests were conducted after the drained sand had been left to dry for 48 hours, 6 days, 7 days, and also immediately after draining.

Figure 4.13 is a plot of the initial dome velocities from the Moist Sand Test Series. The plot contains a curve which is obtained from averaging the position vs. time data from all comparable tests conducted in saturated sand. Note that the initial velocity decreases with decreasing moisture content, and that there are steps in the data of the moist sand domes. This is due to unsatisfactory camera resolution in observing the position of the slower moist sand domes.

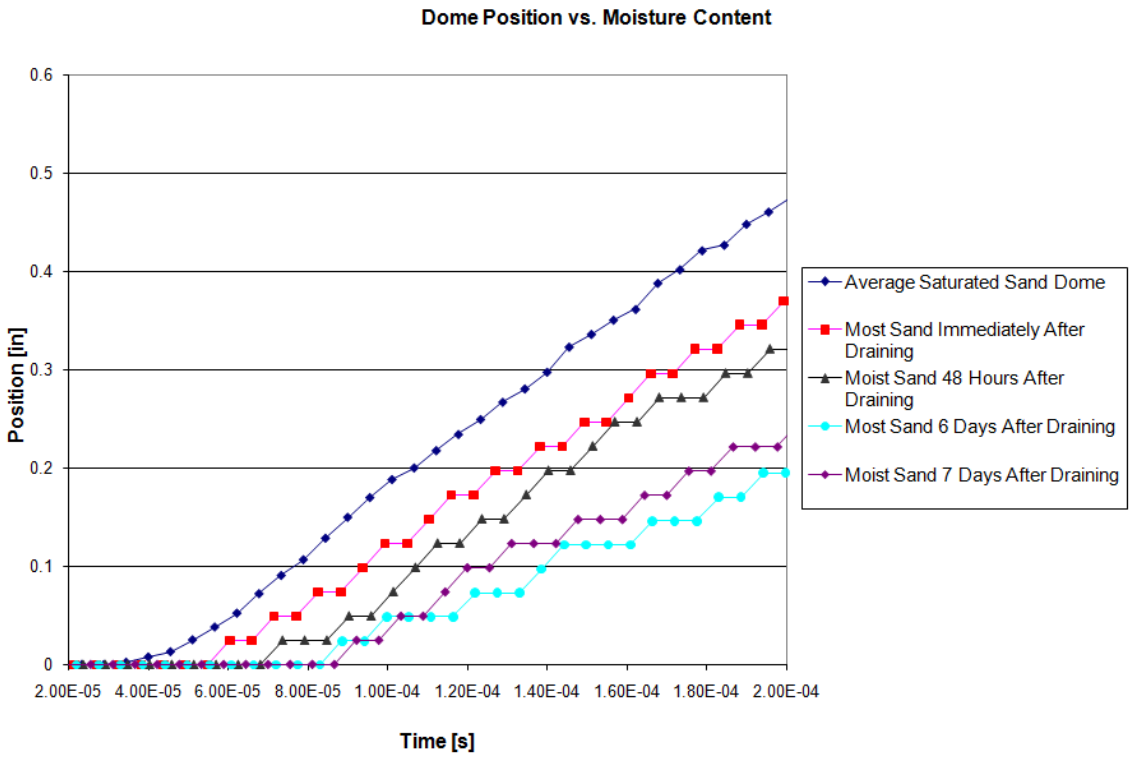

Figure 4.13: Moist and Saturated Sand Dome Position vs. Time Plot

The density of the sand for each test was measured by taking a known volume of sand and measuring the mass prior to each test. The initial velocities of the domes were calculated and the results are plotted in Figure 4.15. The reason for calculating the initial velocity is because the moist sand domes do not remain coherent by the time they would reach the imaginary target at 0.75in above the surface of the sand. Curves were fit to the dome data at the initial movement of the domes to calculate an initial velocity. The high velocity expanding gases make the top of the dome less defined and more difficult to track, thus initial dome velocities are presented rather than dome velocities at the target. An example of this is in Figure 4.14.

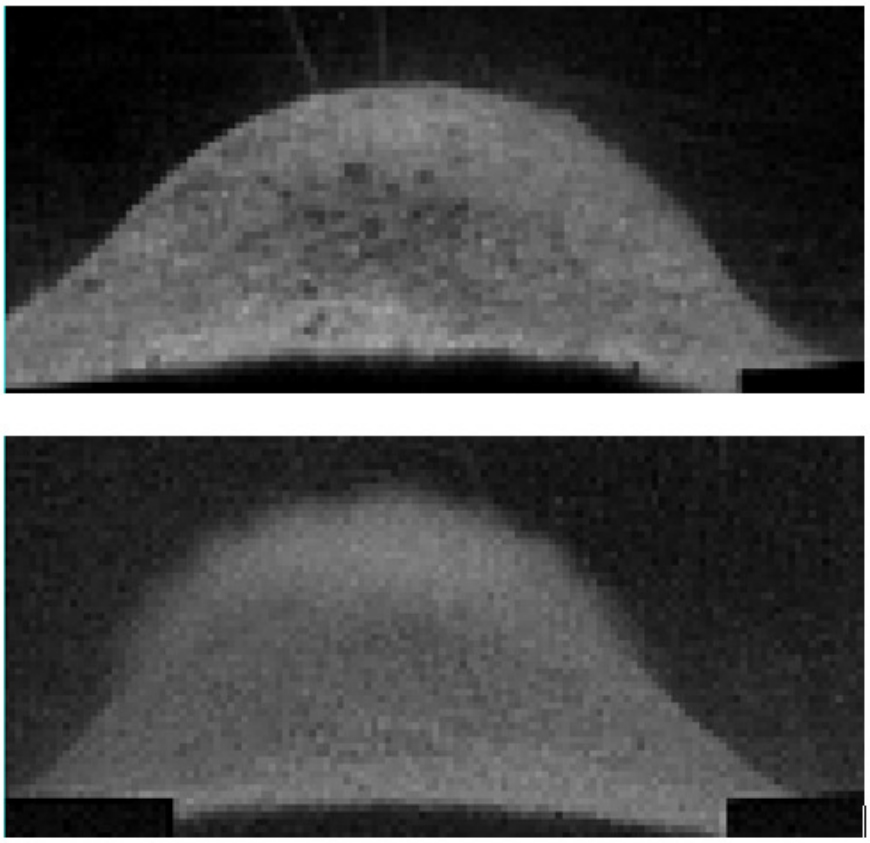

Figure 4.14: A Comparison of Saturated (Test 64) vs. A Moist Sand Dome (Test 69)

The initial velocity values are used in Table 4.6.

Test Number	Cylinder Diameter [in]	DOB [in]	Mass [g]	Depth/Diameter	Sand Density[g/cc]	Initial Dome Velocity [in/s]
67	0.25	1.19	0.5	0.5	1.96	2671
68	NA	1.19	0.5	NA	1.66	1780
69	NA	1.19	0.5	NA	1.65	1402
70	NA	1.19	0.5	NA	1.90	2535

Table 4.6: Moist Sand Test Series Dome Data

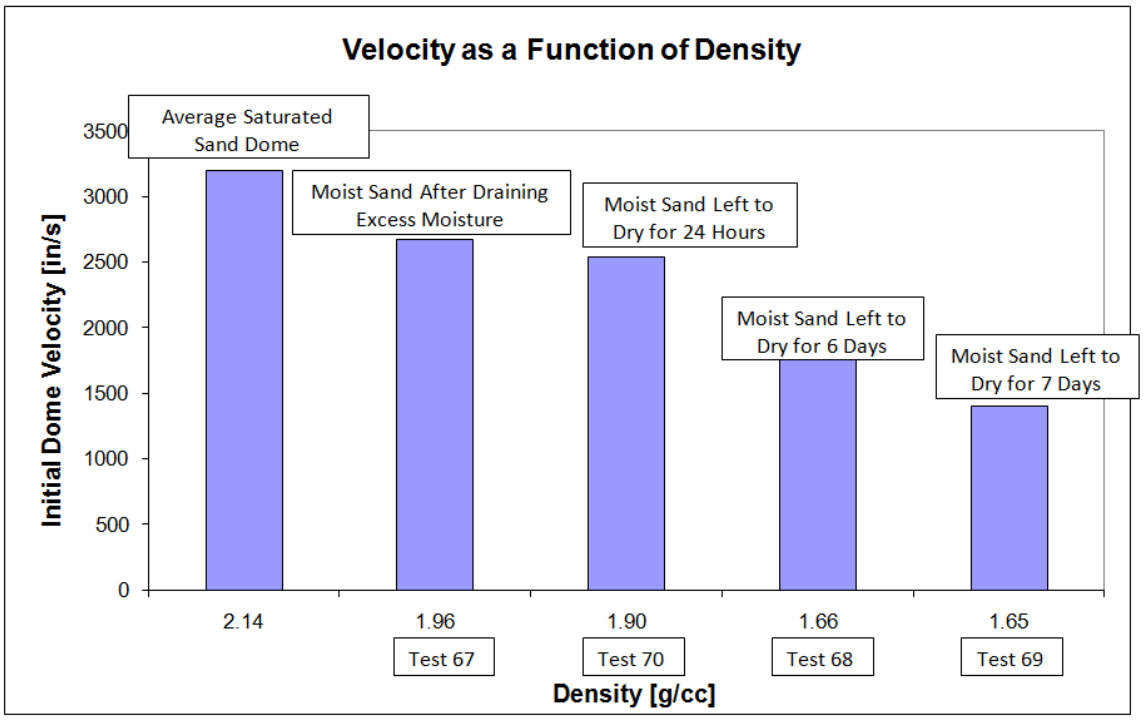

Figure 4.15: Initial Dome Velocity as a Function of Sand Density

Figure 4.15 shows a clear correlation between the density of the sand and the initial velocity of the dome. Tests 67 and 70 have similar velocities while Tests 68 and 69 have similar velocities. Test 67 was conducted using a 0.25 in cylinder imperfection, but produced no jet. Since no jet was formed in the moist sand, the subsequent tests in the series were done without surface imperfections, and thus, focused on the dome behavior.

The results indicate a dependent relationship between the initial velocity of the dome and the moisture content of the medium, which is measured as a change in density. This is because the shockwave can travel more easily and with less dissipation through a medium such as water than a porous mixture like sand. The lack of a jet implies that although the shockwave distance is important in the formation of a jet, the jets are fluid phenomena and need the water to form. By decreasing the moisture content in the sand,

the medium is more porous, less fluid, and thus produces a slower moving dome and no jet.

4.5 Surfactant Test Series

Often in the tests using saturated sand, there is some water present in the cavity in the surface of the sand that was produced by the imperfection. In order to see if surface tension in the water affected the jet or dome of the explosions, a surfactant was added to water before it was added to the tank. The surfactant added was Triton X-100, pictured in Figure 4.16.

Figure 4.16: Surfactant Triton X-100

Triton X-100 reduces the surface tension of water from approximately 70 mN/m to approximately half of that after adding only 0.5mL to the approximately 800in^3 (13L)of

water typically used to saturate the tank[15, 16]. The water with surfactant was mixed via stirring and then added to the tank through a valve at the bottom similar to all of the previous tests. Two tests were conducted using the surfactant. The first was done with no added surface imperfections. The second was done with a 0.25 in cylinder imperfection.

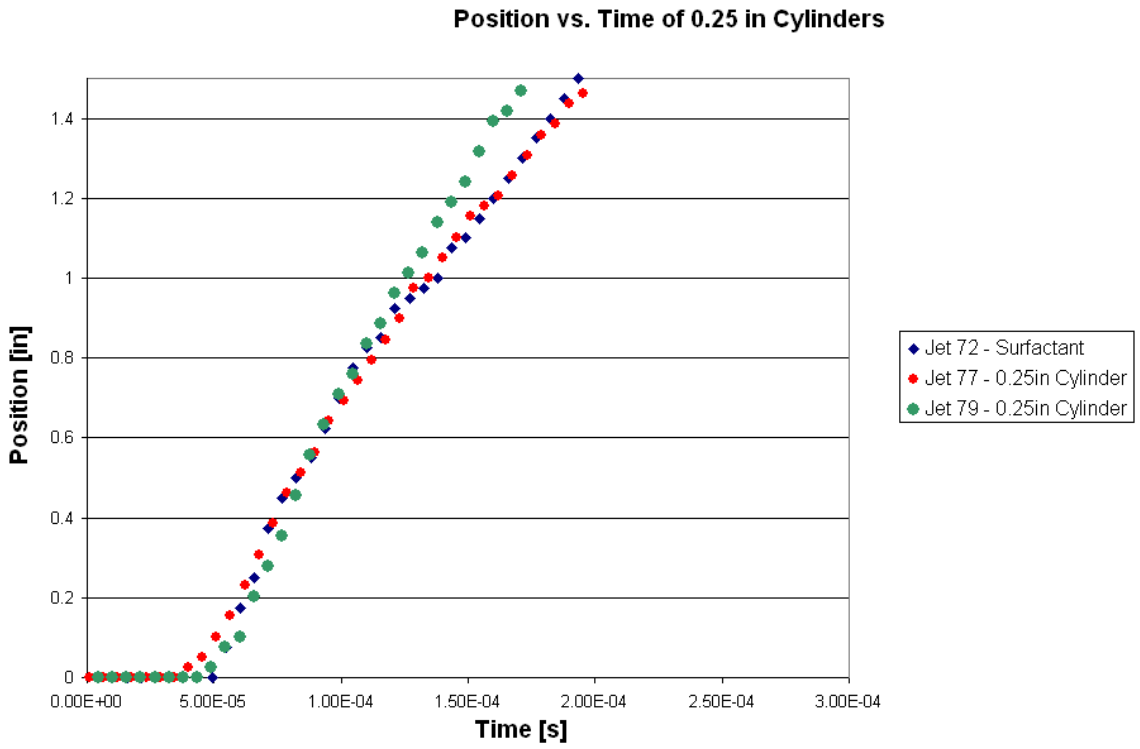

Figure 4.17: Position vs. Time of 0.25 in Cylinder Test with Surfactant Compared to Other 0.25 in Cylinder Tests

Test Number	Cylinder Diameter [in]	DOB [in]	Mass [g]	Depth/Diameter	Jet Velocity [in/s]	Dome Velocity [in/s]
71	NA	1.19	0.5	NA	NA	3046
72	0.25	1.19	0.5	0.5	10259	3421

Table 4.7: Surfactant Test Series Data

The purpose of the surfactant tests was to see if the surface tension in the water was affecting the formation of the jet or the development of the dome. The values in Table 4.7 and plots in Figure 4.17 indicate that the surfactant did not dramatically affect the jet velocity in a way that would differentiate itself from the other 0.25 in cylinder tests with depth to diameter ratio of 0.5. Even the video files produce remarkably similar jets, shown in Figure 4.18.

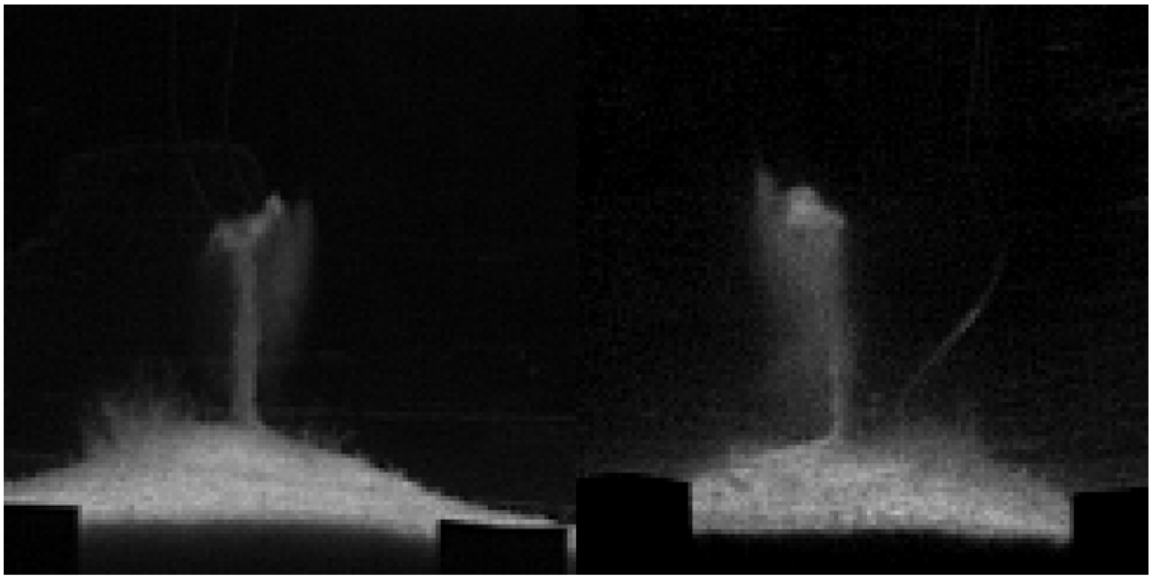

Figure 4.18: Jets from Tests 77 (without surfactant) and 72 (with surfactant) after 250.93μs

The only noticeable difference between the two is the increased amount of "spray" from the dome and jet with surfactant. This is most likely due to the reduced cohesion between the water molecules, but it does not seem to affect the overall jet or dome velocity.

4.6 Coarse Grain Sand Test Series

Finally, the effect of the grain size of the sand is explored in the Coarse Grain Sand Test Series. The Berkeley Springs Sand was replaced with sieved coarse grain sand, which is referred to as the Coarse Grain Sand. Both the Berkeley Springs Sand and the Coarse Grain Sand were analyzed to quantify the particle size distribution. Samples of 2.0 kg of each type of sand were sieved using sieves sizes 16, 20, 30, 40, 50 and 60. These sizes and their corresponding opening diameter are in Table 4.8.

Sieve Number	Opening Diameter
16	1.19mm
20	0.841mm
30	0.595mm
40	0.42mm
50	0.297mm
60	0.25mm

Table 4.8: Sieve Number and Opening Diameters

The results from the sieve analysis are in Figure 4.19. The main difference between the two sands is the percentage of particles present at or above the 0.595, 0.42 and 0.297mm diameter ranges. For example, the Berkeley Springs Sand has over 65% of its mass in the 0.595-0.42mm diameter range, where the Coarse Grain Sand has more than 25% of its mass in the larger 0.841mm-1.19mm diameter and above sizes. The distributions are shown in a column plot and a percent size plot in Figure 4.19.

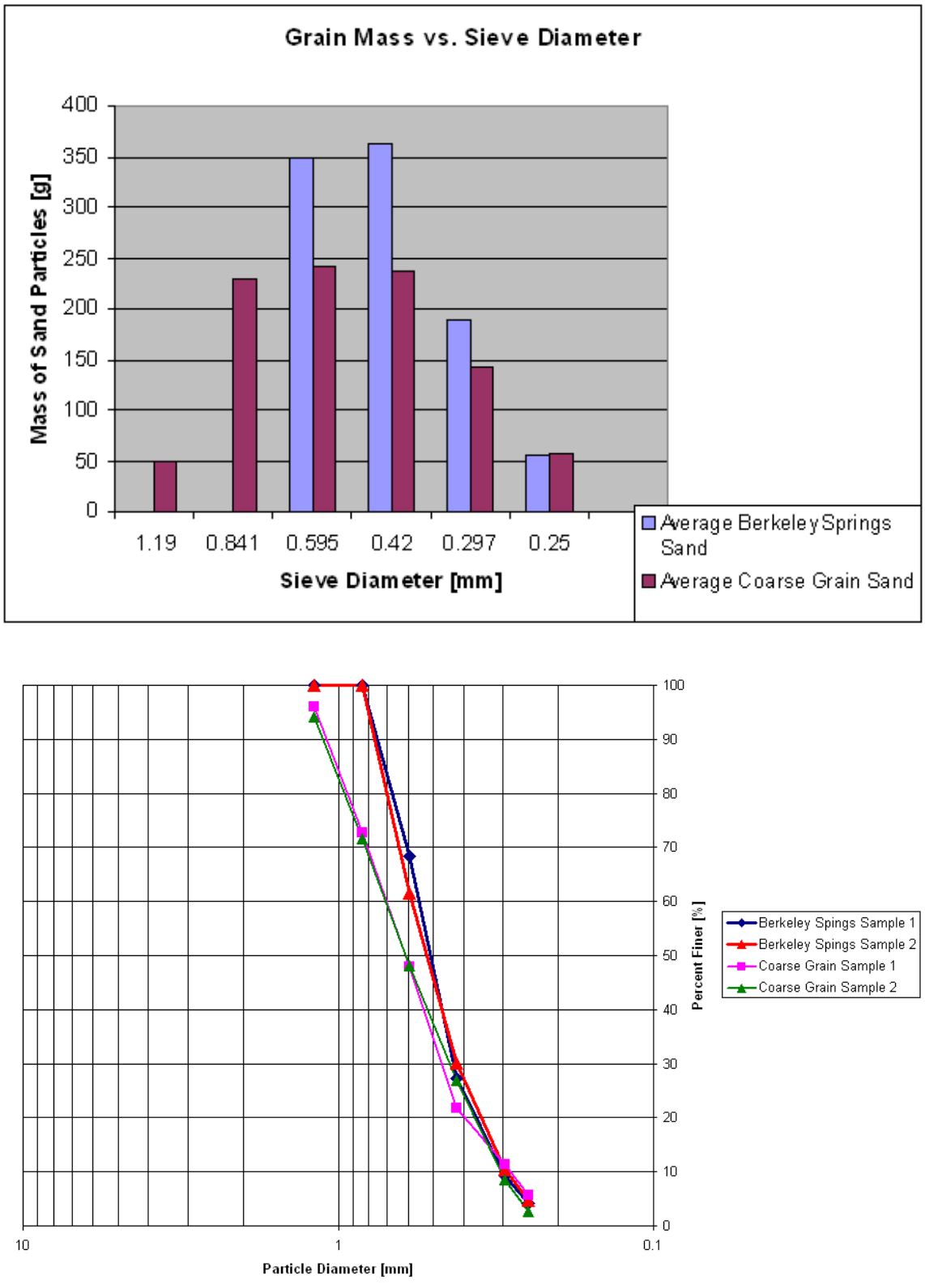

Figure 4.19: Grain Size Analysis – Mass of Sand Particles Present at a Given Sieve Size and Percent Size Plot of Berkeley Springs and Coarse Grain Sand

Finally the density of the Coarse Grain Sand was calculated and compared to the Berkeley Springs Sand. Both density calculations were done after saturating the sand with an average calculated from 5 samples. The density of the saturated Coarse Grain Sand is 2.2 g/cc compared to the 2.14 g/cc of the Berkeley Springs Sand.

The jets from the Coarse Grain Sand are compared to the tests with identical setup in Fine Sand (Berkeley Springs Sand) in Figure 4.20, Figure 4.21 and Figure 4.22.

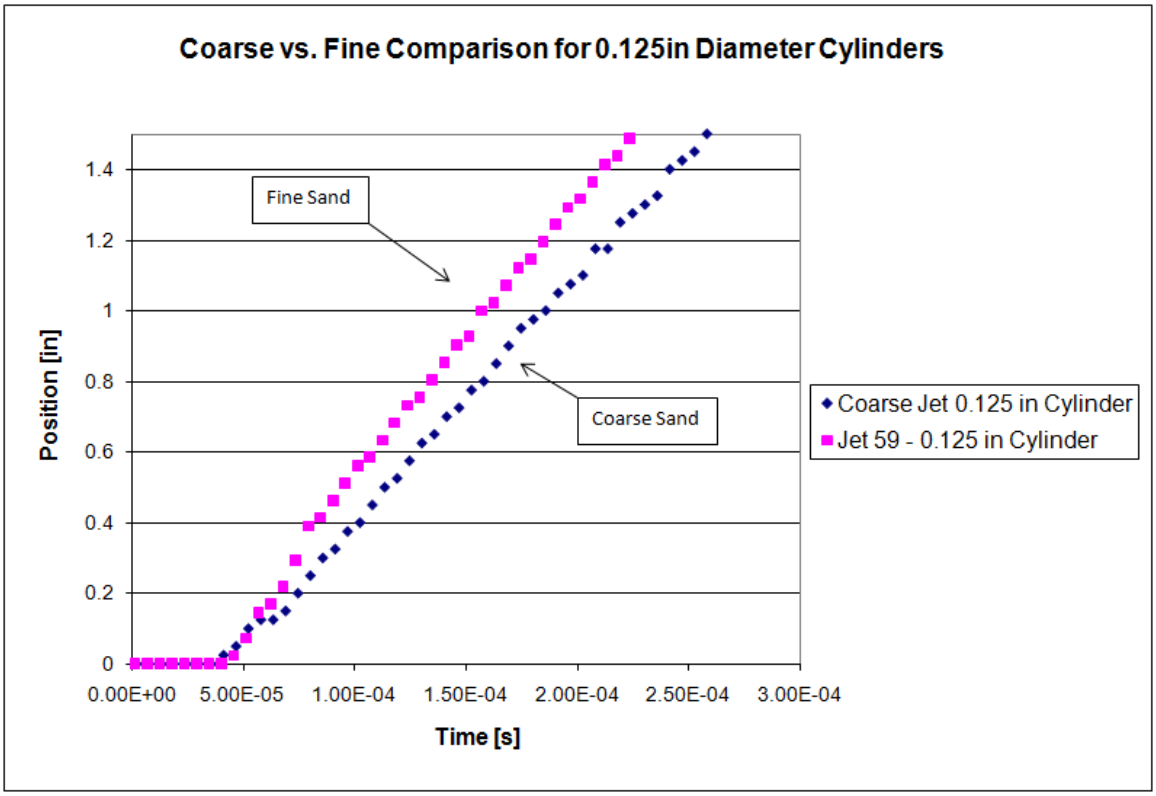

Figure 4.20: Position vs. Time Data of Coarse and Fine (Berkeley Springs) Sand Jets from 0.125 in Cylinders

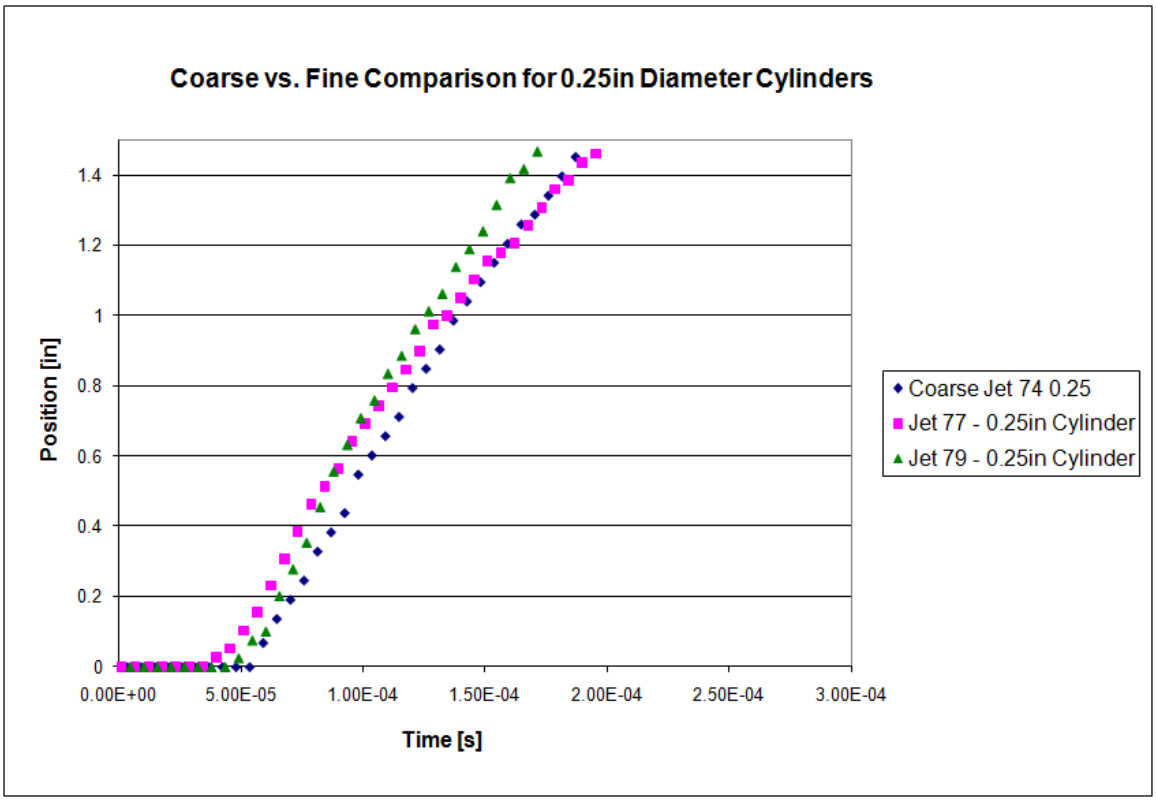

Figure 4.21: Position vs. Time Data for Coarse and Fine (Berkeley Springs) Sand Jets from 0.25 in Cylinders

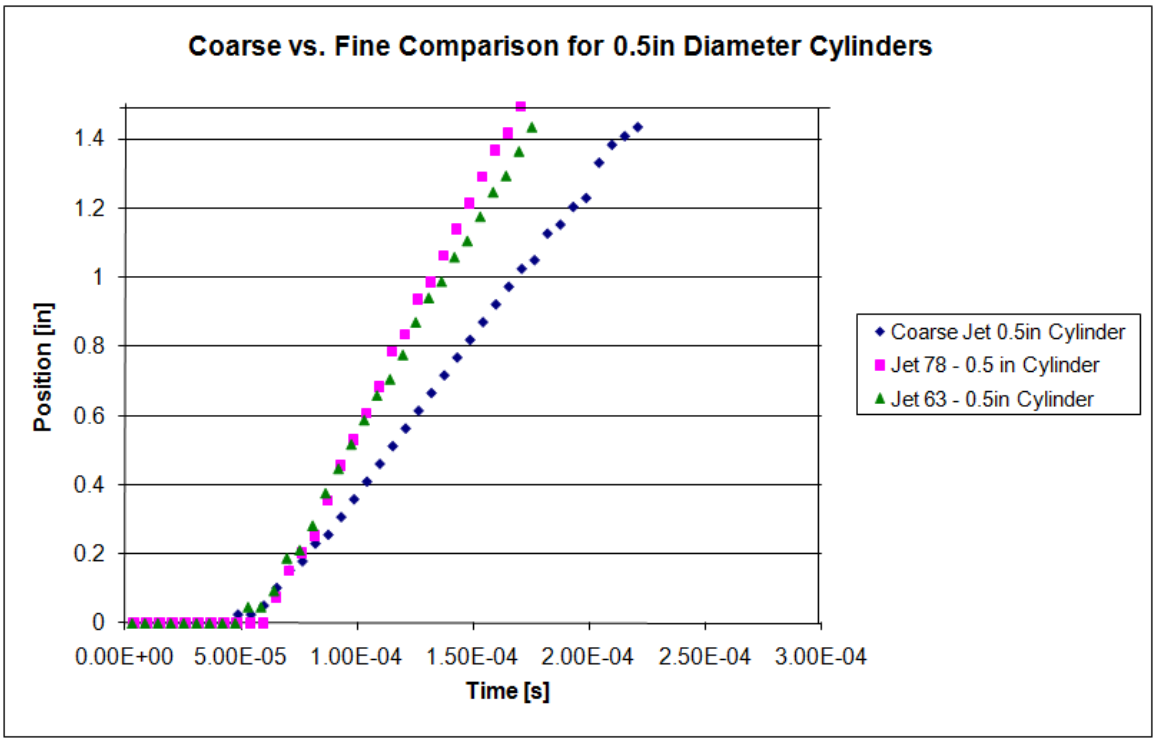

Figure 4.22: Position vs. Time Data for Coarse and Fine (Berkeley Springs) Sand Jets from 0.5 in Cylinders

Test Number	Cylinder Diameter [in]	DOB [in]	Mass [g]	Depth/Diameter	Jet Velocity [in/s]	Dome Velocity [in/s]
73	NA	1.19	0.5	NA	NA	2964
74	0.25	1.19	0.5	0.5	12243	3233
75	0.125	1.19	0.5	0.5	8125	3084
76	0.5	1.19	0.5	0.5	10836	4288

Table 4.9: Coarse Sand Test Data

The values in Table 4.9 are not far off from the corresponding values in Table 4.3 in the case of 0.25 in cylinders. Figure 4.20 yields a jet velocity approximately 16% higher in Test 74 than with the Berkeley Springs Sand in Test 59. But Figure 4.22 illustrates that Test 76 yields a 30% lower velocity compared to Tests 78 and 63. Similar

inconsistencies are seen in the Figure 4.21 results, where the 0.25 in cylinders in Tests 74 and 79 produce velocities that are within 0.5% of one another.

From the velocity analysis, there does not seem to be an apparent trend in the jet velocities when compared to a similar test in Berkeley Springs Sand. It is theorized that this is due to the wider particle size distribution introducing more scatter into the data because of the greater heterogeneity in the sand, but more tests should be done using the Coarse Grain Sand to identify a possible trend.

4.6.1 Error in Cylinder Tests

It is necessary to note that there may be significant error in the results of some of the cylinder tests. This error is presumably due to the difficulty of keeping the cylindrical geometry imprinted in the sand, and the sensitivity of the jet velocity to the geometry of the imperfection. The comparison of the jets from Tests 58 and 66 to 77 and 79 in Figure 4.23 demonstrate this error. All of these tests use the exact same conditions of a 0.25 in diameter cylinder imprinted to a depth of 0.125 in into saturated Berkeley Spring Sand.

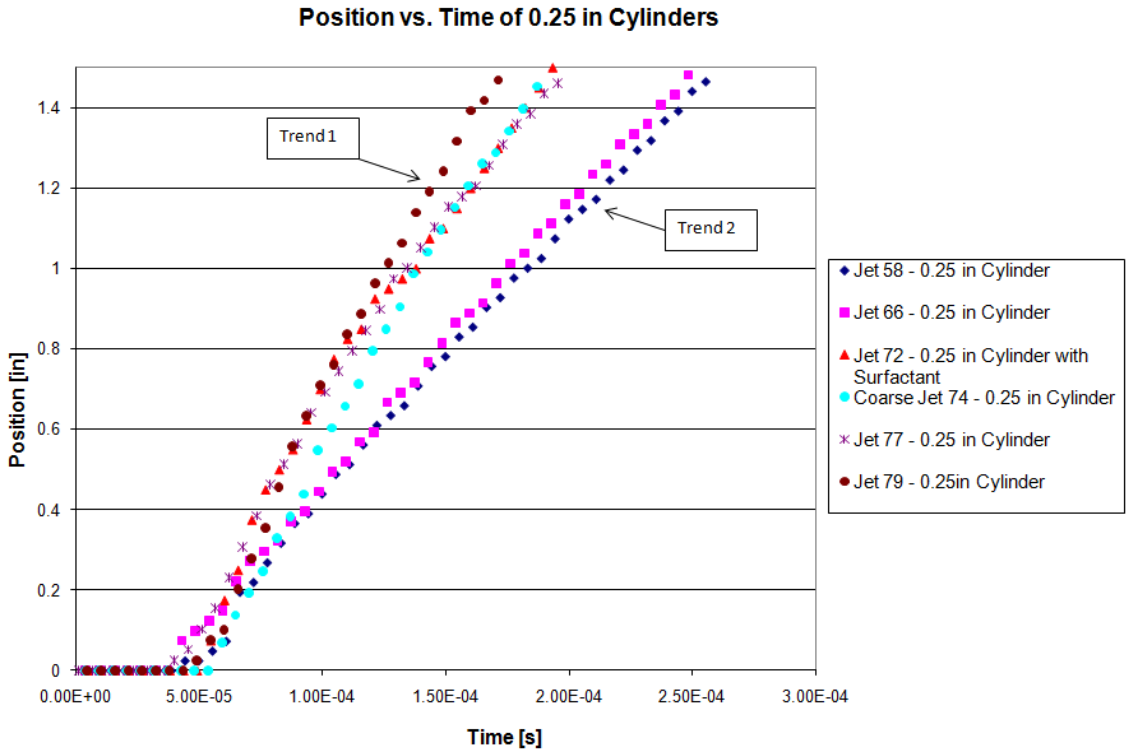

Figure 4.23: Discrepancies in the 0.25 in Diameter Cylinder Position vs. Time Data

It is presumed that this is due to the saturation of the sand and its effect on the imperfection geometry, causing a collapse of the cylinder. When the cylinder shape is preserved, the higher velocities of 77 and 79 are observed (Trend 1). When the cylinder shaped imperfection is "blunted" by the saturated sand, the resulting velocity is lower, and more comparable to that of a hemisphere imperfection from the Hemisphere Imperfection Test Series (Trend 2). This explanation is plausible in that it provides a reason why the data show two different trends in the same exact test.

4.7 Dome Analysis and Time Shift Corrections

Below in Figure 4.24 is a plot of all of the dome velocities in order of their test number.

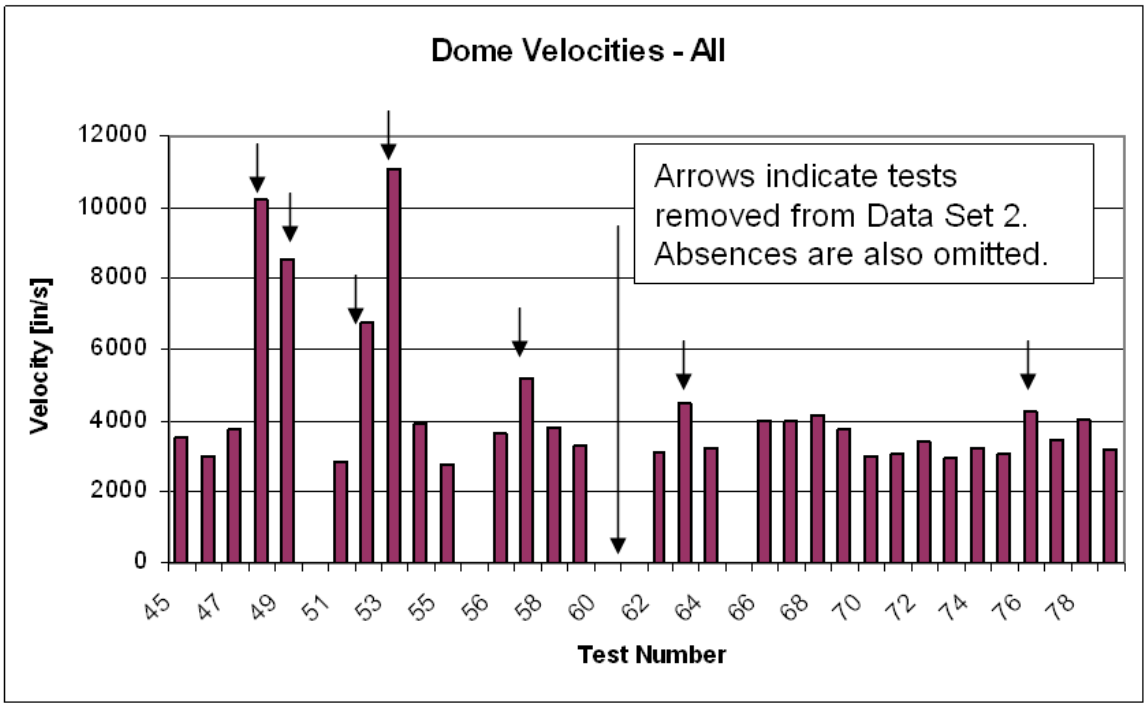

Figure 4.24: Dome Velocity by Test Number

The data in Figure 4.24 are further classified by their test conditions. The moist sand, shallow DOB, and 0.5 in diameter imperfections tests are omitted and the data are plotted again to produce Figure 4.25, which contains the domes from all of the tests that used 1.19 in DOB saturated sand. The 0.5 in diameter DOB tests are omitted because the size of the imperfection was large enough to make tracking the top of the dome difficult.

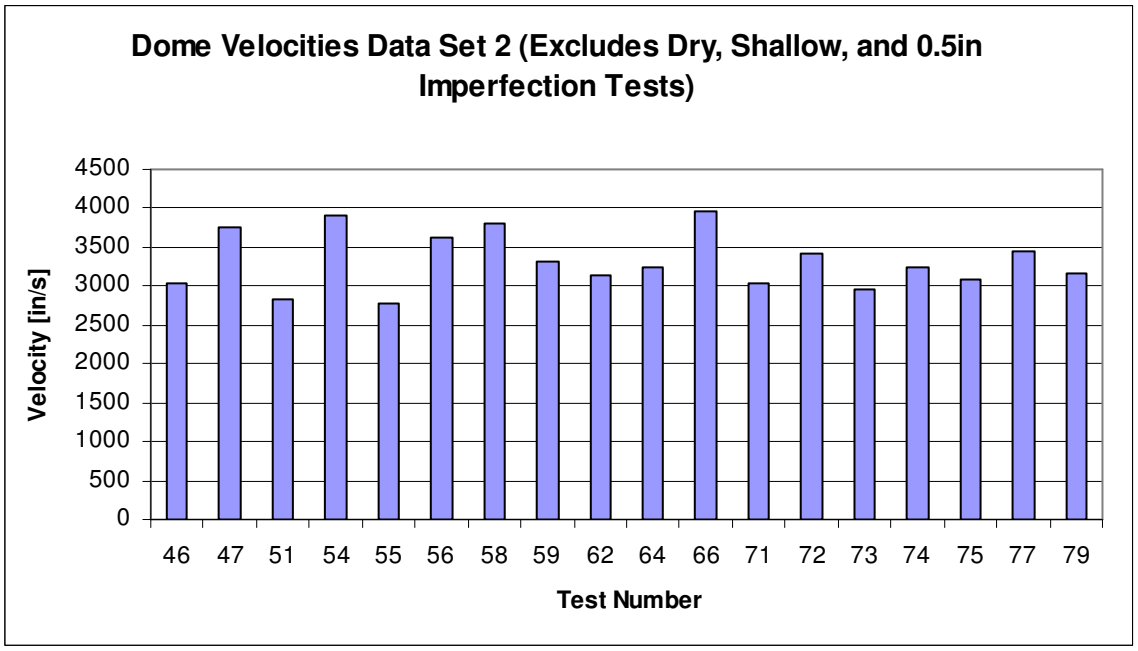

Figure 4.25: Dome Velocity by Test Number (Set 2)

Figure 4.25 provides insight into the repeatability within the tests when calculating velocities. Even though these tests should produce the same results, there is still a large standard deviation of approximately 365 in/s, which is 11% of the average velocity. There many factors that can add error decrease the repeatability in the velocity measurements. The small length scales, porous and heterogeneous medium, and the noise amplifying process of differentiation are significant sources of error for the velocity calculations presented. Despite the error, the calculations do provide valuable quantitative insight into both the velocity (and therefore loading mechanisms) of the dome and jet.

In addition, the image tracking results occasionally show a significant shift in the arrival time of the dome and jet. This error is presumably caused by a slight malfunction in the

FS-17 firing system or in the RP-87 detonator. The error is detected by comparing the resulting dome to the spread of the other domes. Examples of this are Tests 79 and 58.

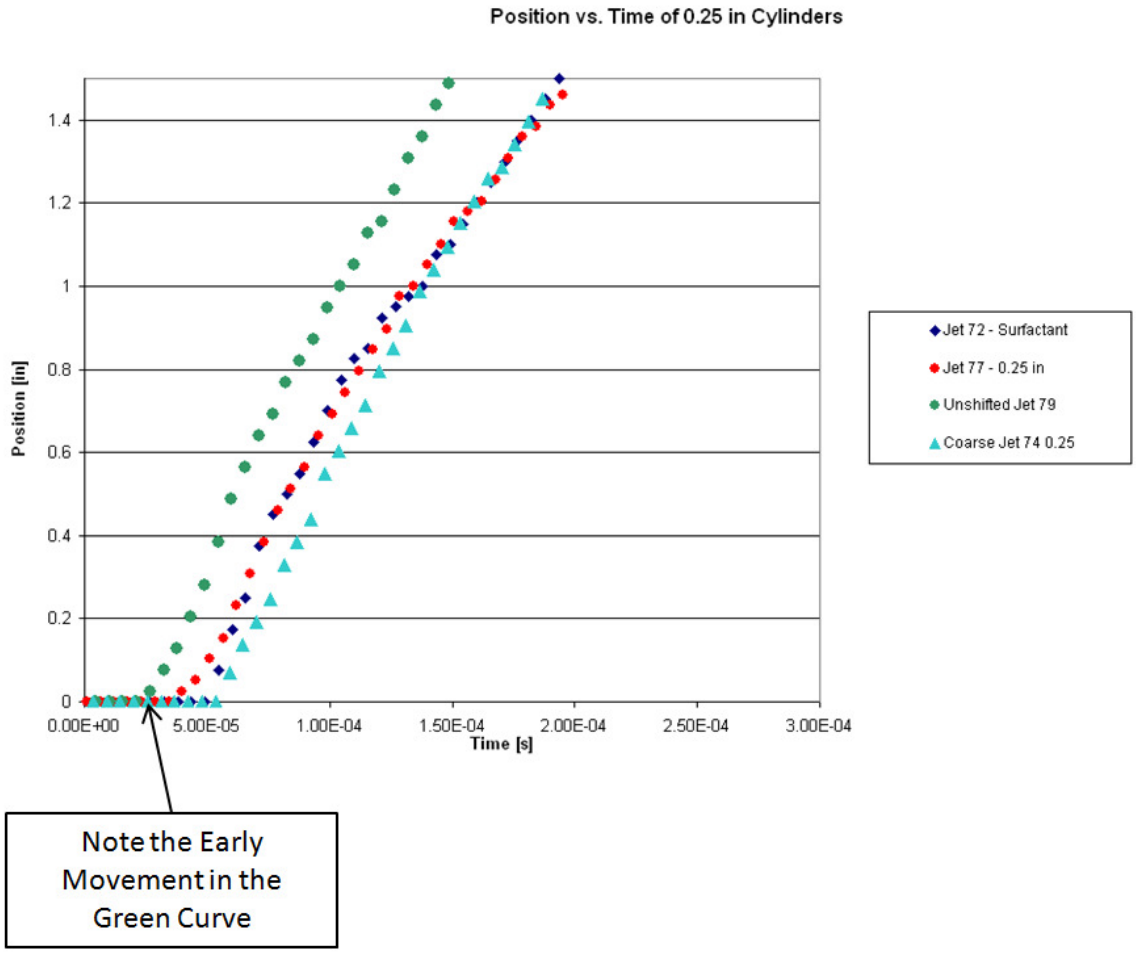

Figure 4.26: Graph of Jets for 0.25 in Cylinder Imperfections with Unshifted Jet 79

The unshifted Jet 79 sticks out from the other jets in Figure 4.26 because it does not have the same x intercept. The data for the dome of Test 79 are plotted against the others to verify that it is not just a jet phenomenon.

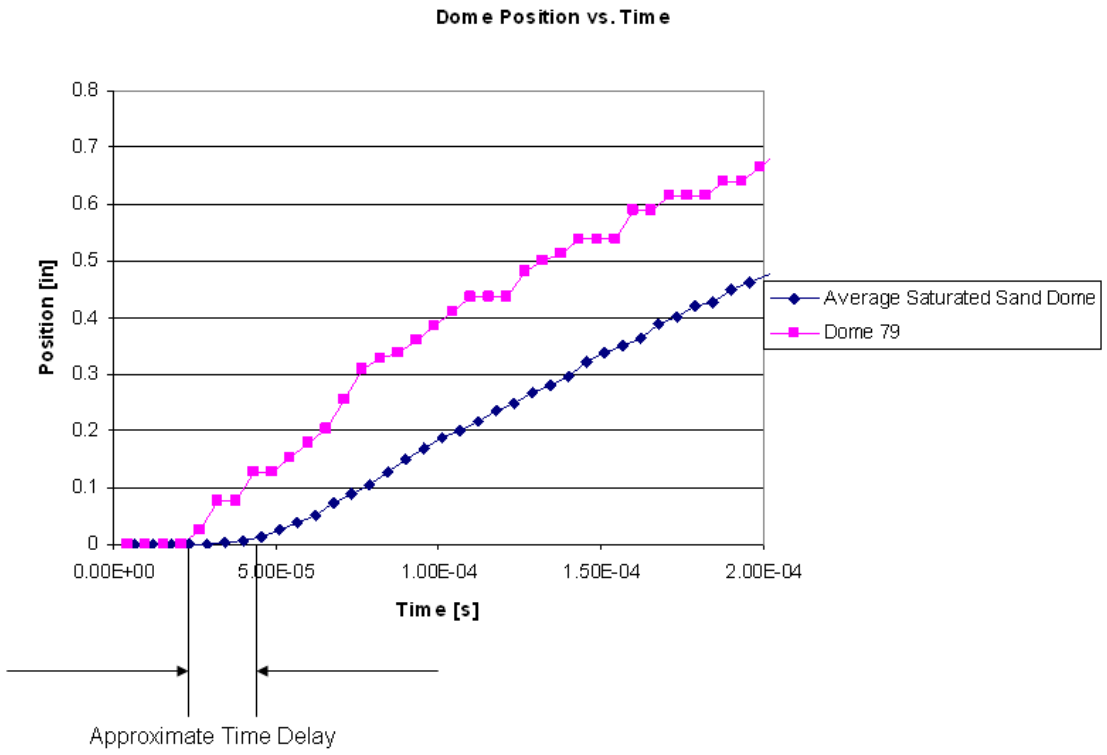

Figure 4.27: Position vs. Time Plot of a Suspicious Dome and the Average Dome

Clearly the dome from Test 79 in Figure 4.27 does not have the same x intercept as the other tests. This is an indication of error because all of the other domes are done with the same depth of burial and conditions unless otherwise noted (the main exceptions being the moist and tests, coarse sand and surfactant tests). The resulting data for Test 79 are shifted by the inclusion of zeroes to ensure that the data are consistent to the many previous tests that have used the exact same setup. The shifted data is then plotted with the rest for verification in Figure 4.28.

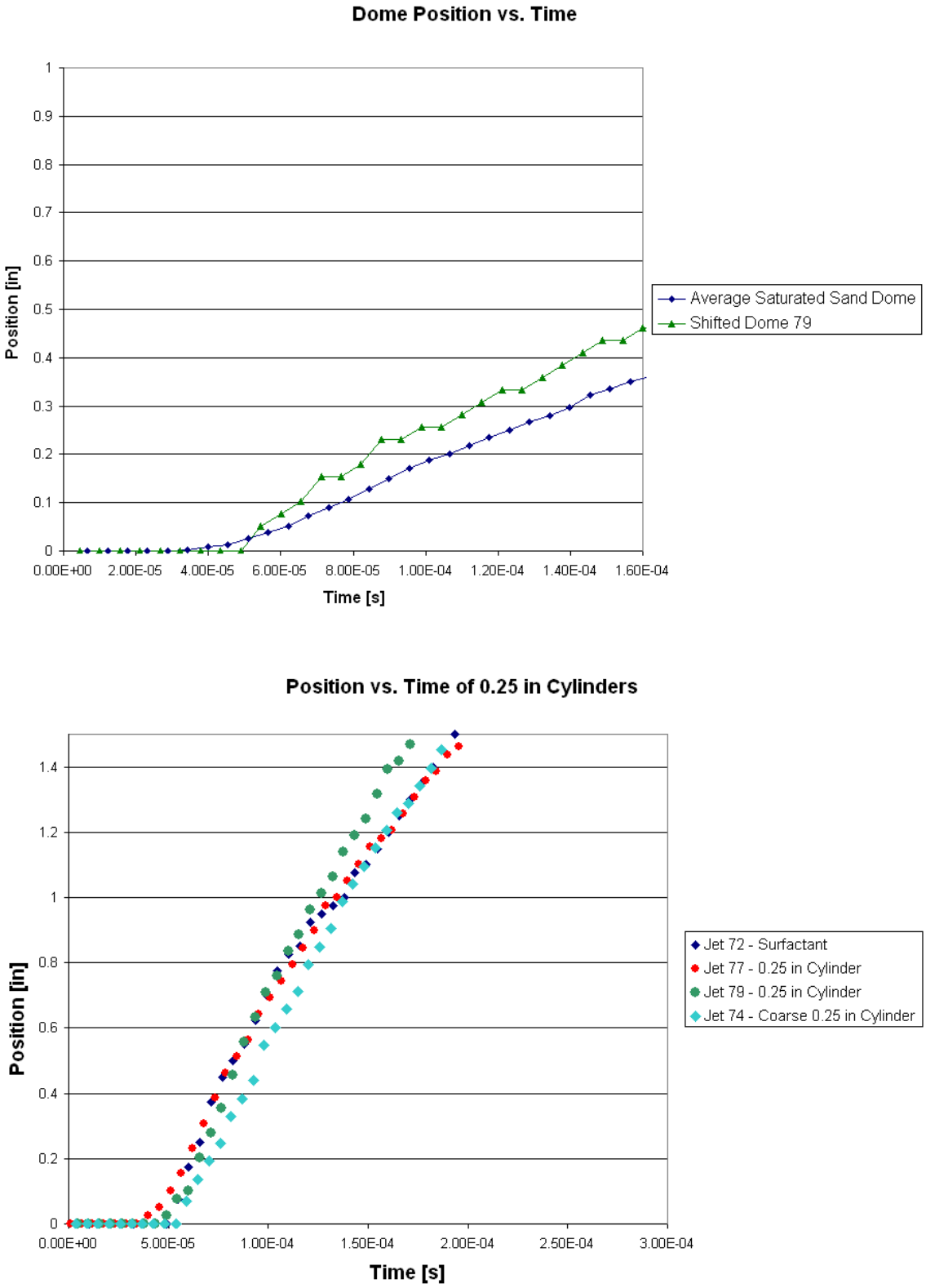

Figure 4.28: Example of Corrected Dome and Jet Position vs. Time Plots

All of the comparisons are done using the shifted jet and dome data. Data shift corrections were only used in Tests 79 and 58.

Chapter 5: Conclusions

The results from the tests demonstrate that the velocity and overall behavior of the jet is very much dependent on the shape and depth of the surface imperfection. In all cases other than the 0.125 in diameter imperfections, the cylinder shapes created the fastest jets. The 0.25 in cylinders pressed to 0.125 in produced velocities that are 200% of cone jet velocities and 300% of hemisphere jet velocities. The largest difference was between the 0.5 in diameter hemispheres and cylinders, which produced an increase in velocity from 3872 to 15393 in/s. The cylindrical imperfection produces a surface area above the charge that has a lower effective depth of burial. The hemispheres and cones in theory only fully reduce the depth of burial at a single point above the charge. The reduction in depth of burial reduces the distance the shockwave has to travel and increases the velocity of the jet. The curvature of the hemispheres and the slope of the cone do not provide a surface with a normal that is parallel to the direction of the shockwave. Additionally they do not displace as much volume as the cylinder imperfections per radius. Both of these factors contribute to lower jet velocities from the cones and hemispheres than the equivalent diameter cylinder.

The velocity vs. imperfection diameter trend reversed in the case of the hemispheres and the cones. This is because of the uncharacteristically high velocity values of the 0.125 in hemispheres and the low velocities for the 0.125 in cones. The small size of the 0.125 in diameter imperfections makes them more comparable in size to the natural or unintentional surface imperfections. The 0.5 in and 0.25 in imperfections tend to be more

consistent in their trends and produce velocities that are more similar to one another. This is evident in the case of cylinders and hemispheres especially.

Next to the depth of burial of the charge, the distance from the charge to the bottom surface of the imperfection is the most important factor in determining jet velocity. The velocities when this distance is kept constant using cylinder imperfections are all with 10% of one another. The only pieces of evidence opposing this idea are the 0.125 in diameter hemispheres which produce jets with the fastest velocities out of all of the tests conducted at the 1.19in DOB. However, their velocity and density dissipated quickly albeit after hitting the hypothetical target. They also exemplify the amorphous shape of the jets and offer insight into how pressures can be different in very small distances on the surface of a target.

The investigations into the effects of coarse grain sand and surfactant show results that do not heavily affect the dome and jet behavior and velocities. The Coarse Grain Series data trends are inconsistent while the surfactant only succeeds in causing more spray from the explosion. Finally, the Moist Sand Tests demonstrate that the moisture level in the sand is critical to the velocity of the dome and the very existence to the jet.

The different imperfection depths, diameters and shapes all produced insight into the peak velocities of the jets. One should consider spatial and time dependent fingers on the jet as well as natural and intentional surface imperfections because they can provide large differences in velocity, and therefore pressure on a target.

Chapter 6: Areas of Further Exploration

The work in this thesis explores avenues by which the jet and explosion domes are affected. Despite the variables that are tested, many new questions arise. The issue of why the 0.125 in hemisphere jets has such high initial velocities should be investigated. The Cylinder Imperfection Tests with Constant Depth to Diameter Ratio and the Hemisphere Imperfection Tests with 1.19in DOB should be supplemented with additional tests to gather more information on imperfection collapse, as well as, the difference between the shockwave physics in the hemisphere vs. the cylinder and the effects on the jet. Further analysis needs be done to investigate why the trend in velocity with respect to the size of the imperfection is reversed from the case of the cones to the case of the hemispheres. Additionally, tests need to be conducted to find DOB's that are thresholds to when one will or will not observe a clear jet.

The main mechanism for obtaining data was to track the tip of the jet and dome through time. There are other ways to characterize the jet that could offer more information than simply a tip position. For instance, the jets could be calculated as a characteristic width, which is the jet's area divided by its height. A parameter like this could provide more information about the jet and is another variable that could indicate trends in behavior. One could also use additional cameras to study the jet in three dimensions to truly capture its shape.

The work in this thesis has a bias toward experimental work due to the resources of the Dynamic Effects Lab which include the Phantom high speed camera along with its

software, and a license for and access to explosive materials. Analytical work along with computational simulations would contribute greatly to the understanding of the phenomena explored in this thesis. The image tracking process could benefit from modern image processing, but this too has limitations, mainly from the resolution limitations at the 180,000 fps frame rate. Improvements to the camera in the form of increased spatial or temporal resolution could increase the precision of all of the results.

Appendices

Appendix A: List of Tests

Test No.	Imperfection Diameter [in]	DOB [in]	Charge Mass [g]	Depth/Diameter	Jet Velocity [in/s]	Dome Velocity [in/s]
45	0.5 Hemisphere	1.19	0.5	0.5	3872	3545
46	0.25 Hemisphere	1.19	0.5	0.5	6488	3027
47	0.125 Hemisphere	1.19	0.5	0.5	15373	3742
48	0.125 Hemisphere	0.69	0.5	0.5	10225	10199
49	0.25 Hemisphere	0.69	0.5	0.5	7739	8567
50	0.5 Hemisphere	0.69	0.5	0.5	12409	NA
51	0.125 Hemisphere	1.19	0.5	0.5	15253	2827
52	0.25 Hemisphere	0.69	0.5	0.5	12632	6725
53	0.25 Hemisphere	0.69	0.5	0.5	14294	11097
54	0.5 Hemisphere	1.19	0.5	0.5	7204	3918
55	0.25 Hemisphere	1.19	0.5	0.5	4226	2782
56	0.25 Cylinder	1.19	0.5	1	6590	3633
57	0.5 Cylinder	1.19	0.5	0.5	10006	5177
58	0.25 Cylinder	1.19	0.5	0.5	6901	3817
59	0.125 Cylinder	1.19	0.5	0.5	10192	3312
60	0.125 Cylinder	1.19	0.5	2	15241	NA
61	0.25 Cylinder	1.19	0.5	1	13975	NA
62	0.25 Hemisphere	1.19	0.5	0.5	8041	3140
63	0.5 Cylinder	1.19	0.5	0.5	14594	4488
64	0	1.19	0.5	NA	NA	3250
65	0.25 Cylinder	1.19	0.5	1.5	16351	NA
66	0.25 Cylinder	1.19	0.5	0.5	7173	3966
67	0.25 Cylinder	1.19	0.5	0.5	NA	3989
68	0.5 Cylinder	1.19	0.5	NA	NA	4148
69	0.125 Cylinder	1.19	0.5	NA	NA	3771
70	0	1.19	0.5	NA	NA	3017
71	0	1.19	0.5	NA	NA	3046
72	0.25 Cylinder	1.19	0.5	0.5	10259	3421
73	0	1.19	0.5	NA	NA	2964
74	0.25 Cylinder	1.19	0.5	0.5	12243	3233
75	0.125 Cylinder	1.19	0.5	0.5	8125	3084
76	0.5 Cylinder	1.19	0.5	0.5	10836	4288
77	0.25 Cylinder	1.19	0.5	0.5	9879	3442
78	0.5 Cylinder	1.19	0.5	0.5	15393	4024
79	0.25 Cylinder	1.19	0.5	0.5	12181	3154

Initial Velocity Data from Moist Sand Tests

Test Number	Cylinder Diameter [in]	DOB [in]	Mass [g]	Depth/Diameter	Sand Density[g/cc]	Initial Dome Velocity [in/s]
67	0.25	1.19	0.5	0.5	1.96	2671
68	NA	1.19	0.5	NA	1.66	1780
69	NA	1.19	0.5	NA	1.65	1402
70	NA	1.19	0.5	NA	1.90	2535

Appendix B: Test Graphs and Representative Photos

Note: all images from .cine files are taken 139.86μs after camera trigger for comparison purposes.

Test 45

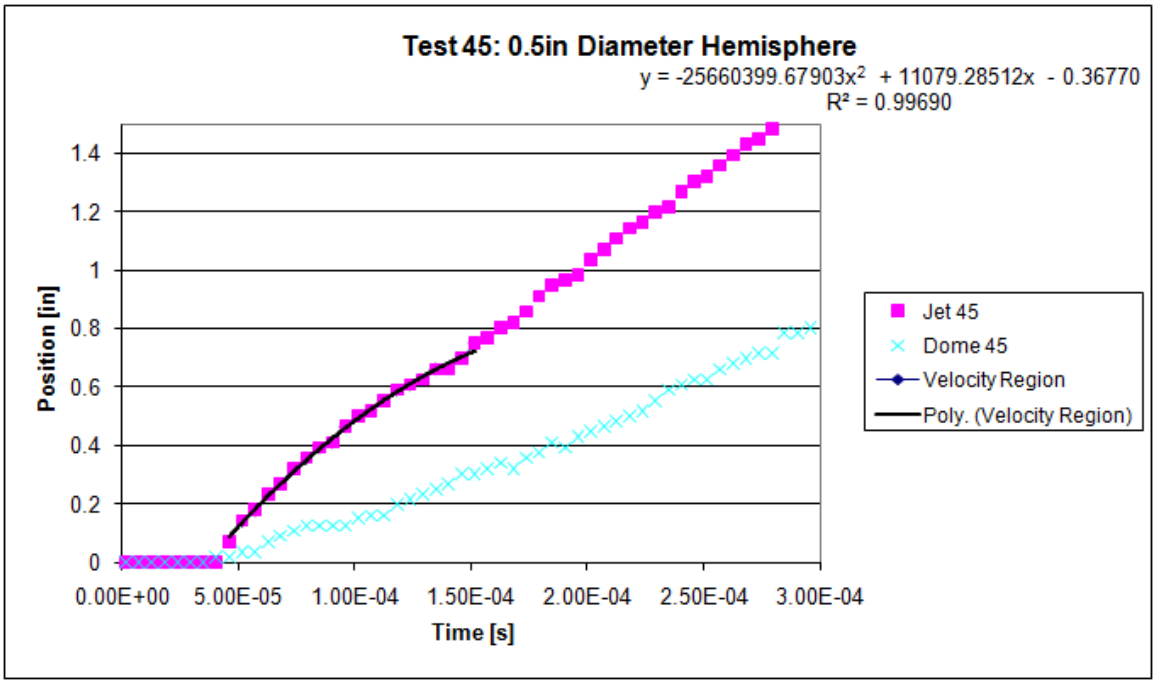

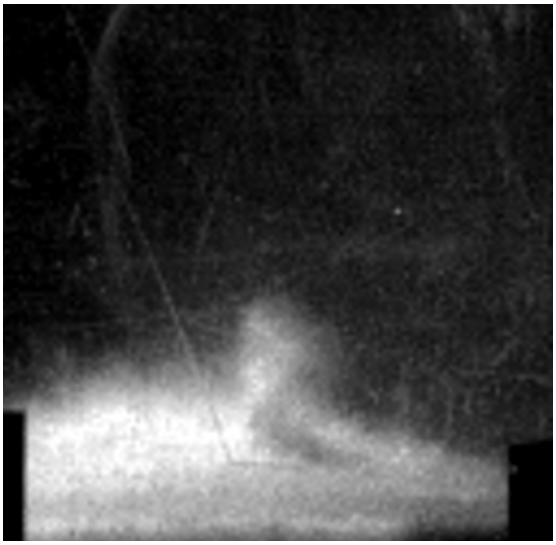

Test 46

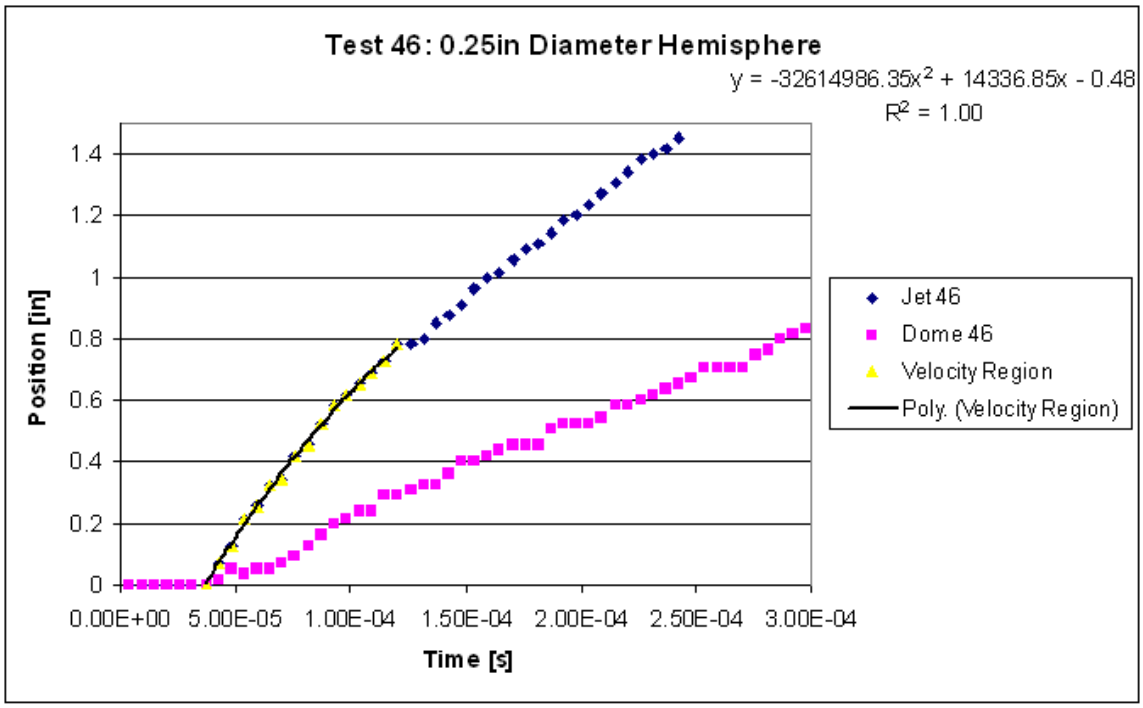
Test 46: 0.25in Diameter Hemisphere
y = -32614986.35x² + 14336.85x - 0.48
R² = 1.00
Position [in]
1.4
1.2
1
0.8
0.6
0.4
0.2
0
0.00E+00
5.00E-05
1.00E-04
1.50E-04
2.00E-04
2.50E-04
3.00E-04
Time [s]
Jet 46
Dome 46
Velocity Region
Poly. (Velocity Region)

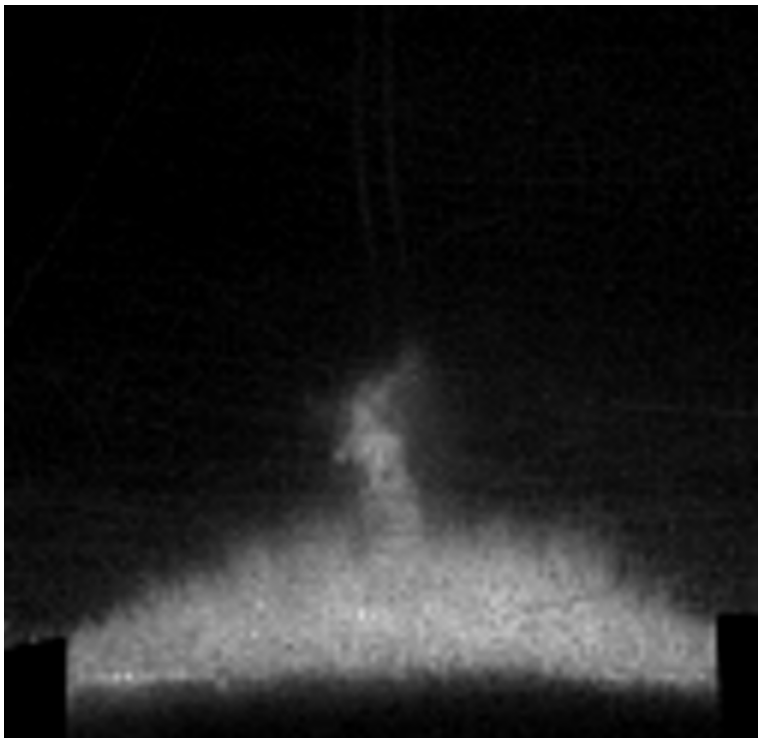

Test 47

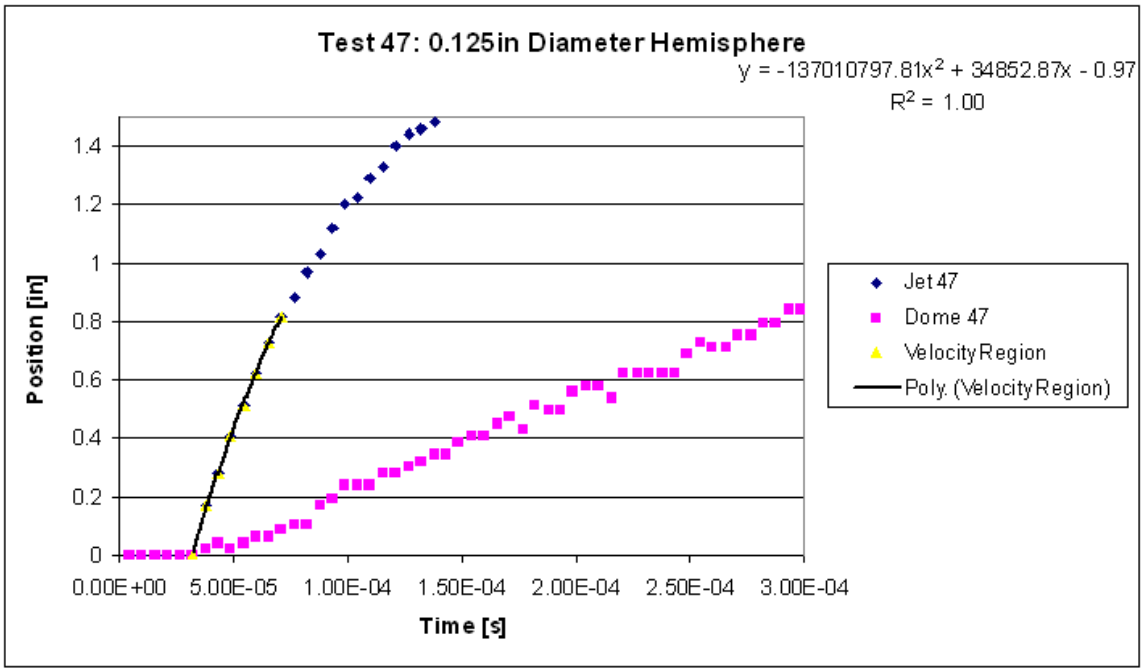
Test 47: 0.125in Diameter Hemisphere
y = -137010797.81x² + 34852.87x - 0.97
R² = 1.00
Position [in]
Time [s]
0
0.2
0.4
0.6
0.8
1
1.2
1.4
0.00E+00
5.00E-05
1.00E-04
1.50E-04
2.00E-04
2.50E-04
3.00E-04
Jet 47
Dome 47
Velocity Region
Poly. (Velocity Region)

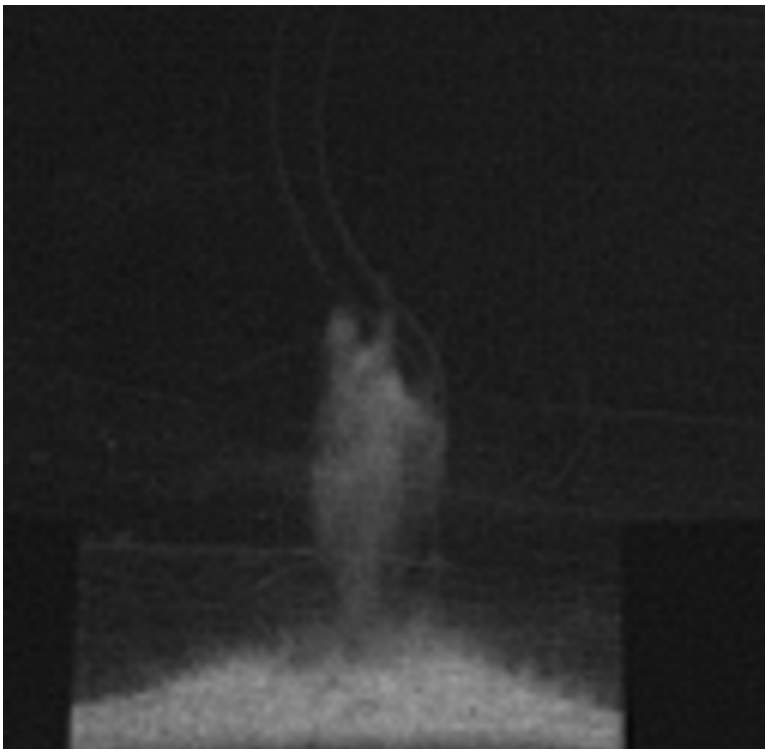

Test 48

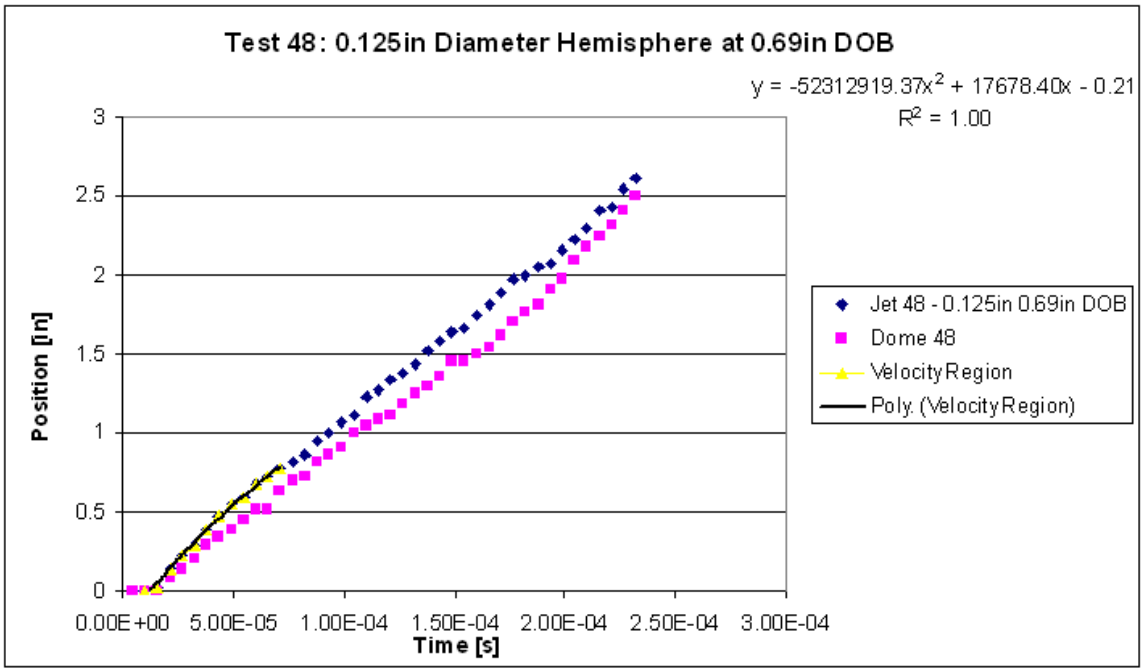
Test 48: 0.125in Diameter Hemisphere at 0.69in DOB
y = -52312919.37x² + 17678.40x - 0.21
R² = 1.00
Position [in]
Time [s]
0
0.5
1
1.5
2
2.5
3
0.00E+00
5.00E-05
1.00E-04
1.50E-04
2.00E-04
2.50E-04
3.00E-04
Jet 48 - 0.125in 0.69in DOB
Dome 48
Velocity Region
Poly. (Velocity Region)

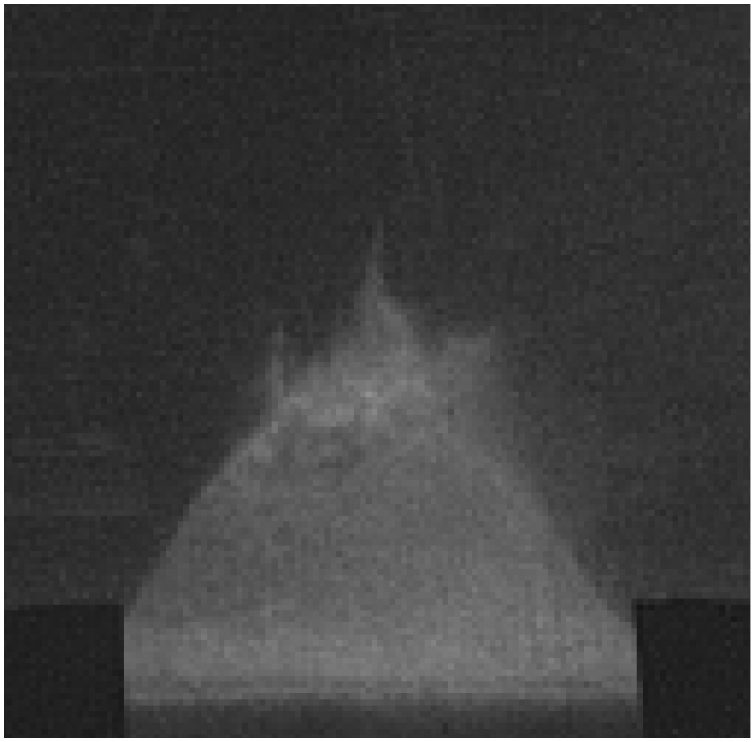

Test 49

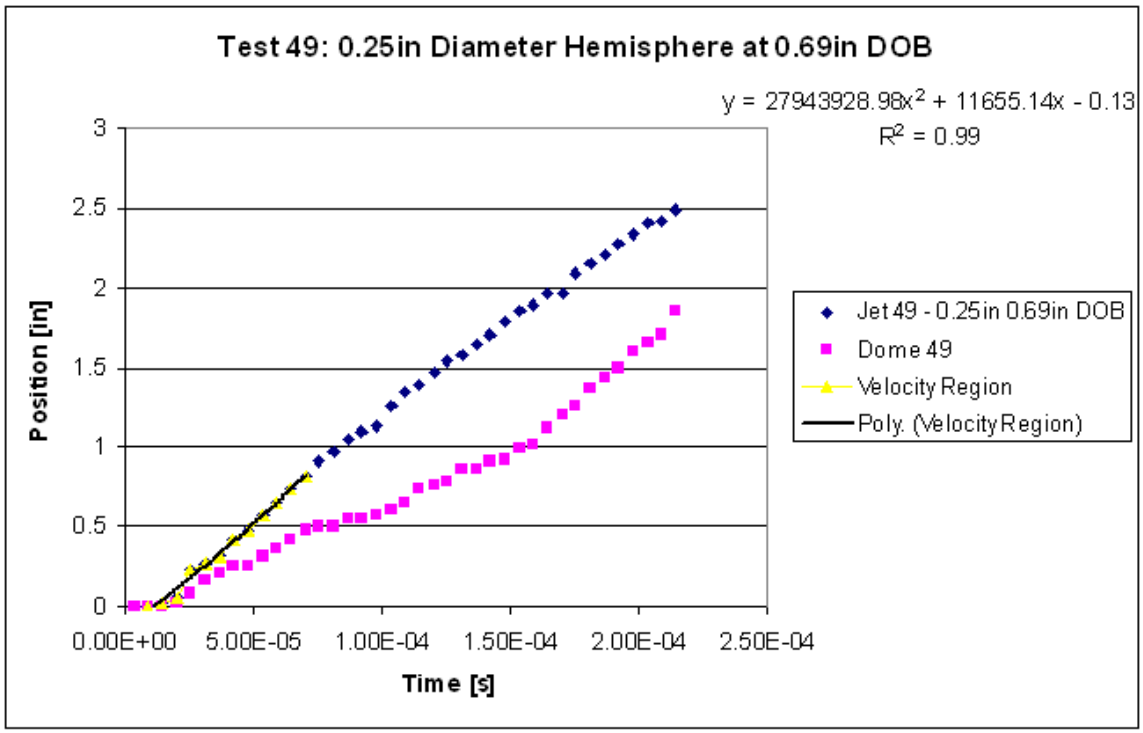
Test 49: 0.25in Diameter Hemisphere at 0.69in DOB
y = 27943928.98x2 + 11655.14x - 0.13
R2 = 0.99
Position [in]
Time [s]
0
0.5
1
1.5
2
2.5
3
0.00E+00
5.00E-05
1.00E-04
1.50E-04
2.00E-04
2.50E-04
Jet 49 - 0.25in 0.69in DOB
Dome 49
Velocity Region
Poly. (Velocity Region)

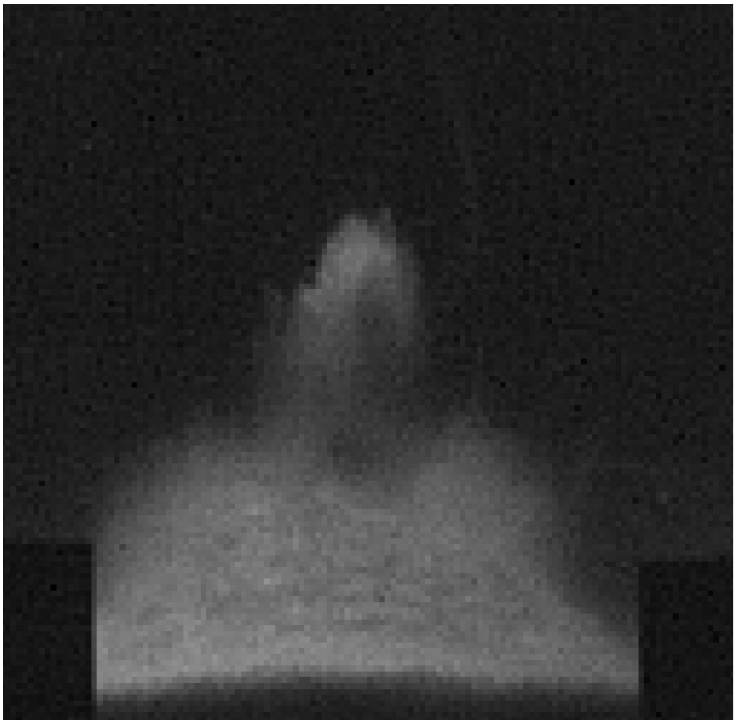

Test 50

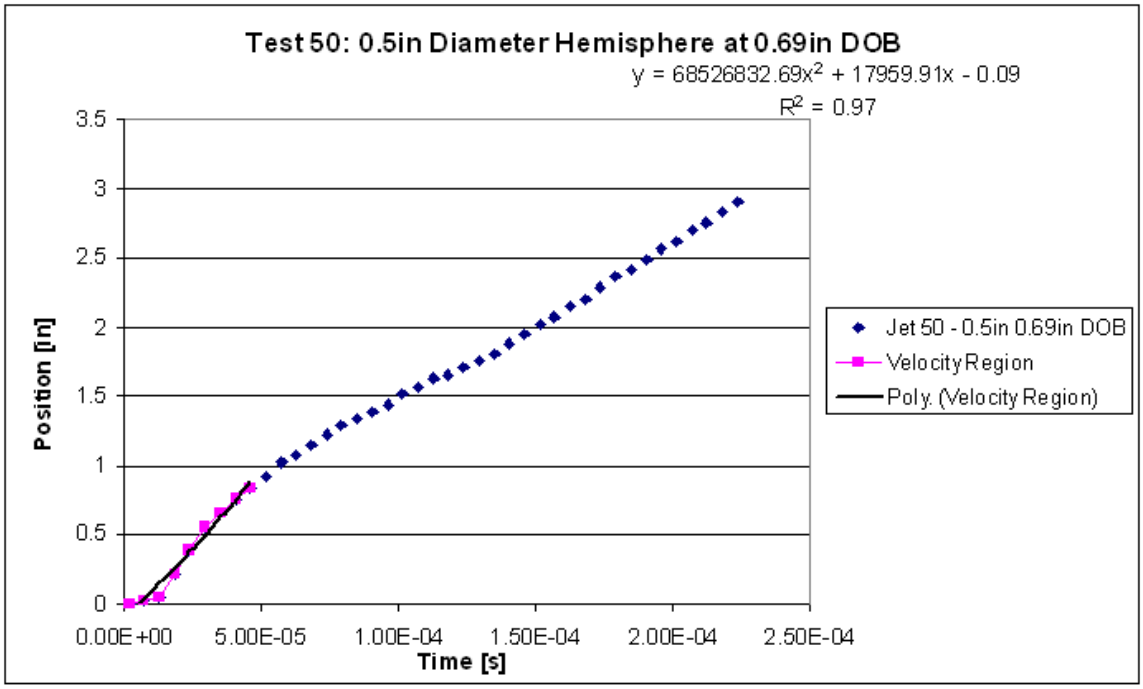
Test 50: 0.5in Diameter Hemisphere at 0.69in DOB
y = 68526832.69x2 + 17959.91x - 0.09
R2 = 0.97
Position [in]
Time [s]
0
0.5
1
1.5
2
2.5
3
3.5
0.00E+00
5.00E-05
1.00E-04
1.50E-04
2.00E-04
2.50E-04
Jet 50 - 0.5in 0.69in DOB
Velocity Region
Poly. (Velocity Region)

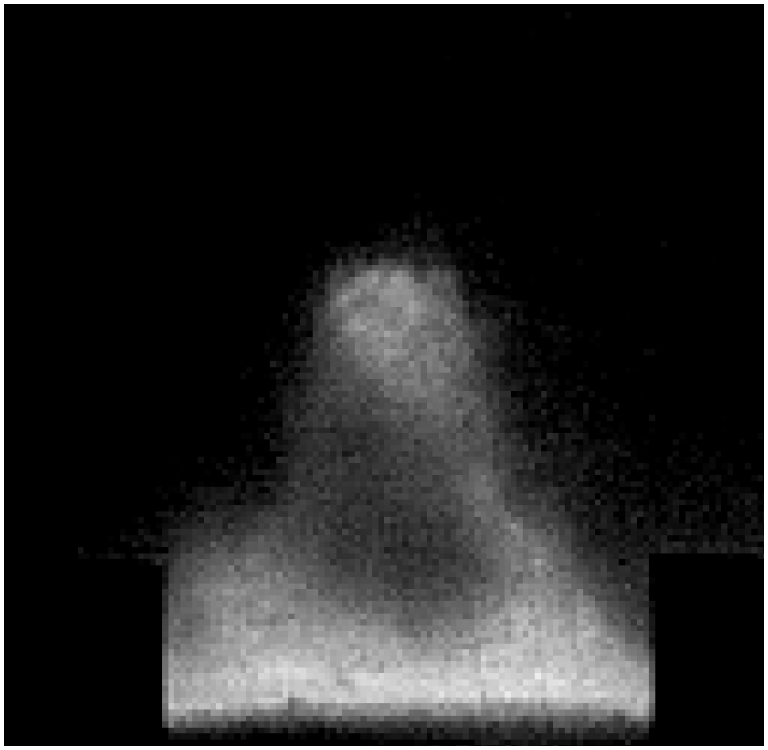

Test 51

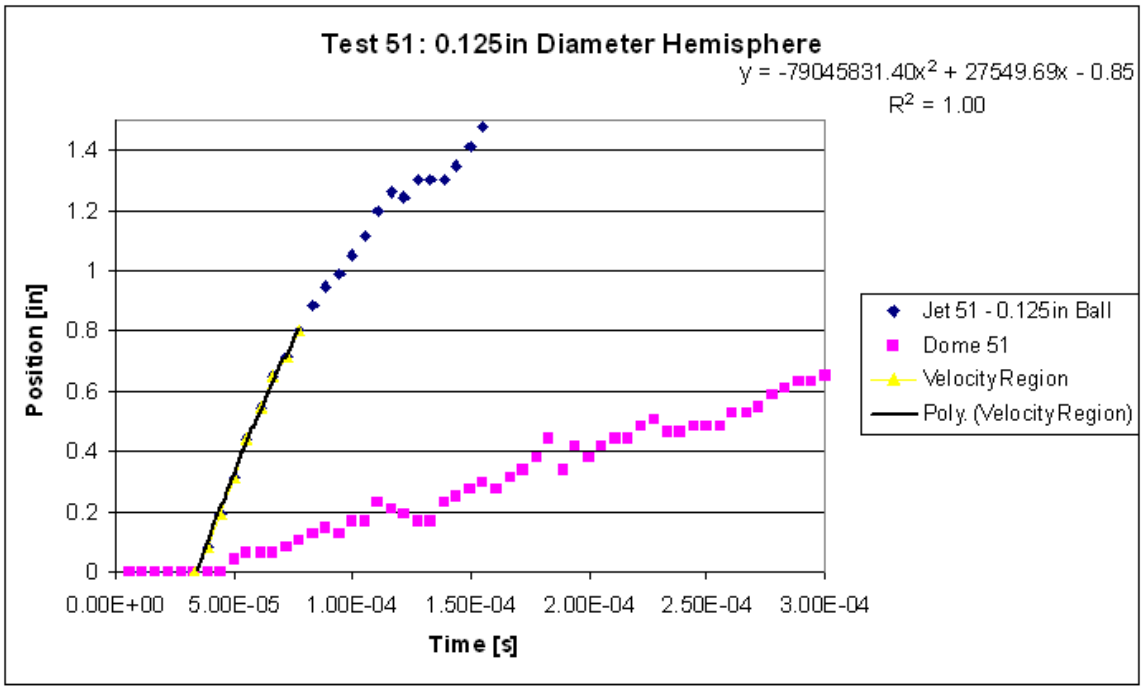
Test 51: 0.125in Diameter Hemisphere
y = -79045831.40x² + 27549.69x - 0.85
R² = 1.00
Position [in]
1.4
1.2
1
0.8
0.6
0.4
0.2
0
0.00E+00
5.00E-05
1.00E-04
1.50E-04
2.00E-04
2.50E-04
3.00E-04
Time [s]
Jet 51 - 0.125in Ball
Dome 51
Velocity Region
Poly. (Velocity Region)

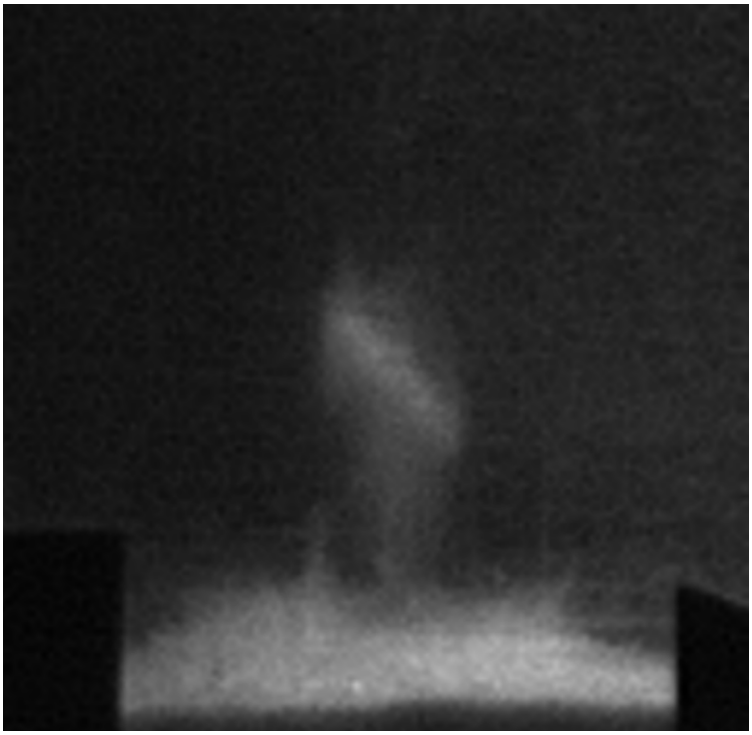

Test 52

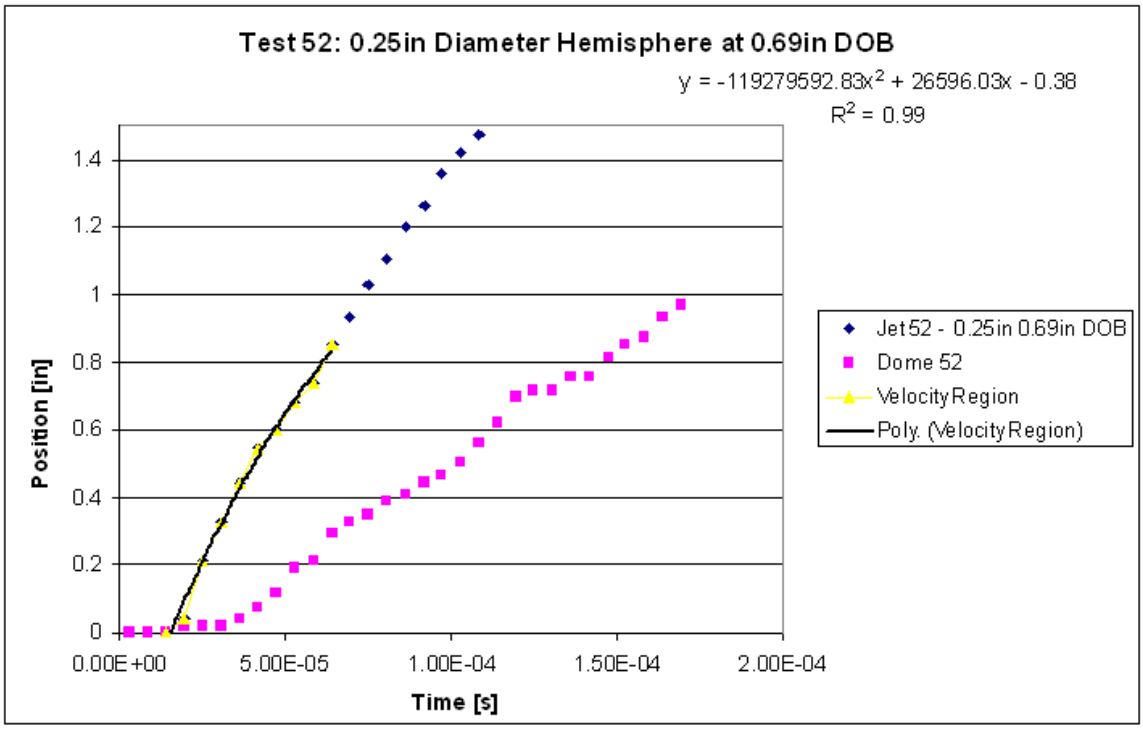
Test 52: 0.25in Diameter Hemisphere at 0.69in DOB
y = -119279592.83x² + 26596.03x - 0.38
R² = 0.99
Position [in]
Time [s]
0
0.2
0.4
0.6
0.8
1
1.2
1.4
0.00E+00
5.00E-05
1.00E-04
1.50E-04
2.00E-04
Jet 52 - 0.25in 0.69in DOB
Dome 52
Velocity Region
Poly. (Velocity Region)

Test 53

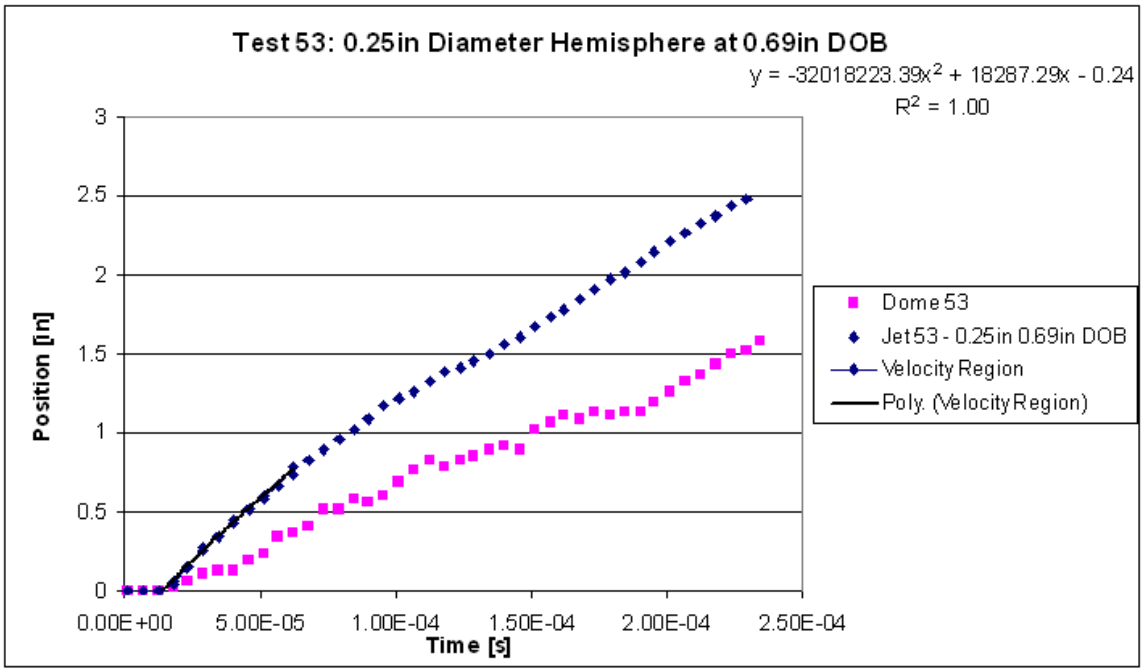
Test 53: 0.25in Diameter Hemisphere at 0.69in DOB
y = -32018223.39x2 + 18287.29x - 0.24
R2 = 1.00
Position [in]
Time [s]
0
0.5
1
1.5
2
2.5
3
0.00E+00
5.00E-05
1.00E-04
1.50E-04
2.00E-04
2.50E-04
Dome 53
Jet 53 - 0.25in 0.69in DOB
Velocity Region
Poly. (Velocity Region)

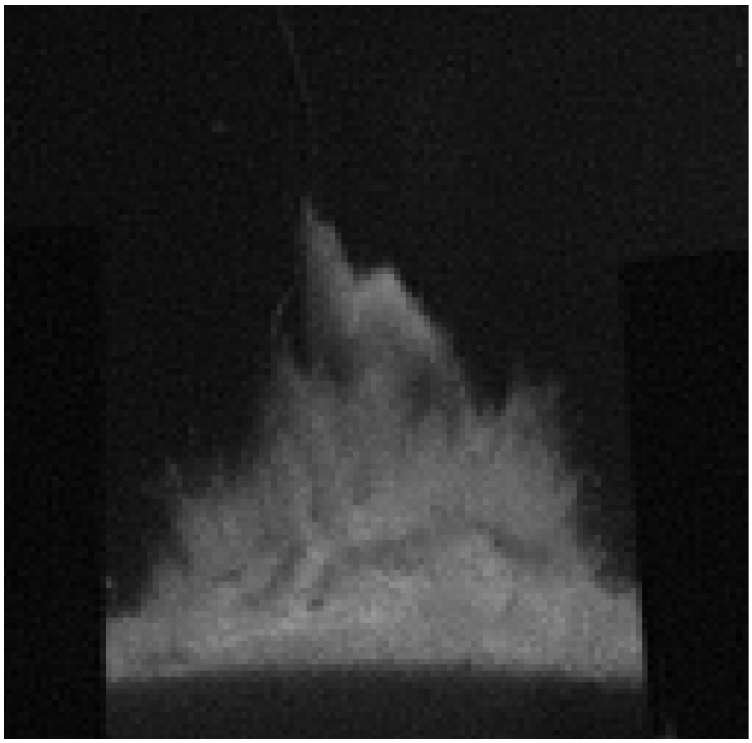

Test 54

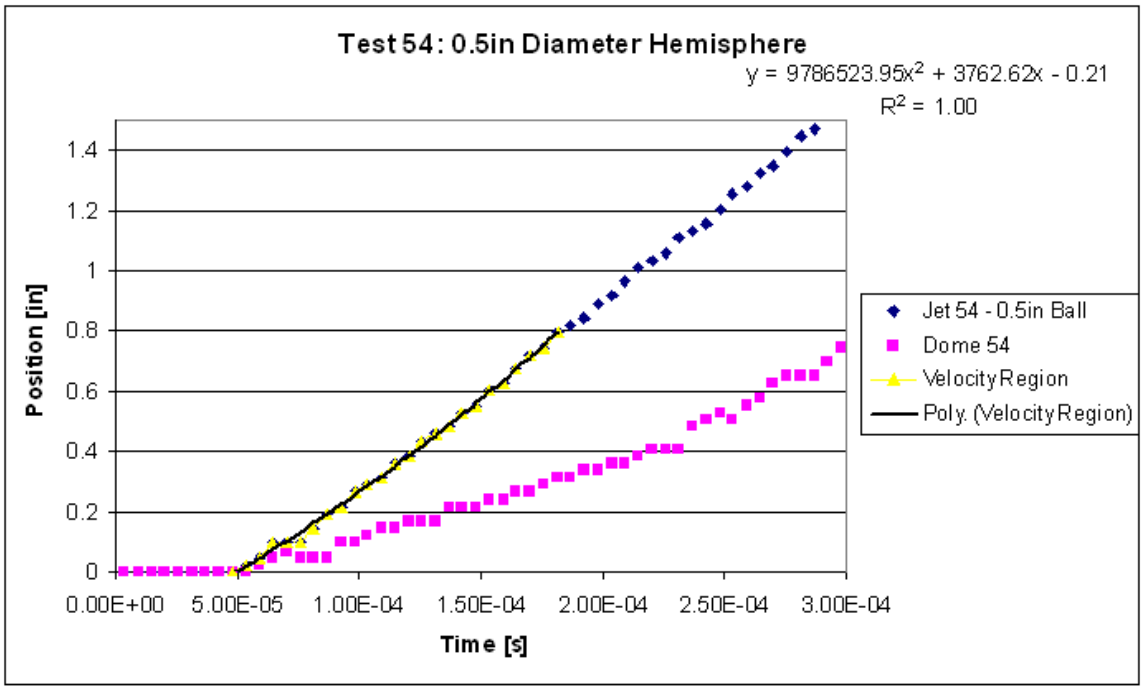
Test 54: 0.5in Diameter Hemisphere
y = 9786523.95x2 + 3762.62x - 0.21
R2 = 1.00
Position [in]
1.4
1.2
1
0.8
0.6
0.4
0.2
0
0.00E+00
5.00E-05
1.00E-04
1.50E-04
2.00E-04
2.50E-04
3.00E-04
Time [s]
Jet 54 - 0.5in Ball
Dome 54
Velocity Region
Poly. (Velocity Region)

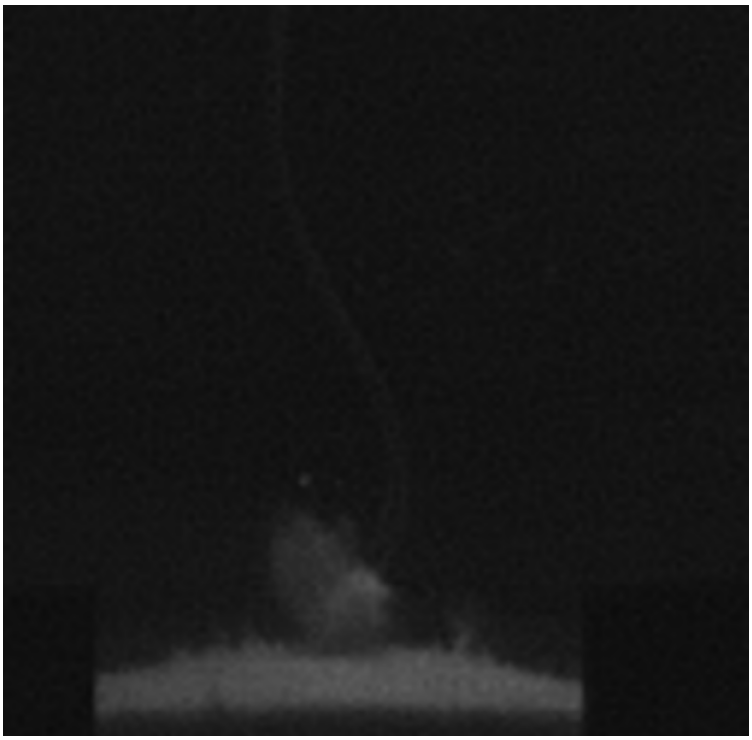

Test 55

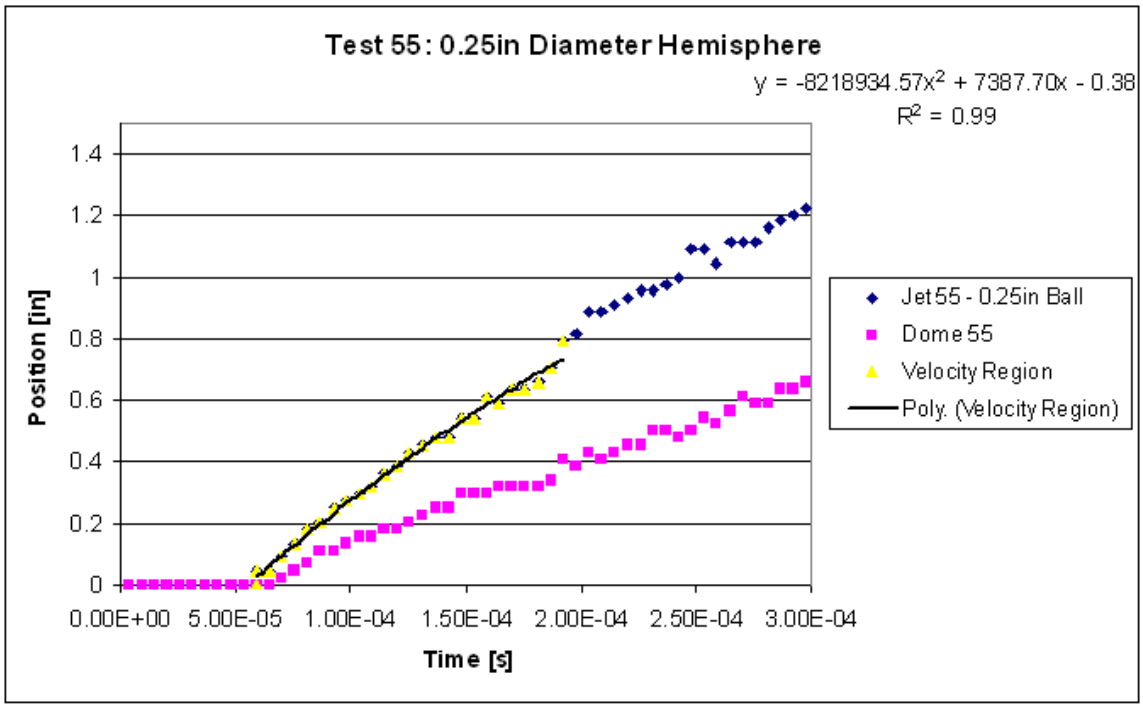
Test 55: 0.25in Diameter Hemisphere
y = -8218934.57x² + 7387.70x - 0.38
R² = 0.99
Position [in]
1.4
1.2
1
0.8
0.6
0.4
0.2
0
0.00E+00
5.00E-05
1.00E-04
1.50E-04
2.00E-04
2.50E-04
3.00E-04
Time [s]
Jet 55 - 0.25in Ball
Dome 55
Velocity Region
Poly. (Velocity Region)

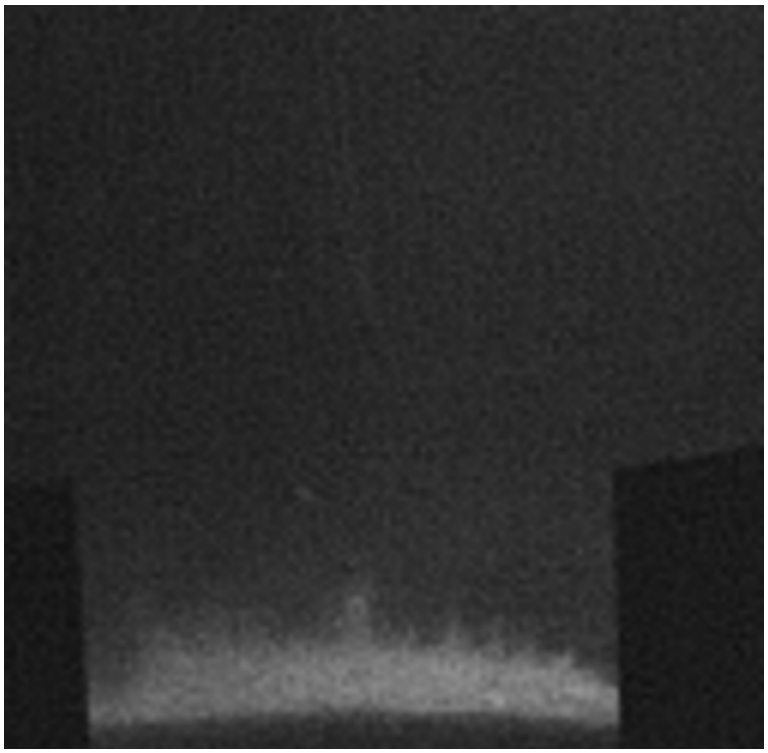

Test 56

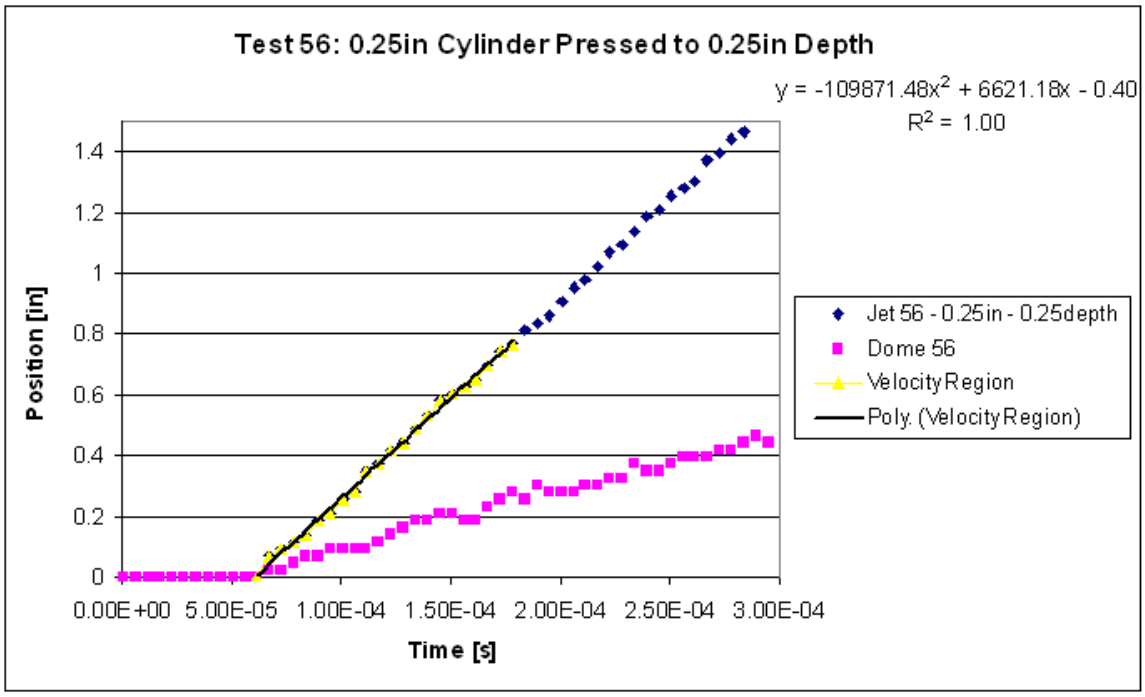
Test 56: 0.25in Cylinder Pressed to 0.25in Depth
y = -109871.48x2 + 6621.18x - 0.40
R2 = 1.00
Position [in]
1.4
1.2
1
0.8
0.6
0.4
0.2
0
0.00E+00
5.00E-05
1.00E-04
1.50E-04
2.00E-04
2.50E-04
3.00E-04
Time [s]
Jet 56 - 0.25in - 0.25depth
Dome 56
Velocity Region
Poly. (Velocity Region)

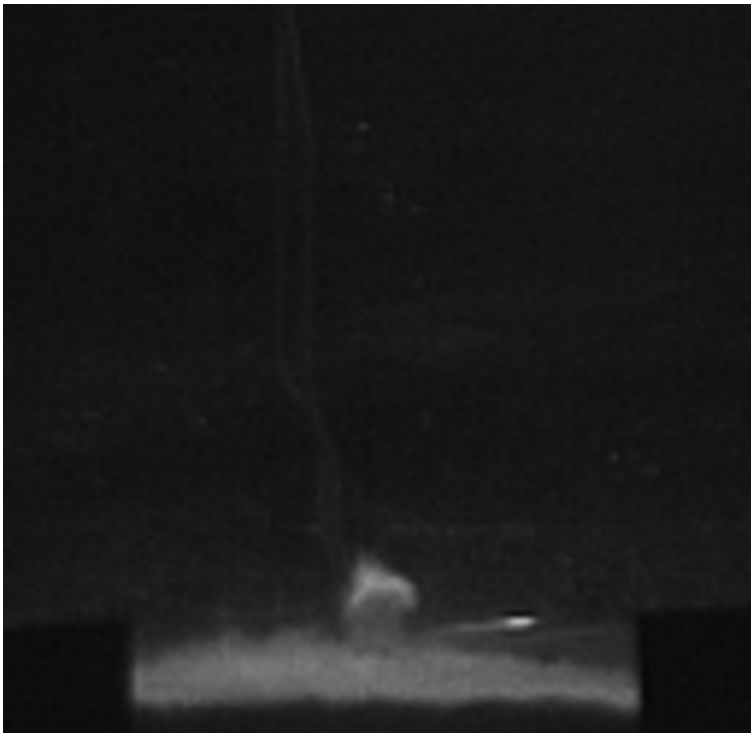

Test 57

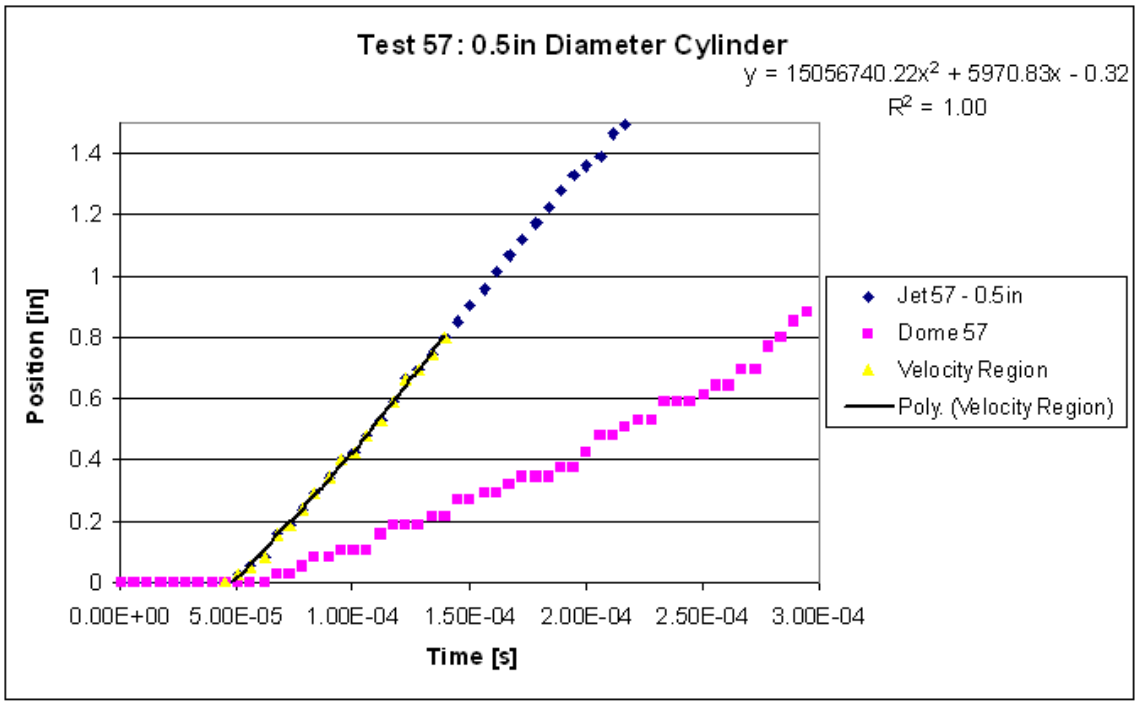
Test 57: 0.5in Diameter Cylinder
y = 15056740.22x2 + 5970.83x - 0.32
R2 = 1.00
Position [in]
1.4
1.2
1
0.8
0.6
0.4
0.2
0
0.00E+00
5.00E-05
1.00E-04
1.50E-04
2.00E-04
2.50E-04
3.00E-04
Time [s]
Jet 57 - 0.5in
Dome 57
Velocity Region
Poly. (Velocity Region)

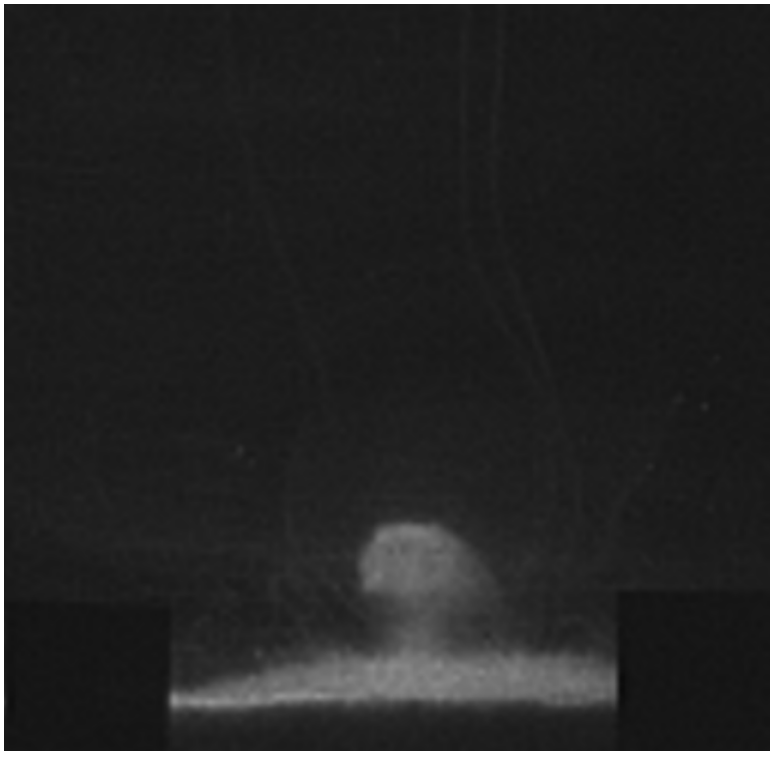

Test 58

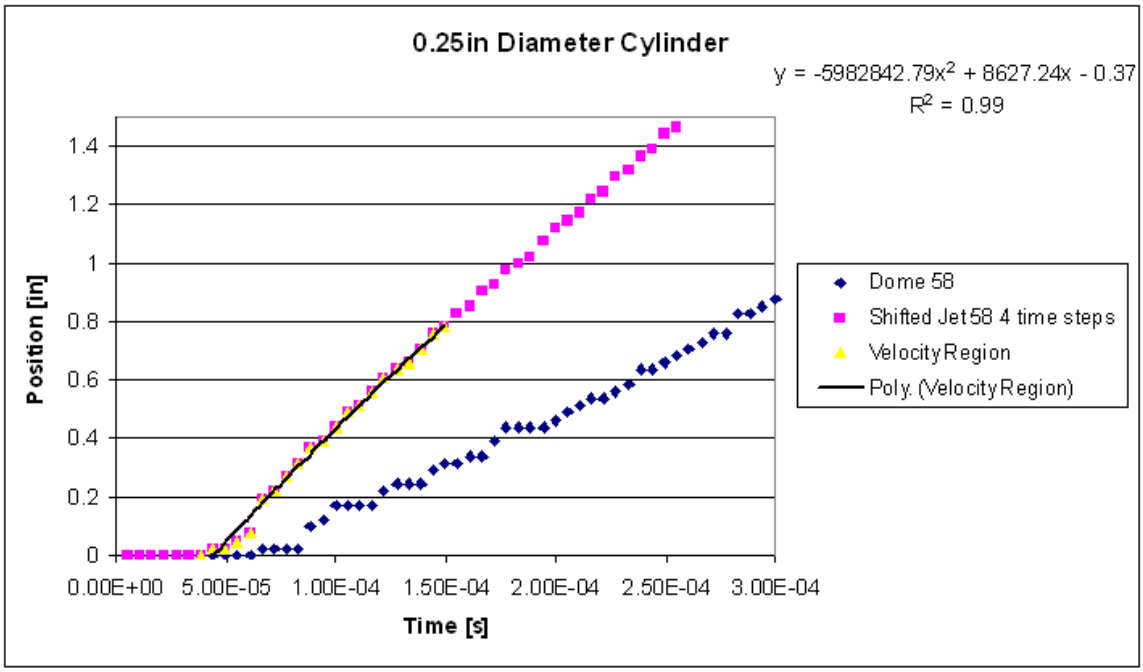
0.25in Diameter Cylinder
y = -5982842.79x2 + 8627.24x - 0.37
R2 = 0.99
Position [in]
1.4
1.2
1
0.8
0.6
0.4
0.2
0
0.00E+00
5.00E-05
1.00E-04
1.50E-04
2.00E-04
2.50E-04
3.00E-04
Time [s]
Dome 58
Shifted Jet 58 4 time steps
Velocity Region
Poly. (Velocity Region)

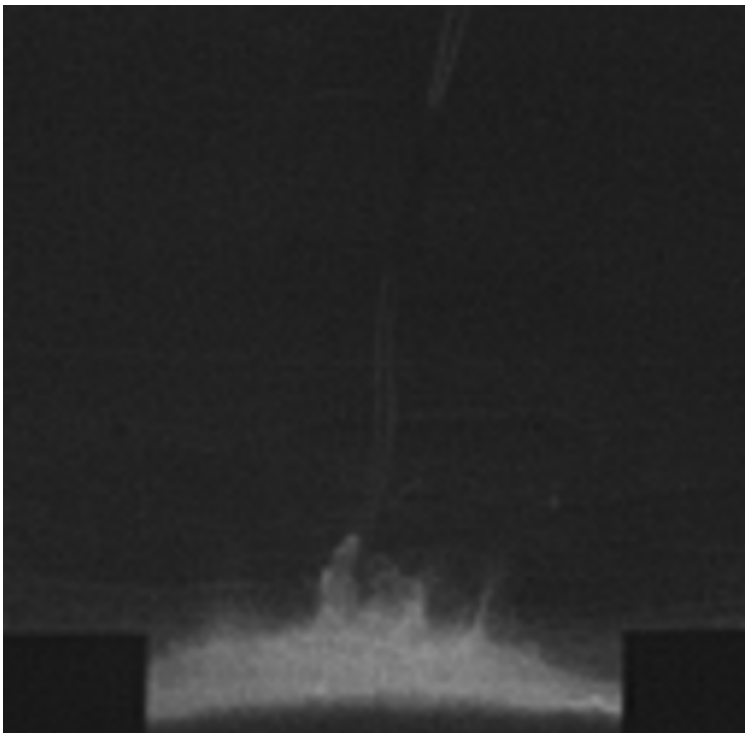

Test 59

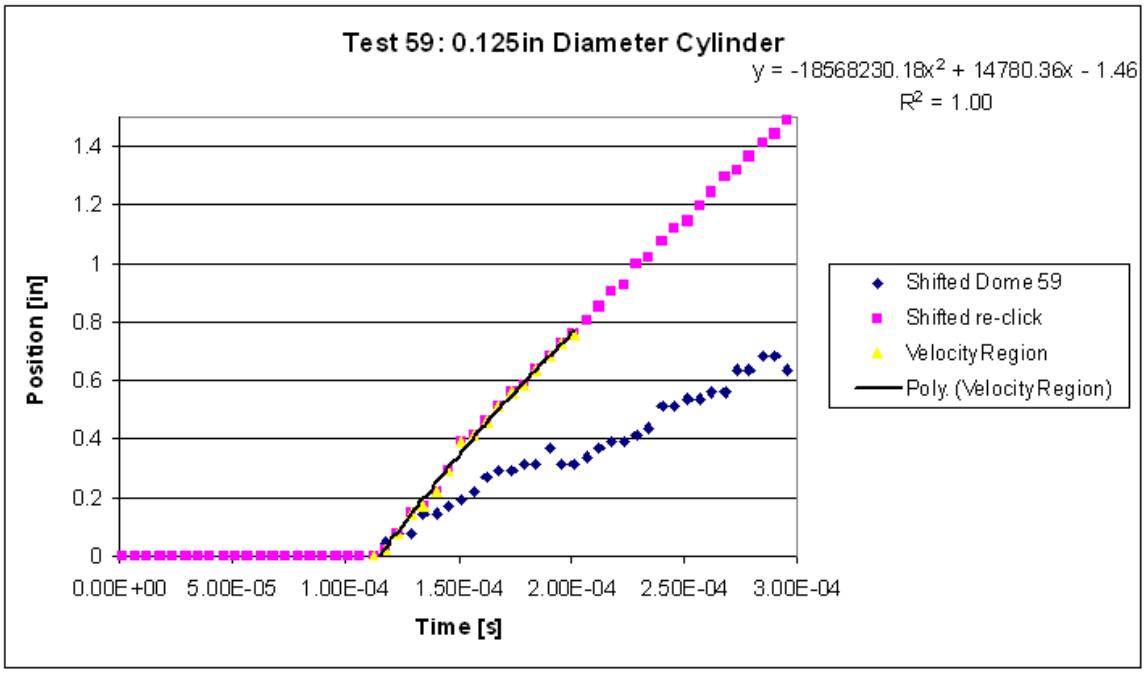
Test 59: 0.125in Diameter Cylinder
y = -18568230.18x2 + 14780.36x - 1.46
R2 = 1.00
Position [in]
1.4
1.2
1
0.8
0.6
0.4
0.2
0
0.00E+00
5.00E-05
1.00E-04
1.50E-04
2.00E-04
2.50E-04
3.00E-04
Time [s]
Shifted Dome 59
Shifted re-click
Velocity Region
Poly. (Velocity Region)

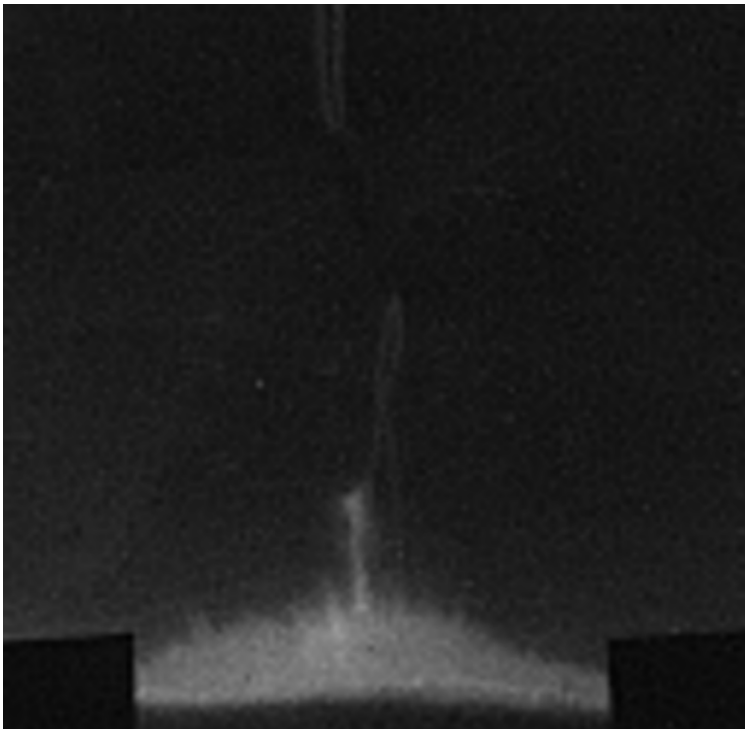

Test 60

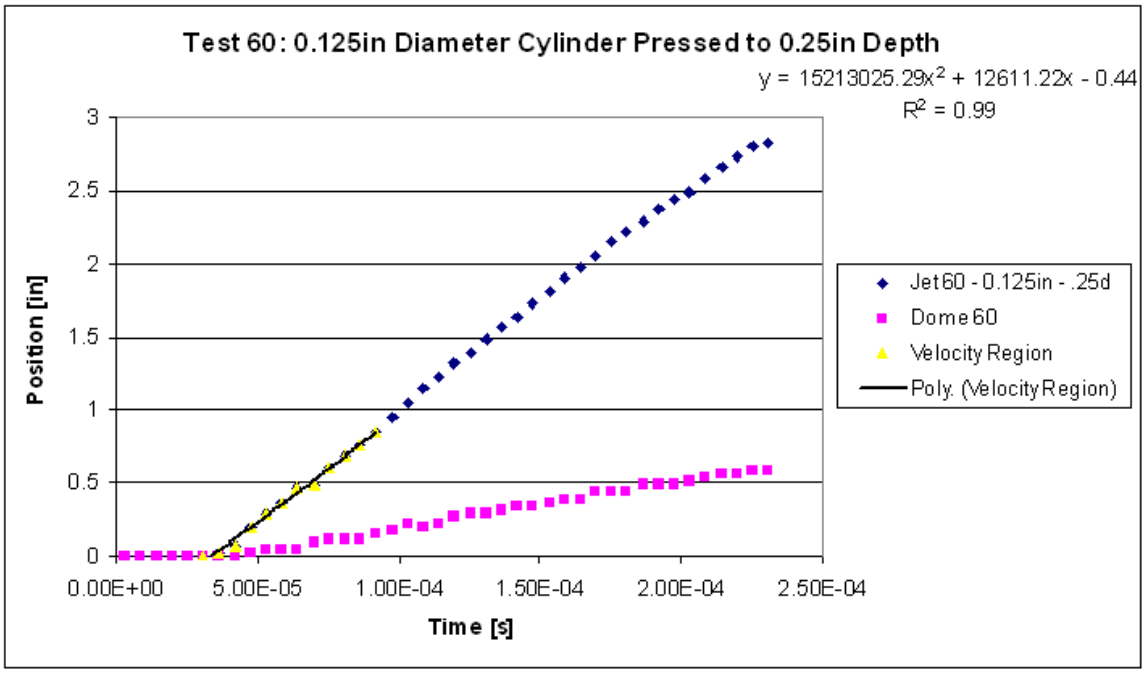
Test 60: 0.125in Diameter Cylinder Pressed to 0.25in Depth
y = 15213025.29x2 + 12611.22x - 0.44
R2 = 0.99
Position [in]
Time [s]
0
0.5
1
1.5
2
2.5
3
0.00E+00
5.00E-05
1.00E-04
1.50E-04
2.00E-04
2.50E-04
Jet60 - 0.125in - .25d
Dome60
Velocity Region
Poly. (Velocity Region)

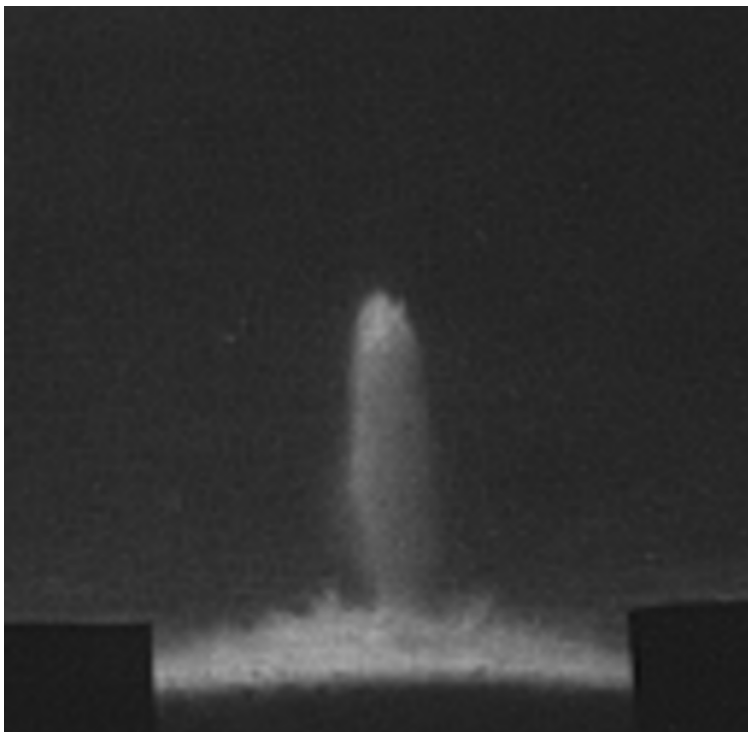

Test 61

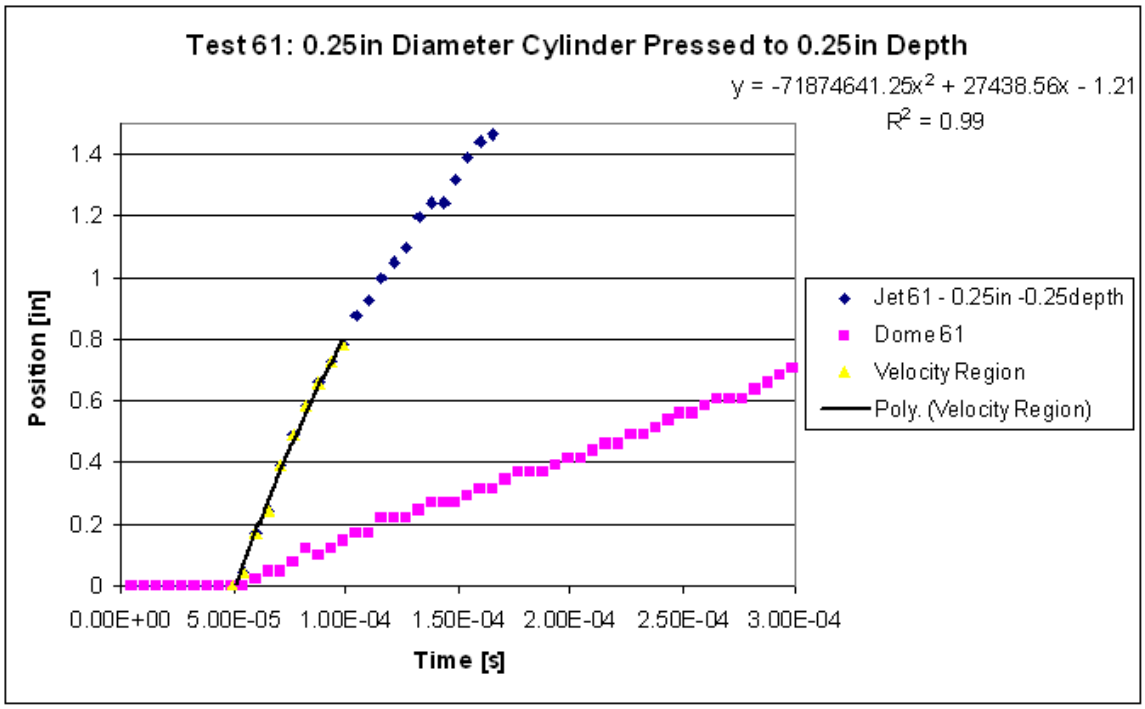
Test 61: 0.25in Diameter Cylinder Pressed to 0.25in Depth
y = -71874641.25x² + 27438.56x - 1.21
R² = 0.99
Position [in]
1.4
1.2
1
0.8
0.6
0.4
0.2
0
0.00E+00
5.00E-05
1.00E-04
1.50E-04
2.00E-04
2.50E-04
3.00E-04
Time [s]
Jet 61 - 0.25in -0.25depth
Dome 61
Velocity Region
Poly. (Velocity Region)

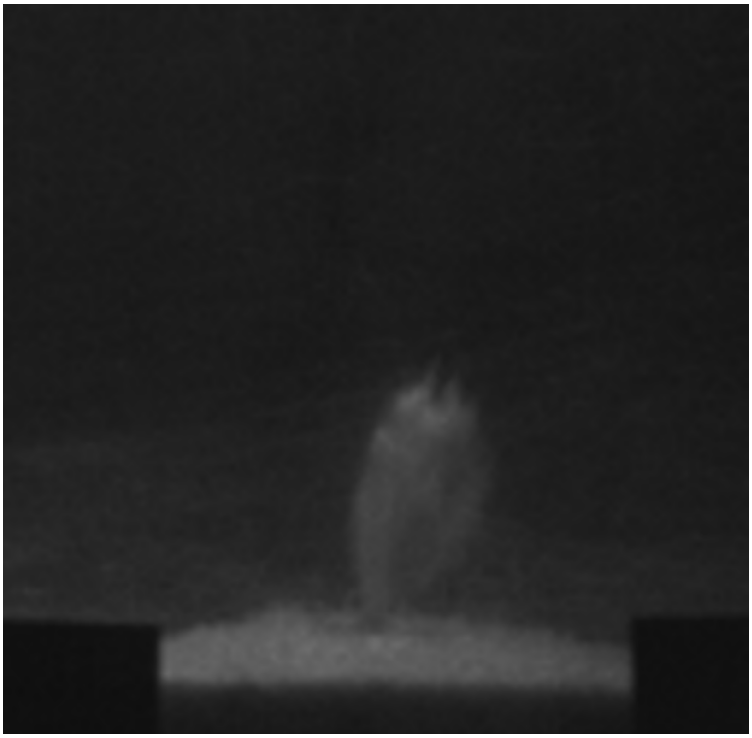

Test 62

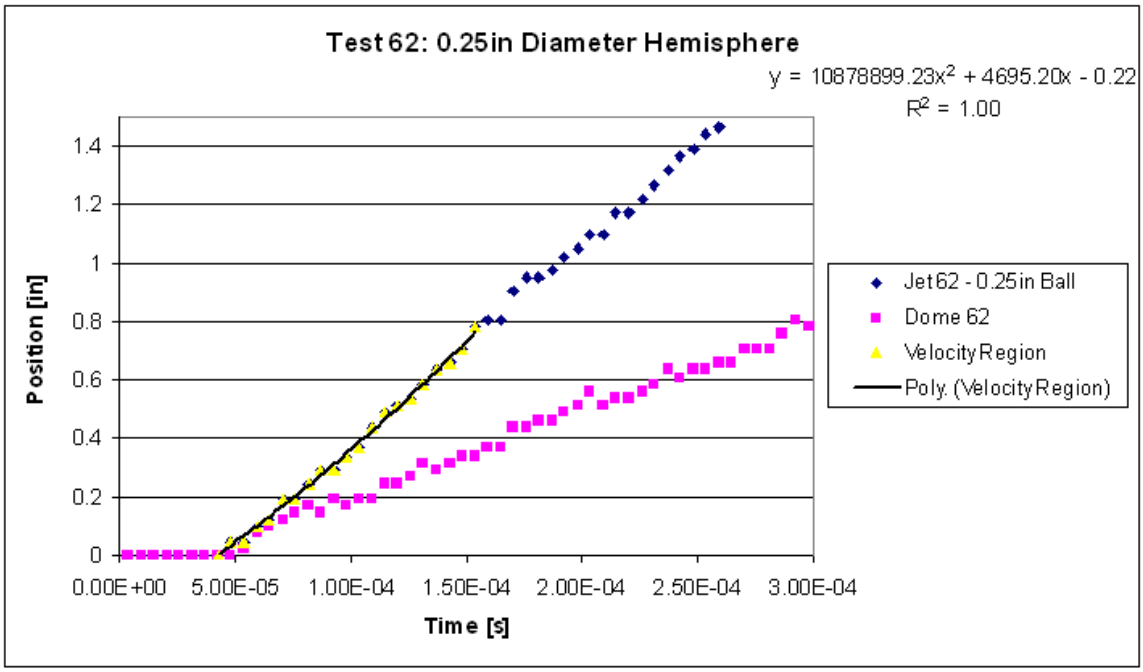
Test 62: 0.25in Diameter Hemisphere
y = 10878899.23x2 + 4695.20x - 0.22
R2 = 1.00
Position [in]
Time [s]
0
0.2
0.4
0.6
0.8
1
1.2
1.4
0.00E+00
5.00E-05
1.00E-04
1.50E-04
2.00E-04
2.50E-04
3.00E-04
Jet62 - 0.25in Ball
Dome 62
Velocity Region
Poly. (Velocity Region)

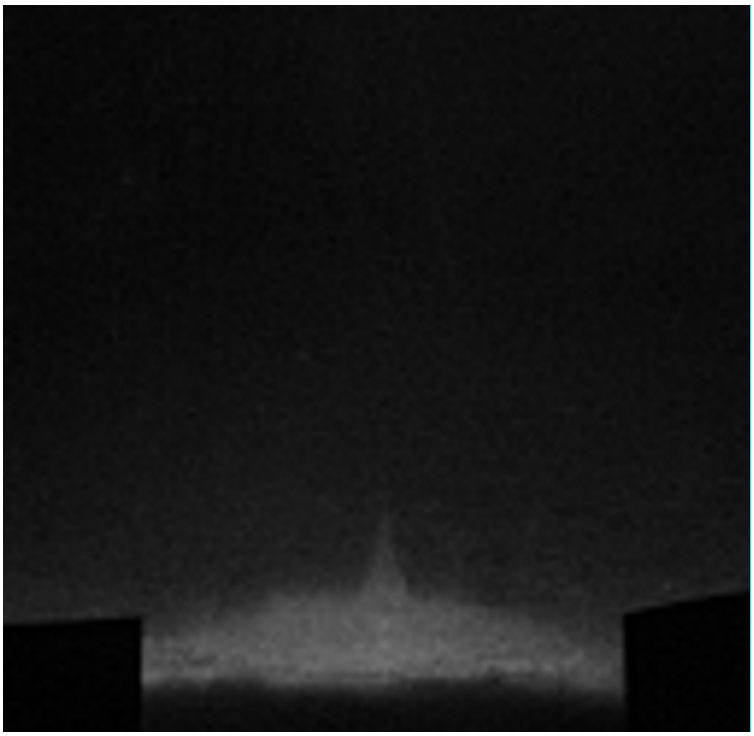

Test 63

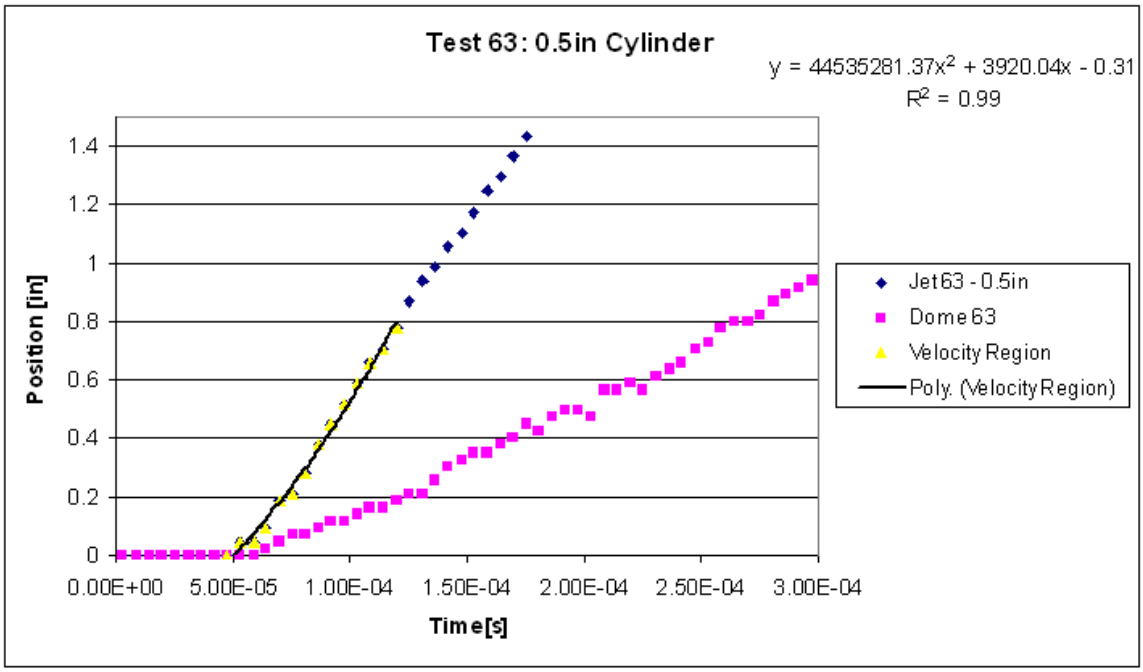
Test 63: 0.5in Cylinder
y = 44535281.37x² + 3920.04x - 0.31
R² = 0.99
Position [in]
Time[s]
0
0.2
0.4
0.6
0.8
1
1.2
1.4
0.00E+00
5.00E-05
1.00E-04
1.50E-04
2.00E-04
2.50E-04
3.00E-04
Jet63 - 0.5in
Dome 63
Velocity Region
Poly. (Velocity Region)

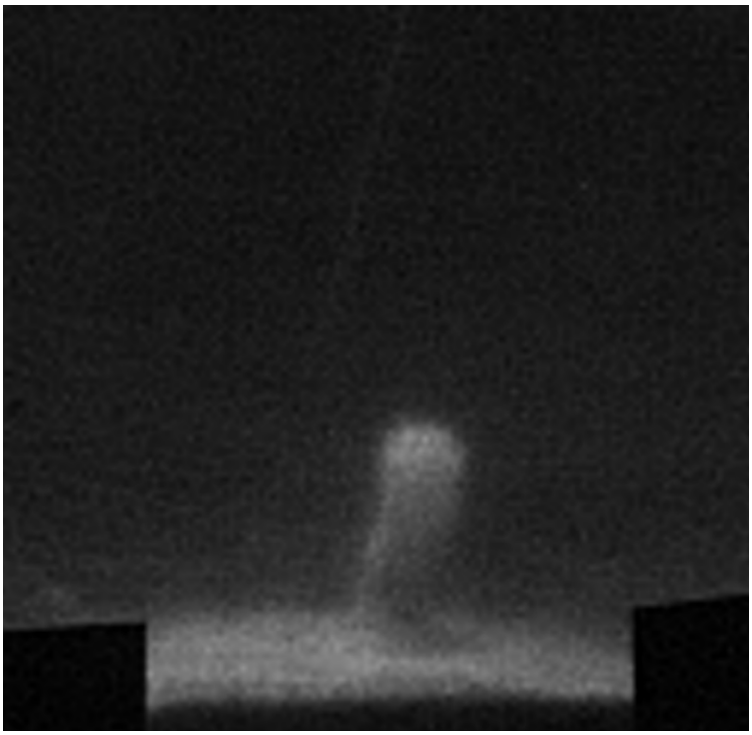

Test 64

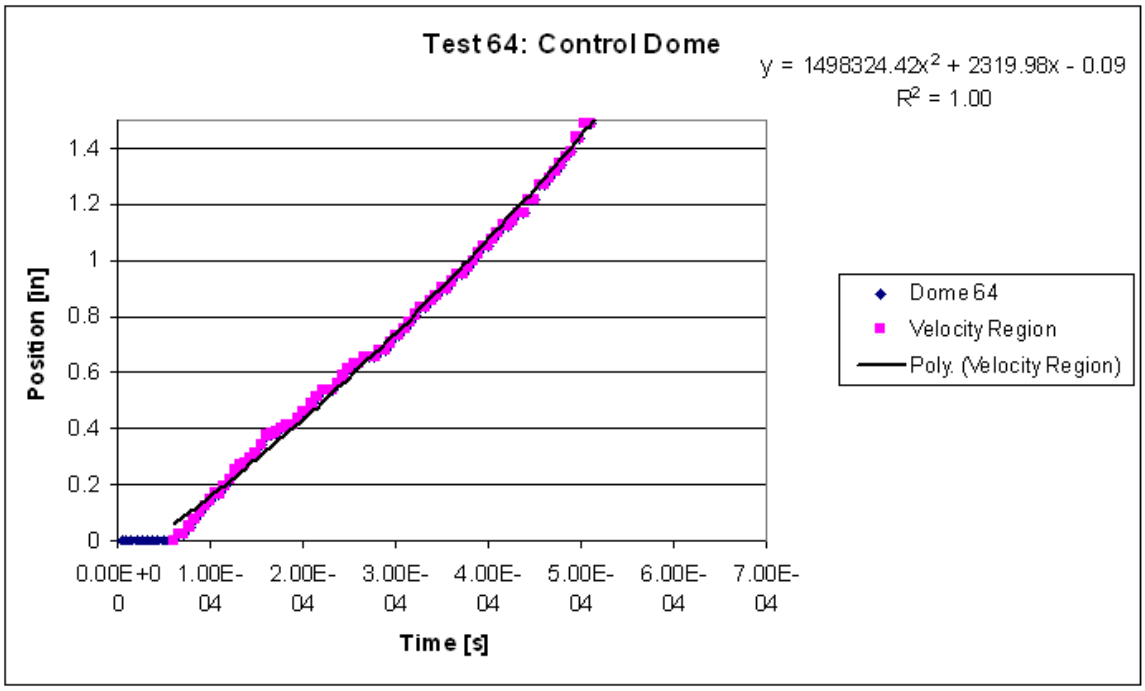
Test 64: Control Dome
y = 1498324.42x² + 2319.98x - 0.09
R² = 1.00
Position [in]
1.4
1.2
1
0.8
0.6
0.4
0.2
0
0.00E+00
1.00E-04
2.00E-04
3.00E-04
4.00E-04
5.00E-04
6.00E-04
7.00E-04
Time [s]
Dome 64
Velocity Region
Poly. (Velocity Region)

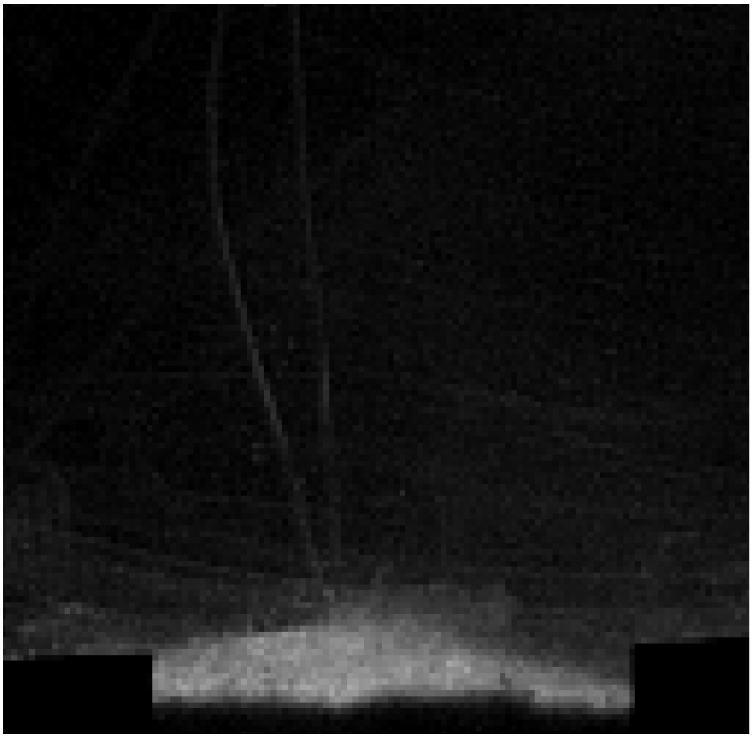

Test 65

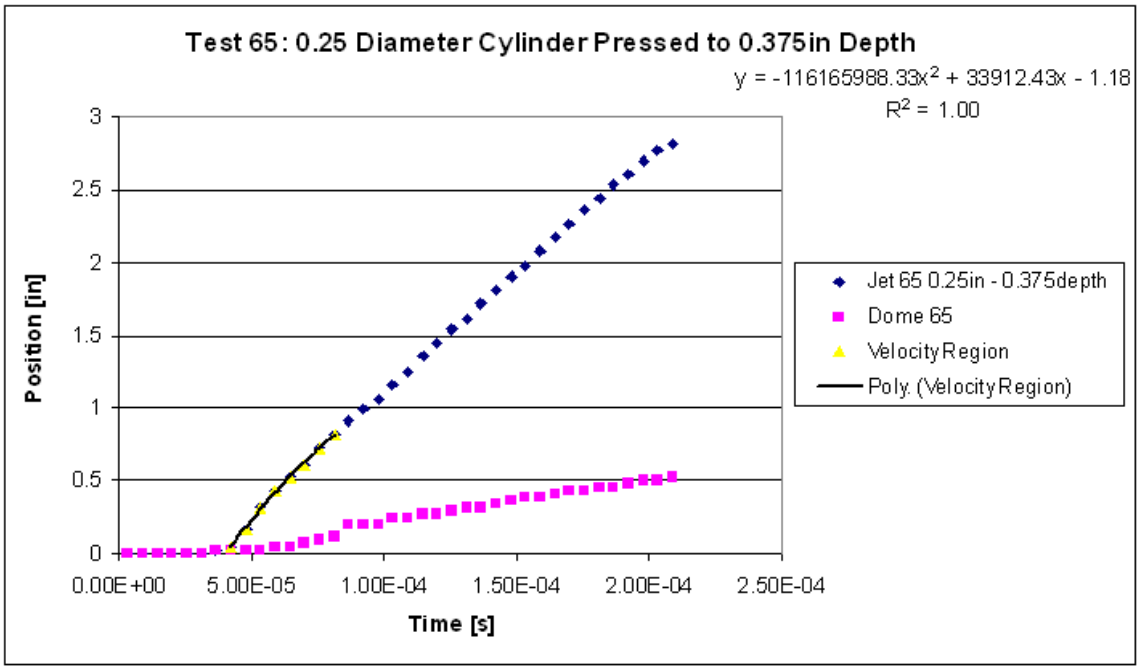
Test 65: 0.25 Diameter Cylinder Pressed to 0.375in Depth
y = -116165988.33x2 + 33912.43x - 1.18
R2 = 1.00
Position [in]
Time [s]
0
0.5
1
1.5
2
2.5
3
0.00E+00
5.00E-05
1.00E-04
1.50E-04
2.00E-04
2.50E-04
Jet 65 0.25in - 0.375depth
Dome 65
Velocity Region
Poly. (Velocity Region)

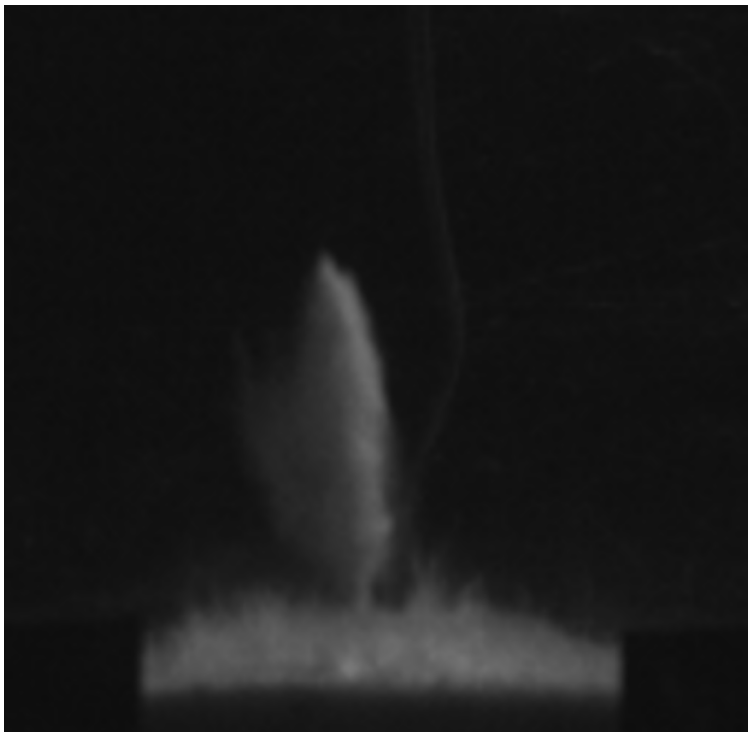

Test 66

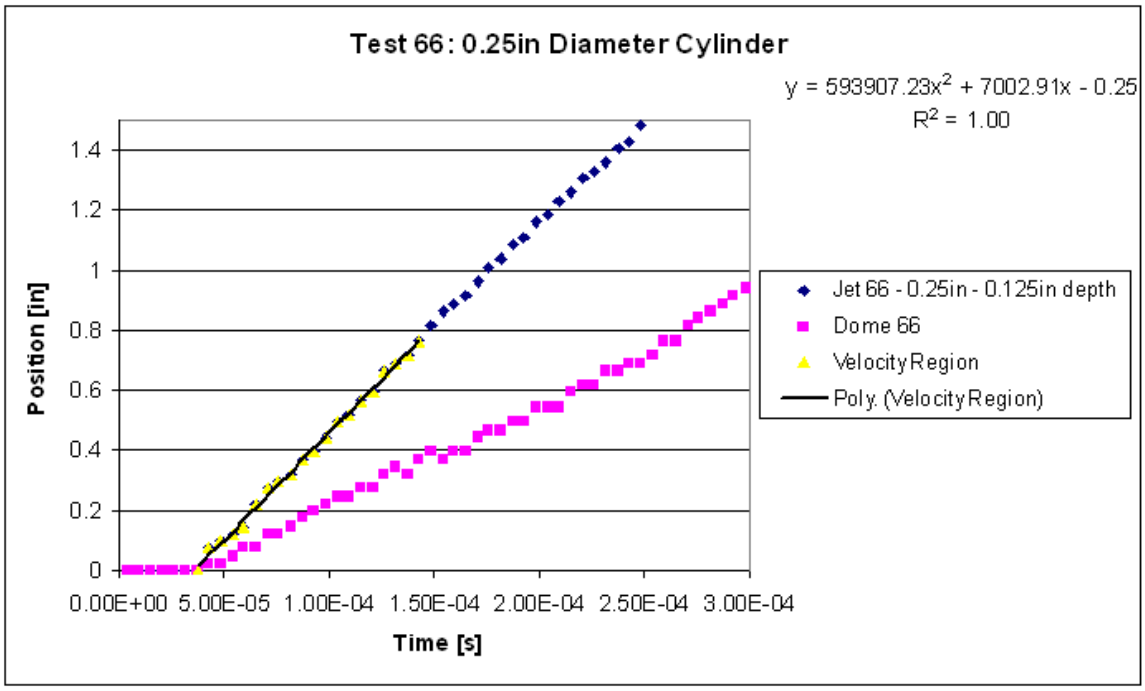
Test 66: 0.25in Diameter Cylinder
y = 593907.23x2 + 7002.91x - 0.25
R2 = 1.00
Position [in]
1.4
1.2
1
0.8
0.6
0.4
0.2
0
0.00E+00
5.00E-05
1.00E-04
1.50E-04
2.00E-04
2.50E-04
3.00E-04
Time [s]
Jet 66 - 0.25in - 0.125in depth
Dome 66
Velocity Region
Poly. (Velocity Region)

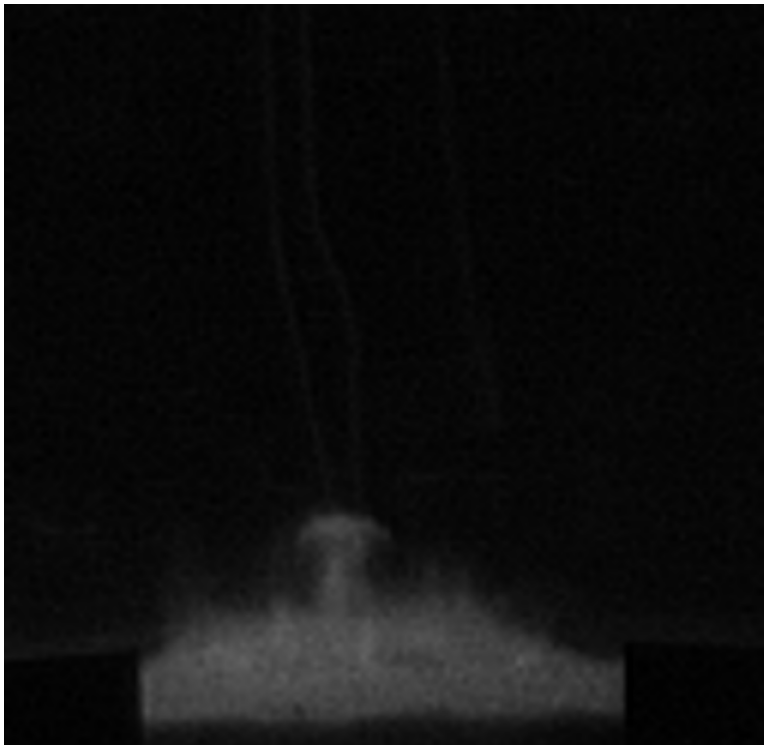

Test 67

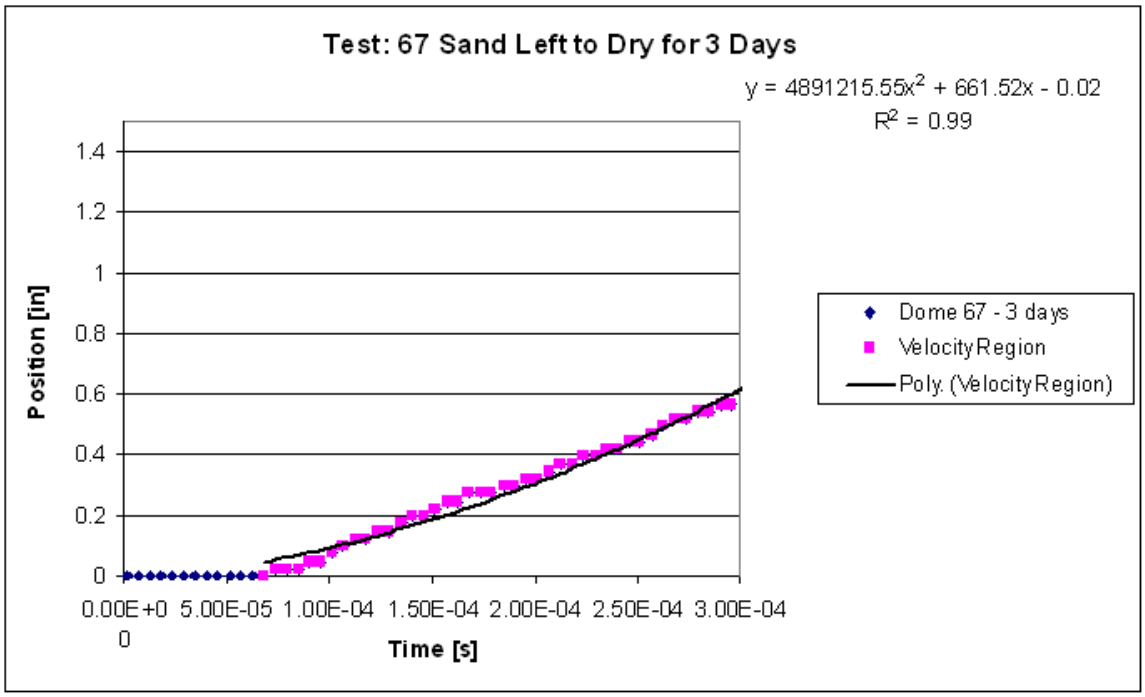
Test: 67 Sand Left to Dry for 3 Days
y = 4891215.55x2 + 661.52x - 0.02
R2 = 0.99
Position [in]
1.4
1.2
1
0.8
0.6
0.4
0.2
0
0.00E+00
5.00E-05
1.00E-04
1.50E-04
2.00E-04
2.50E-04
3.00E-04
Time [s]
Dome 67 - 3 days
Velocity Region
Poly. (Velocity Region)

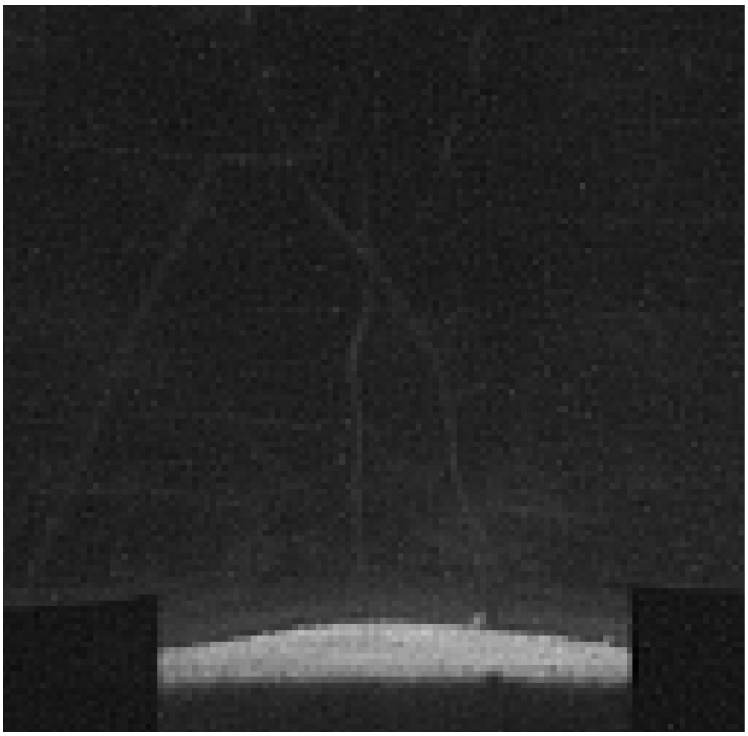

Test 68

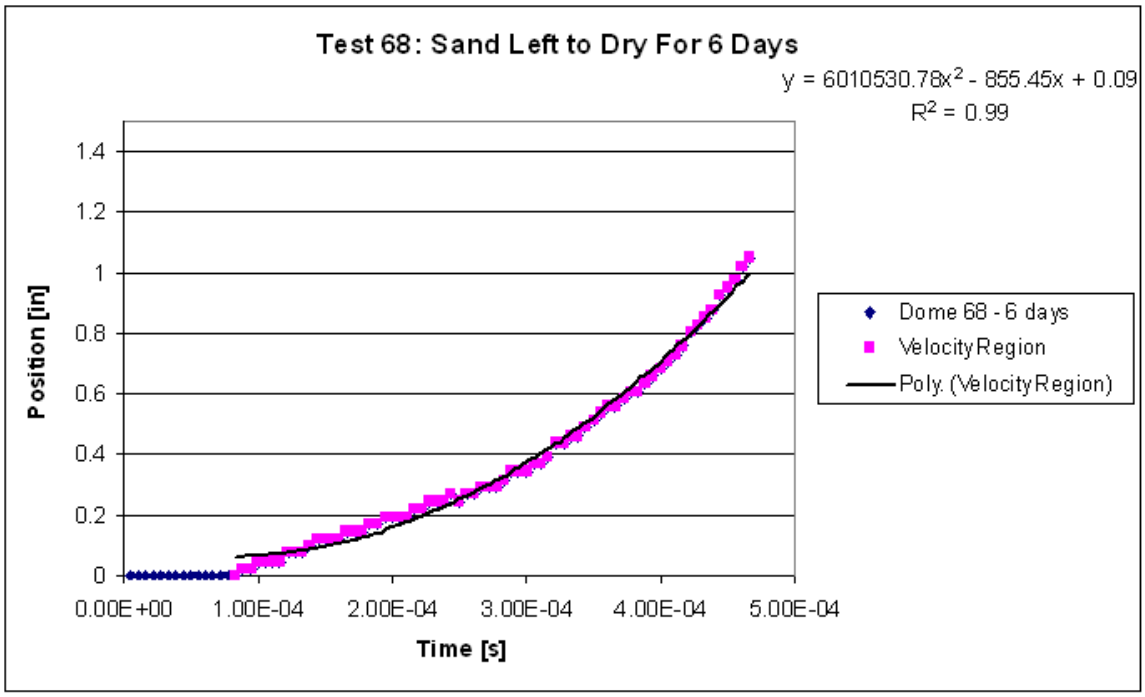
Test 68: Sand Left to Dry For 6 Days
y = 6010530.78x2 - 855.45x + 0.09
R2 = 0.99
Position [in]
1.4
1.2
1
0.8
0.6
0.4
0.2
0
0.00E+00
1.00E-04
2.00E-04
3.00E-04
4.00E-04
5.00E-04
Time [s]
Dome 68 - 6 days
Velocity Region
Poly. (Velocity Region)

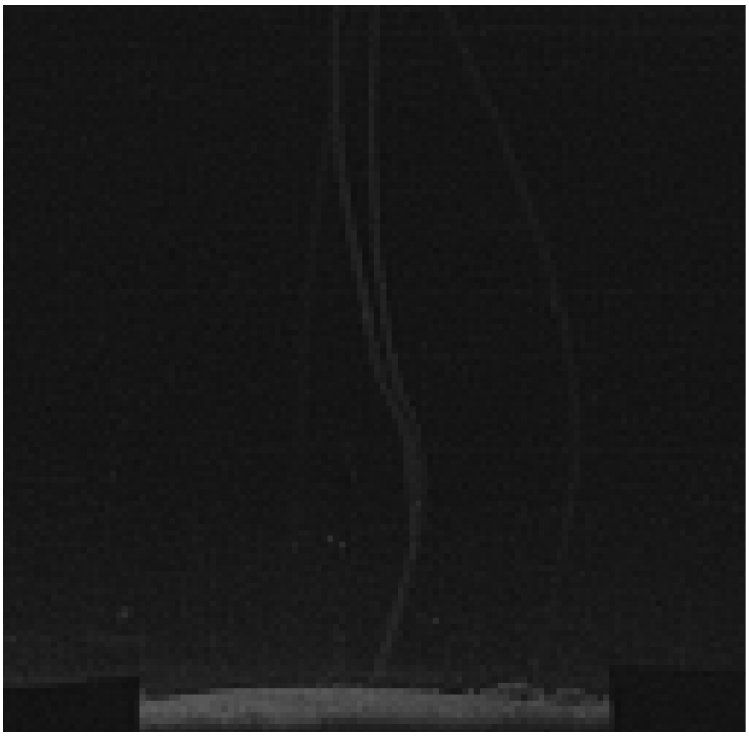

Test 69

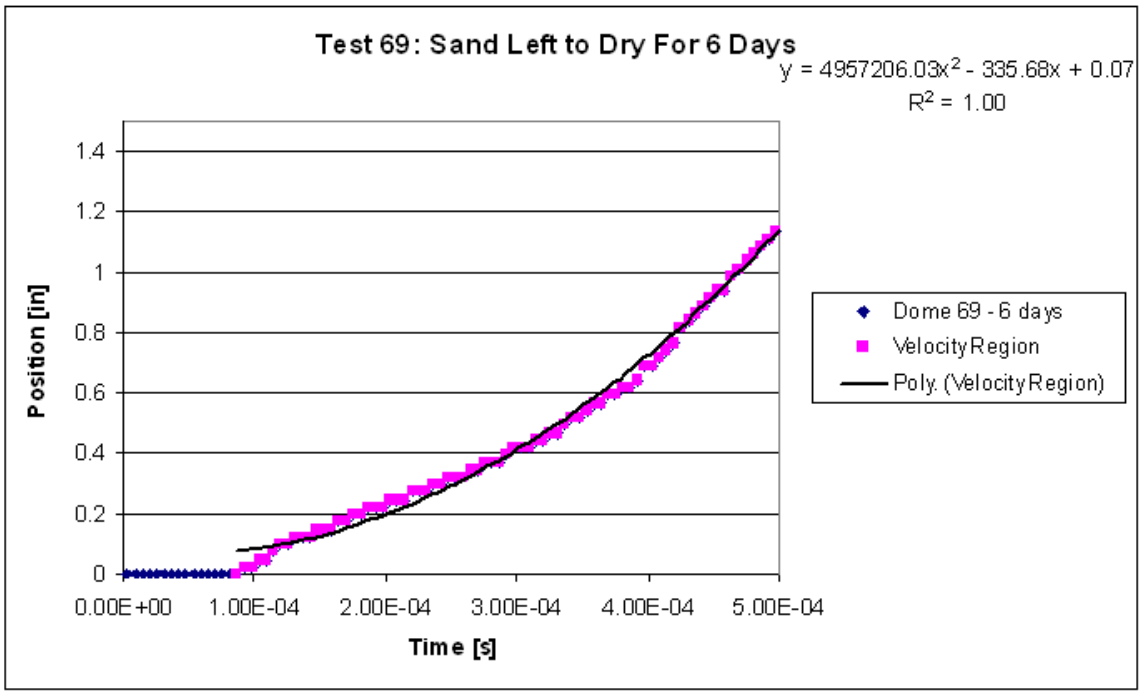
Test 69: Sand Left to Dry For 6 Days
y = 4957206.03x² - 335.68x + 0.07
R² = 1.00
Position [in]
1.4
1.2
1
0.8
0.6
0.4
0.2
0
0.00E+00
1.00E-04
2.00E-04
3.00E-04
4.00E-04
5.00E-04
Time [s]
Dome 69 - 6 days
Velocity Region
Poly. (Velocity Region)

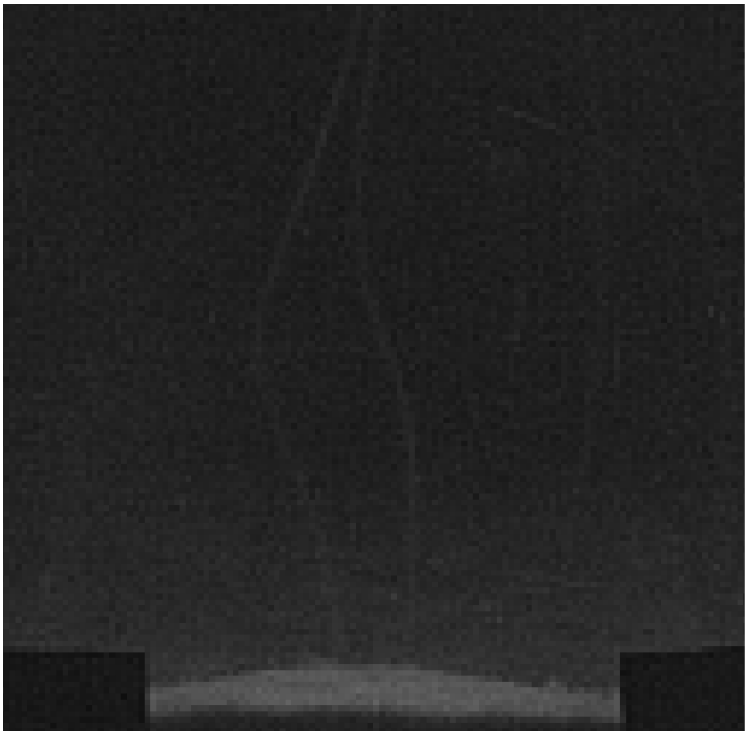

Test 70

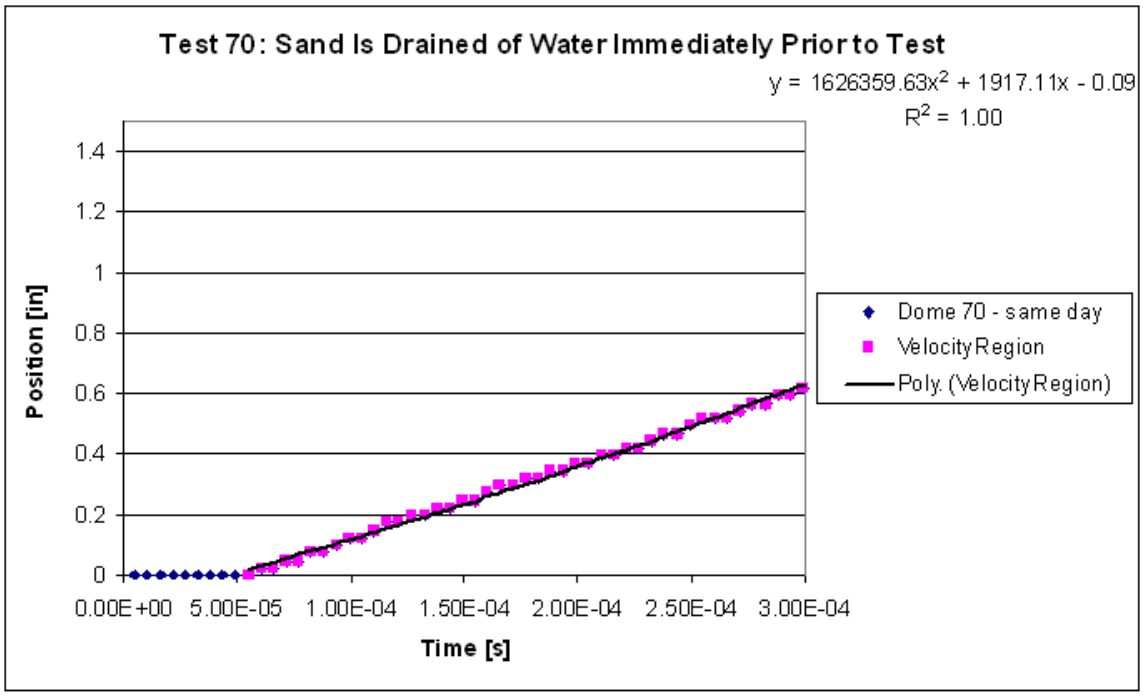
Test 70: Sand Is Drained of Water Immediately Prior to Test
y = 1626359.63x2 + 1917.11x - 0.09
R2 = 1.00
Position [in]
1.4
1.2
1
0.8
0.6
0.4
0.2
0
0.00E+00
5.00E-05
1.00E-04
1.50E-04
2.00E-04
2.50E-04
3.00E-04
Time [s]
Dome 70 - same day
Velocity Region
Poly. (Velocity Region)

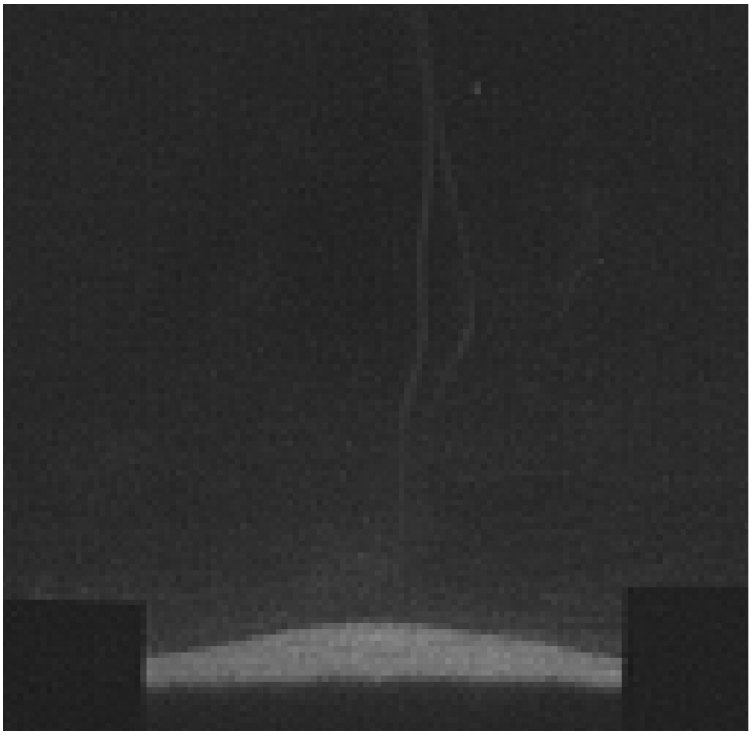

Test 71

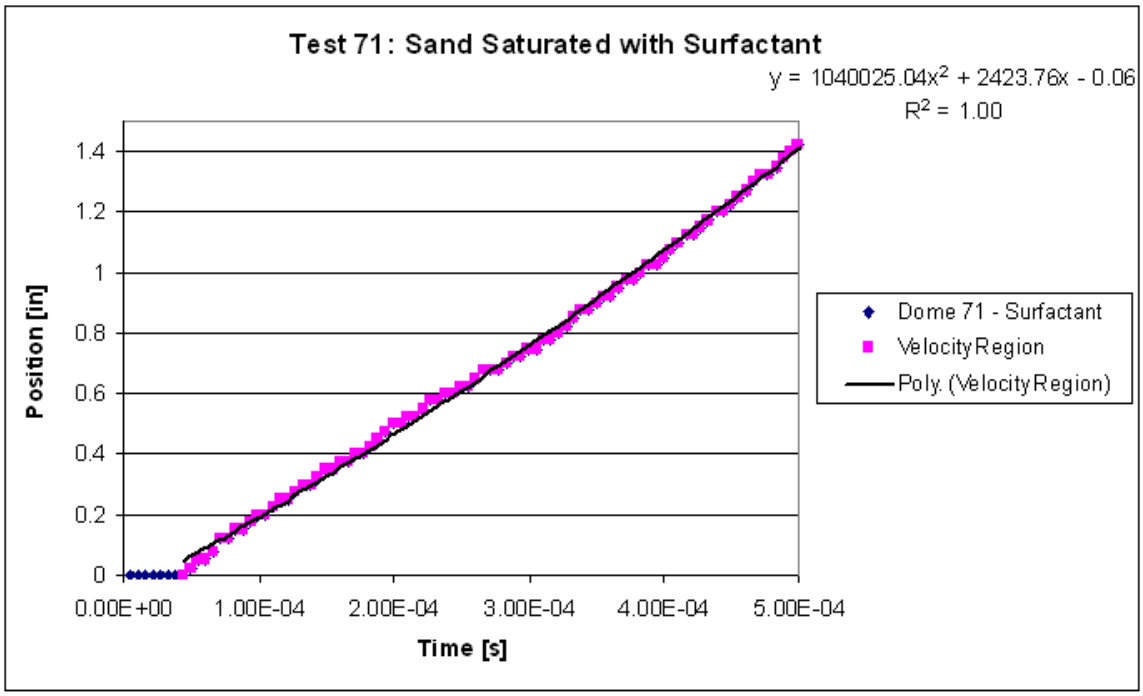
Test 71: Sand Saturated with Surfactant
y = 1040025.04x² + 2423.76x - 0.06
R² = 1.00
Position [in]
1.4
1.2
1
0.8
0.6
0.4
0.2
0
0.00E+00
1.00E-04
2.00E-04
3.00E-04
4.00E-04
5.00E-04
Time [s]
Dome 71 - Surfactant
Velocity Region
Poly. (Velocity Region)

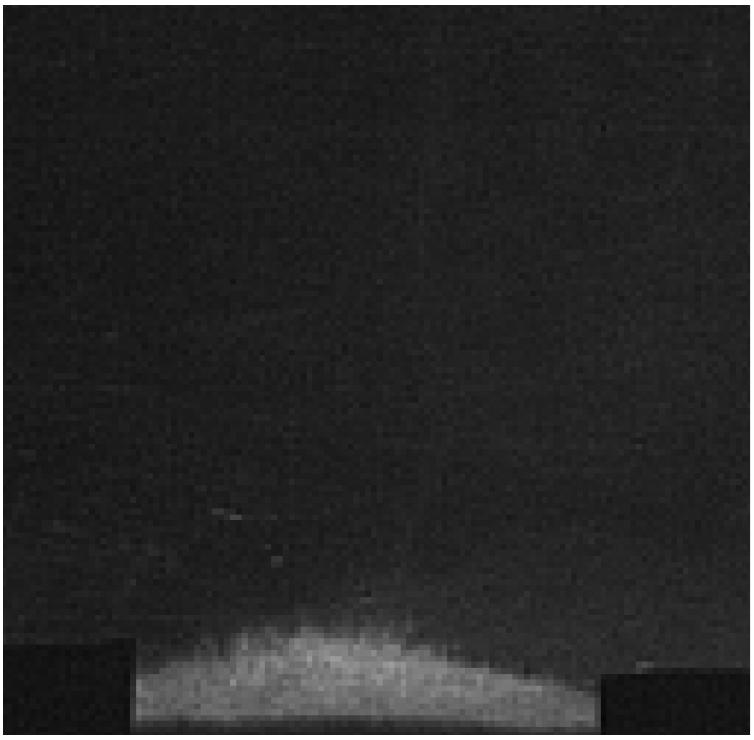

Test 72

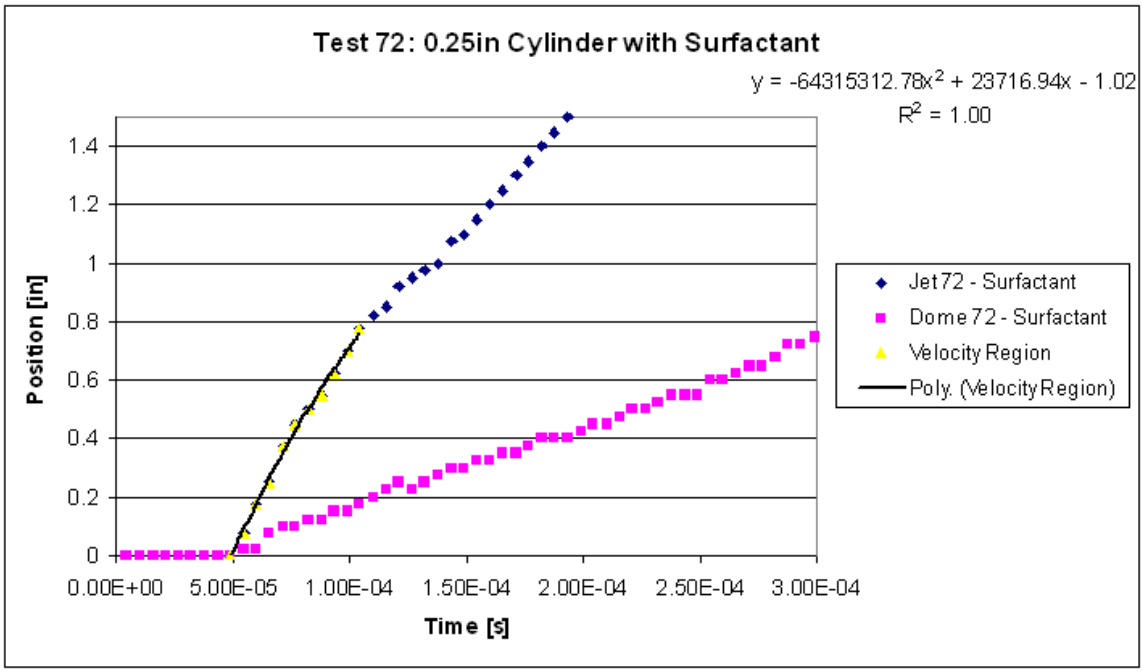
Test 72: 0.25in Cylinder with Surfactant
y = -64315312.78x² + 23716.94x - 1.02
R² = 1.00
Position [in]
Time [s]
0
0.2
0.4
0.6
0.8
1
1.2
1.4
0.00E+00
5.00E-05
1.00E-04
1.50E-04
2.00E-04
2.50E-04
3.00E-04
Jet 72 - Surfactant
Dome 72 - Surfactant
Velocity Region
Poly. (Velocity Region)

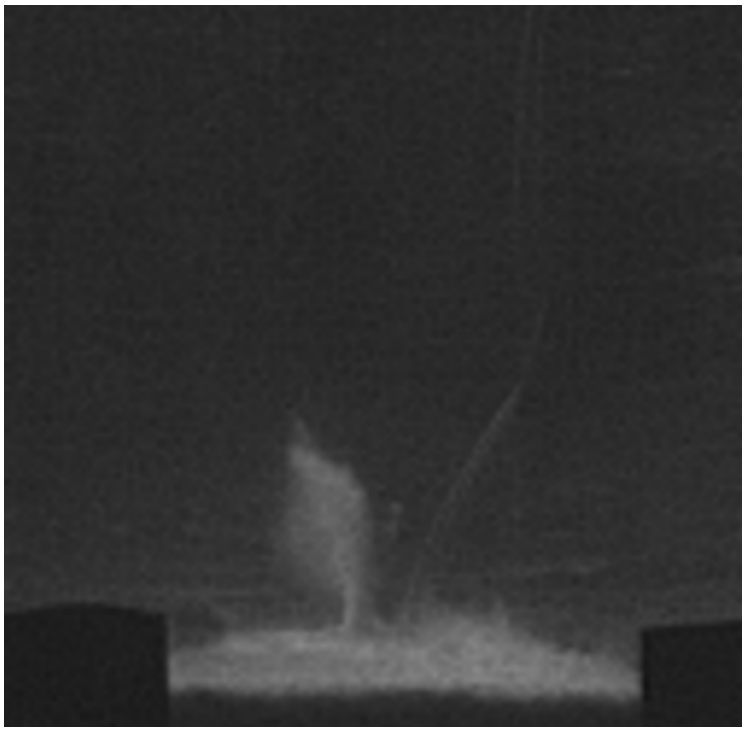

Test 73

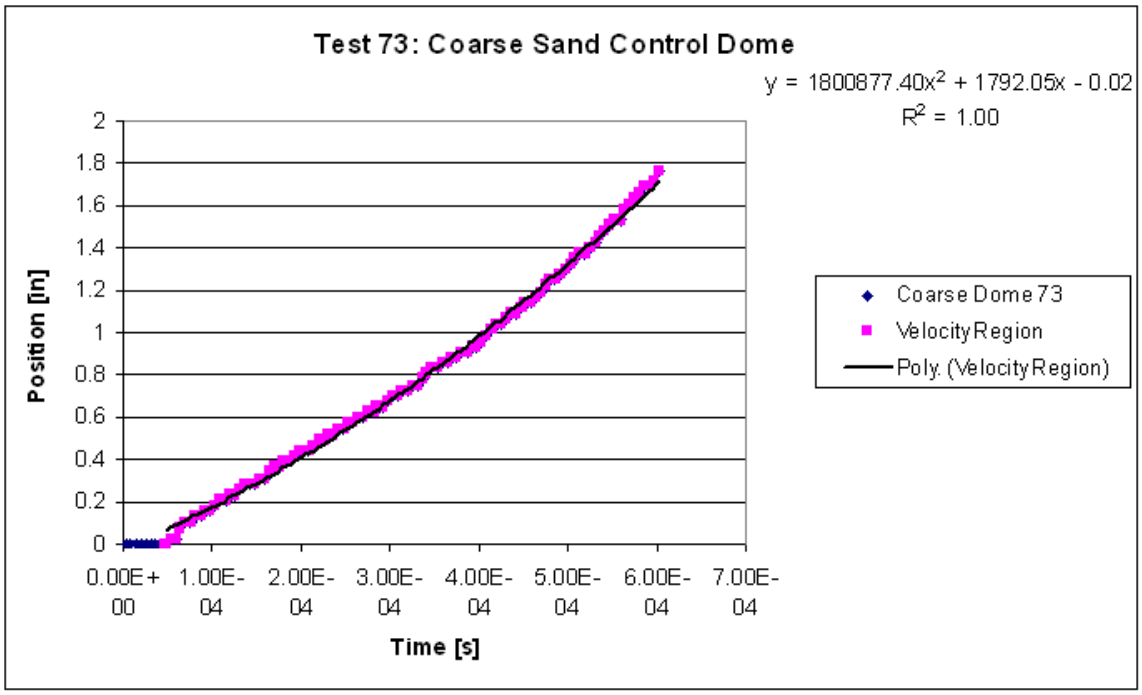
Test 73: Coarse Sand Control Dome
y = 1800877.40x² + 1792.05x - 0.02
R² = 1.00
Position [in]
Time [s]
0
0.2
0.4
0.6
0.8
1
1.2
1.4
1.6
1.8
2
0.00E+00
1.00E-04
2.00E-04
3.00E-04
4.00E-04
5.00E-04
6.00E-04
7.00E-04
Coarse Dome 73
Velocity Region
Poly. (Velocity Region)

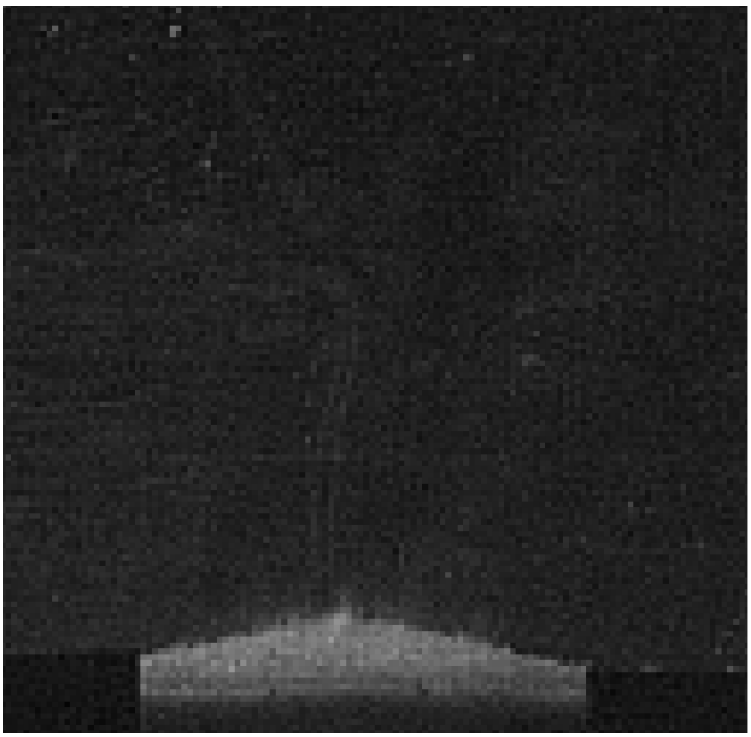

Test 74

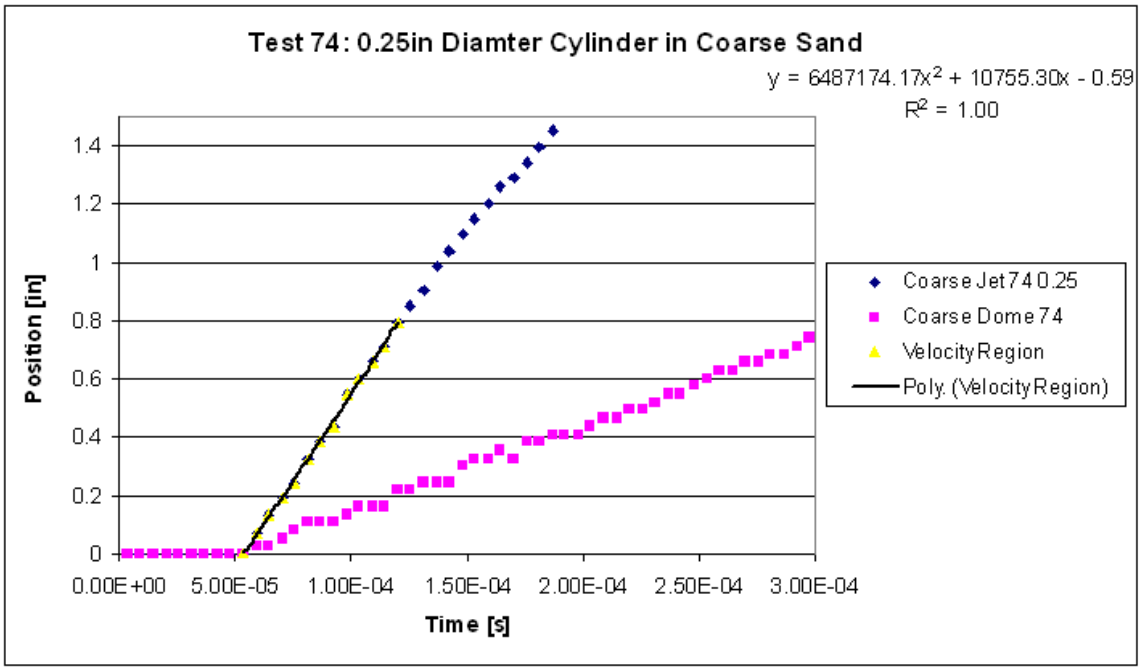
Test 74: 0.25in Diamter Cylinder in Coarse Sand
y = 6487174.17x² + 10755.30x - 0.59
R² = 1.00
Position [in]
1.4
1.2
1
0.8
0.6
0.4
0.2
0
0.00E+00
5.00E-05
1.00E-04
1.50E-04
2.00E-04
2.50E-04
3.00E-04
Time [s]
Coarse Jet 74 0.25
Coarse Dome 74
Velocity Region
Poly. (Velocity Region)

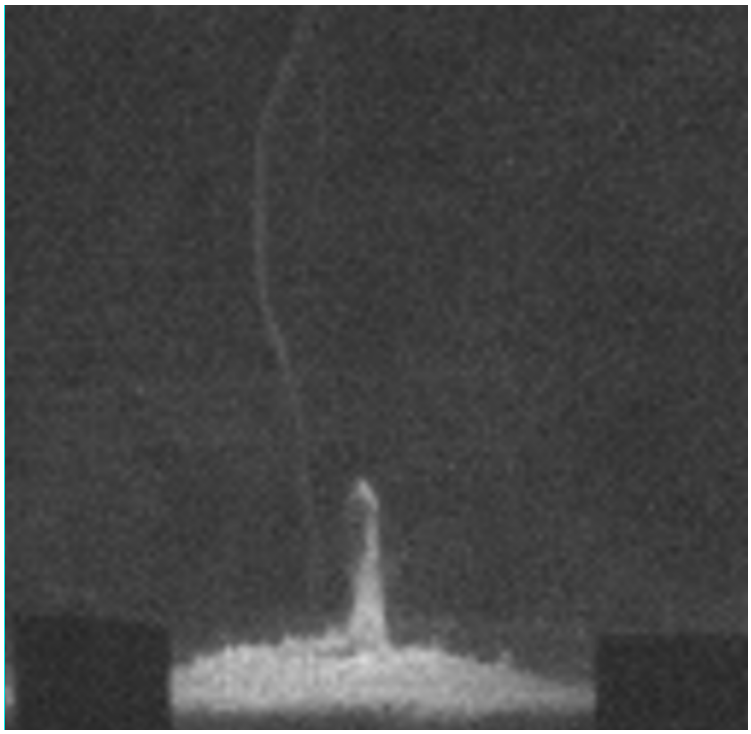

Test 75

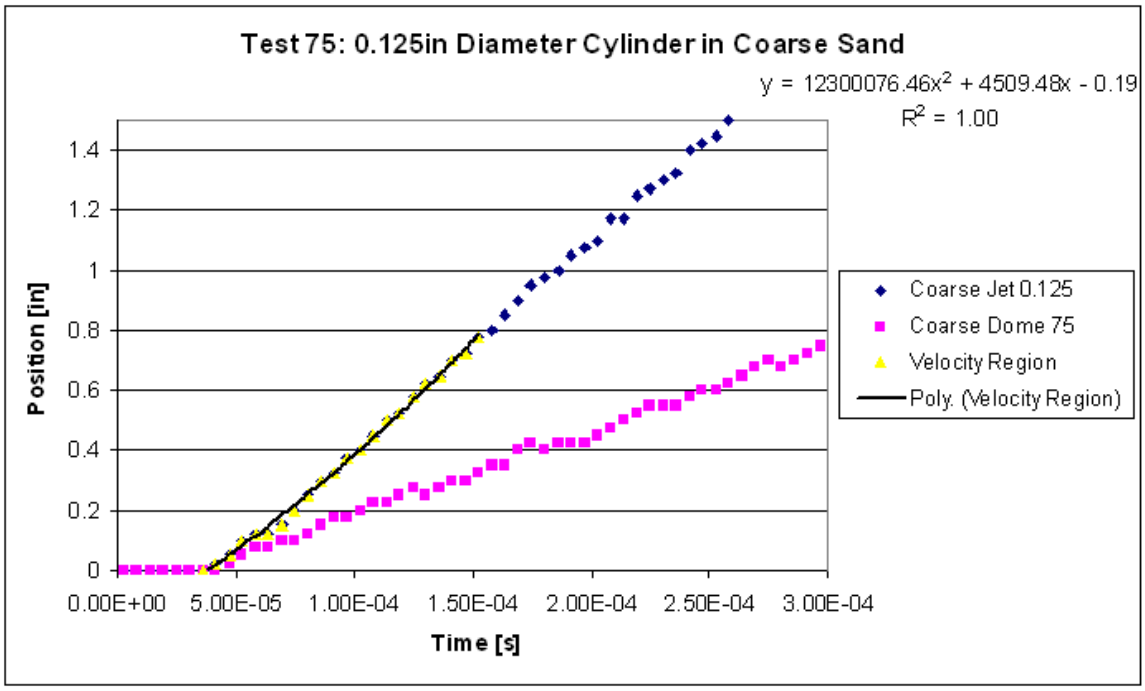
Test 75: 0.125in Diameter Cylinder in Coarse Sand
y = 12300076.46x² + 4509.48x - 0.19
R² = 1.00
Position [in]
Time [s]
0
0.2
0.4
0.6
0.8
1
1.2
1.4
0.00E+00
5.00E-05
1.00E-04
1.50E-04
2.00E-04
2.50E-04
3.00E-04
Coarse Jet 0.125
Coarse Dome 75
Velocity Region
Poly. (Velocity Region)

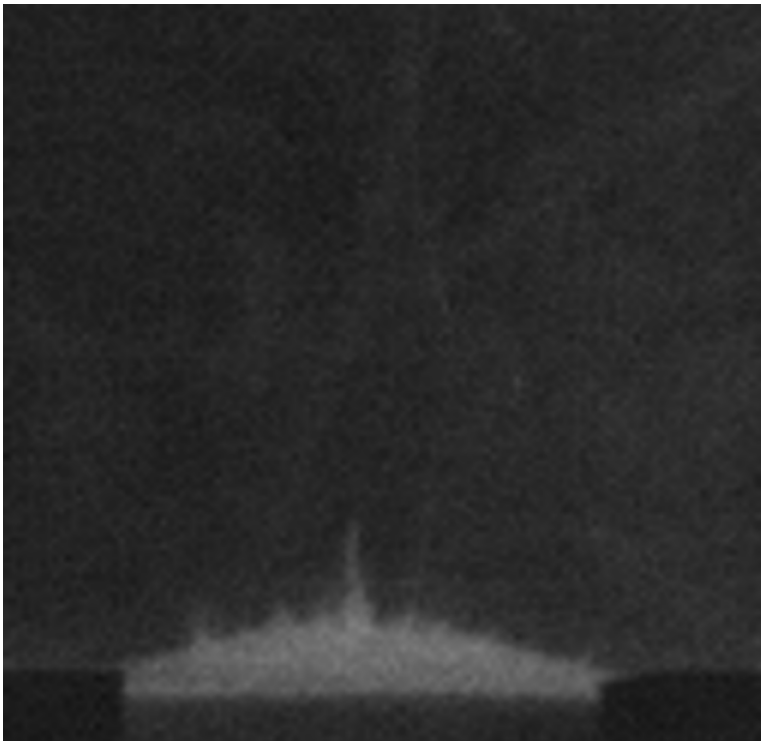

Test 76

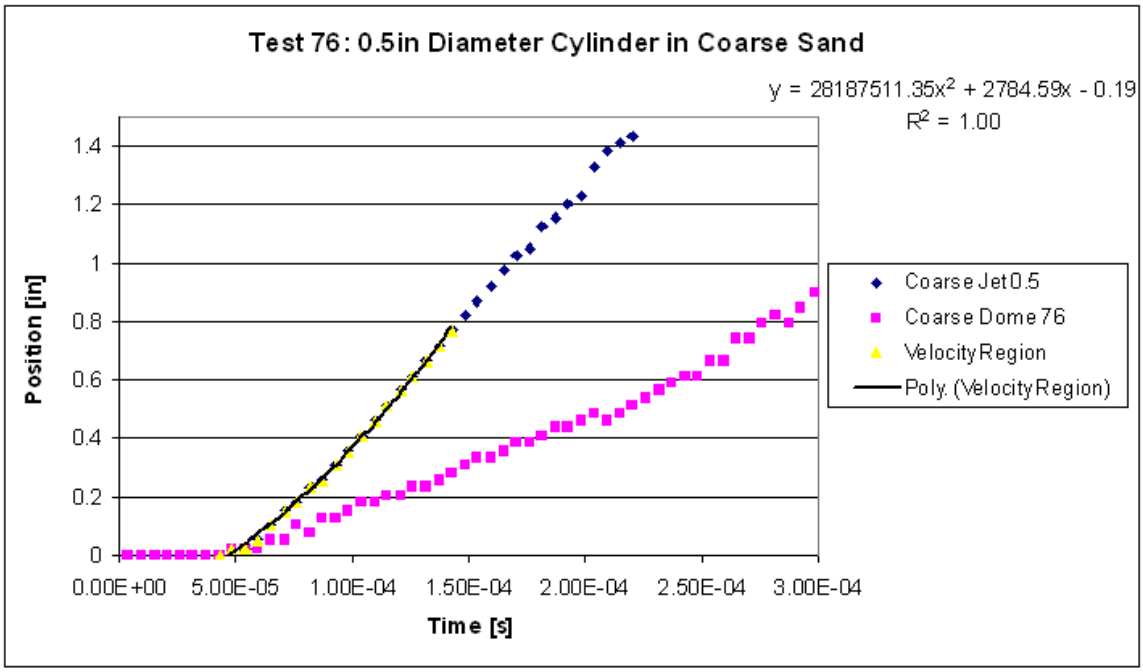
Test 76: 0.5in Diameter Cylinder in Coarse Sand
y = 28187511.35x2 + 2784.59x - 0.19
R2 = 1.00
Position [in]
Time [s]
0
0.2
0.4
0.6
0.8
1
1.2
1.4
0.00E+00
5.00E-05
1.00E-04
1.50E-04
2.00E-04
2.50E-04
3.00E-04
Coarse Jet 0.5
Coarse Dome 76
Velocity Region
Poly. (Velocity Region)

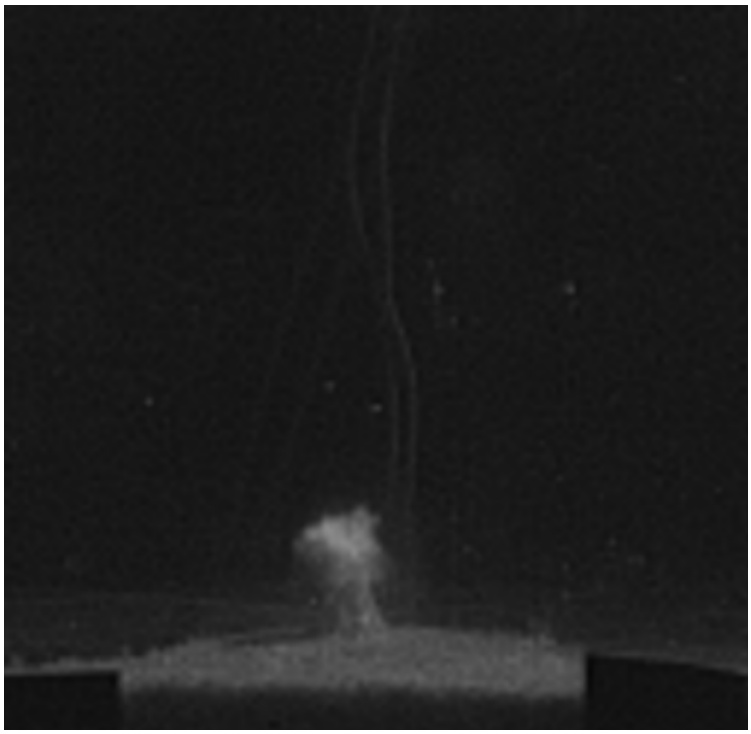

Test 77

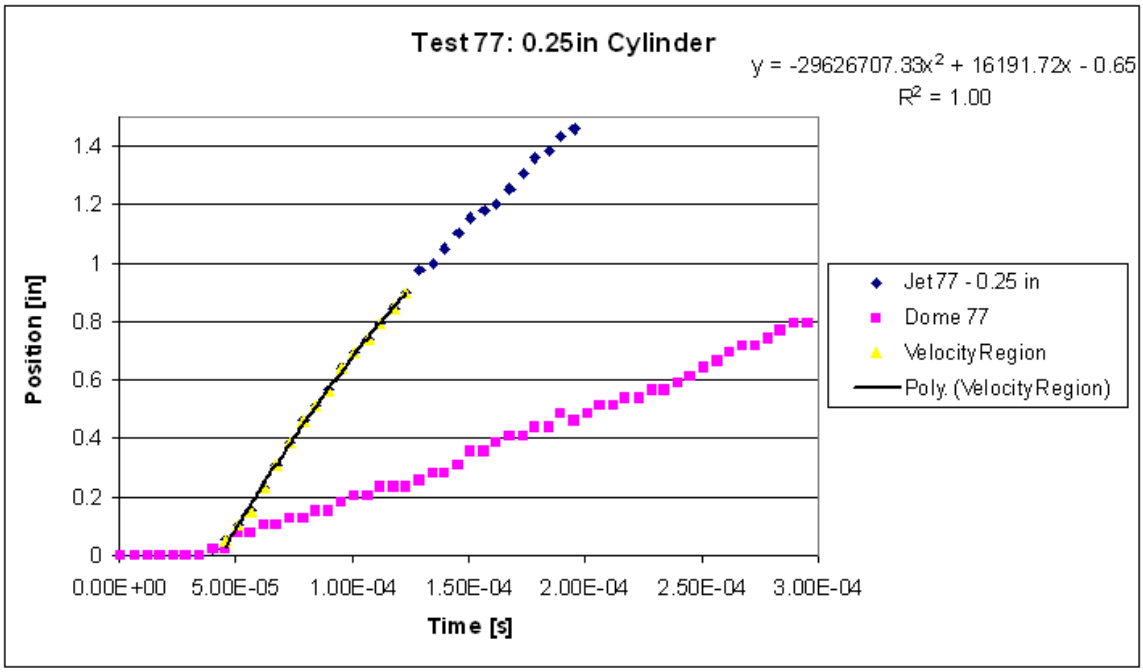
Test 77: 0.25in Cylinder
y = -29626707.33x² + 16191.72x - 0.65
R² = 1.00
Position [in]
1.4
1.2
1
0.8
0.6
0.4
0.2
0
0.00E+00
5.00E-05
1.00E-04
1.50E-04
2.00E-04
2.50E-04
3.00E-04
Time [s]
Jet 77 - 0.25 in
Dome 77
Velocity Region
Poly. (Velocity Region)

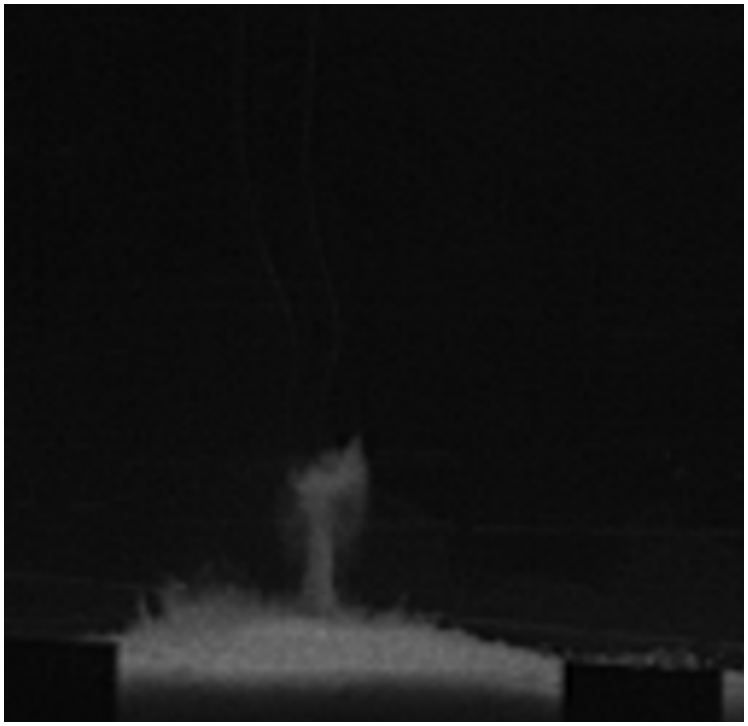

Test 78

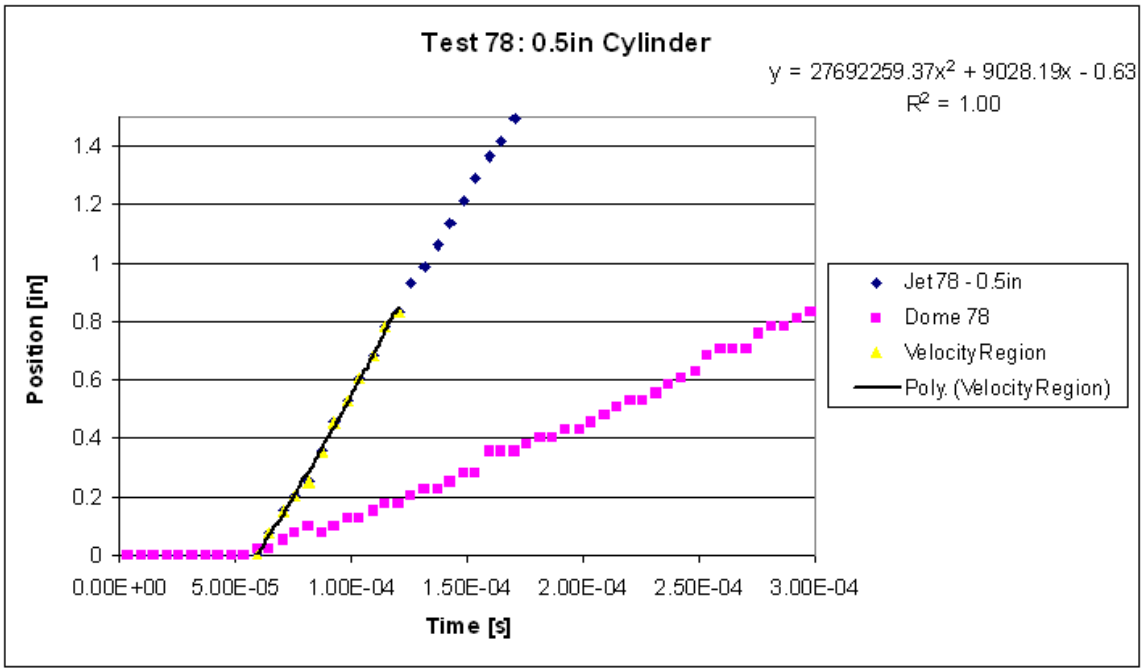
Test 78: 0.5in Cylinder
y = 27692259.37x² + 9028.19x - 0.63
R² = 1.00
Position [in]
Time [s]
0
0.2
0.4
0.6
0.8
1
1.2
1.4
0.00E+00
5.00E-05
1.00E-04
1.50E-04
2.00E-04
2.50E-04
3.00E-04
Jet 78 - 0.5in
Dome 78
Velocity Region
Poly. (Velocity Region)

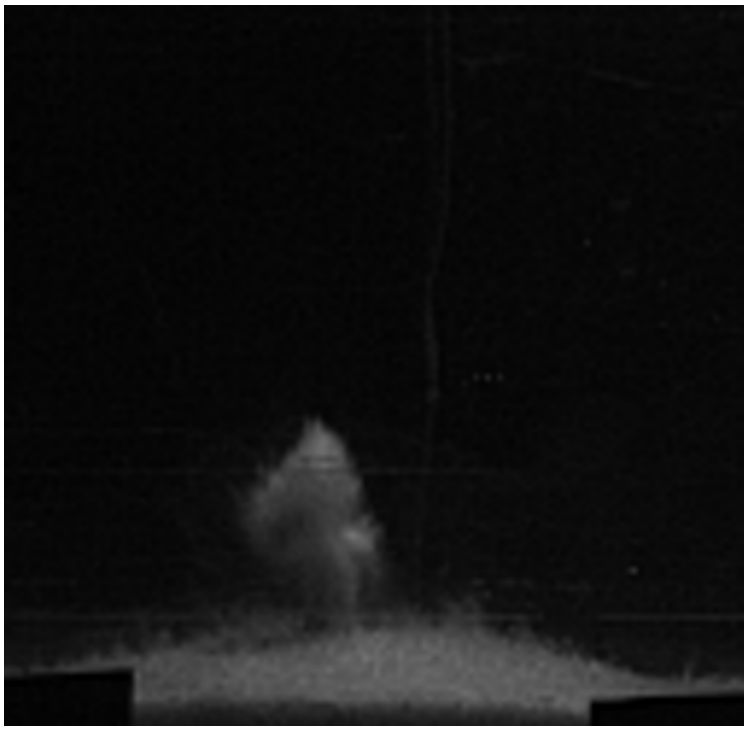

Test 79

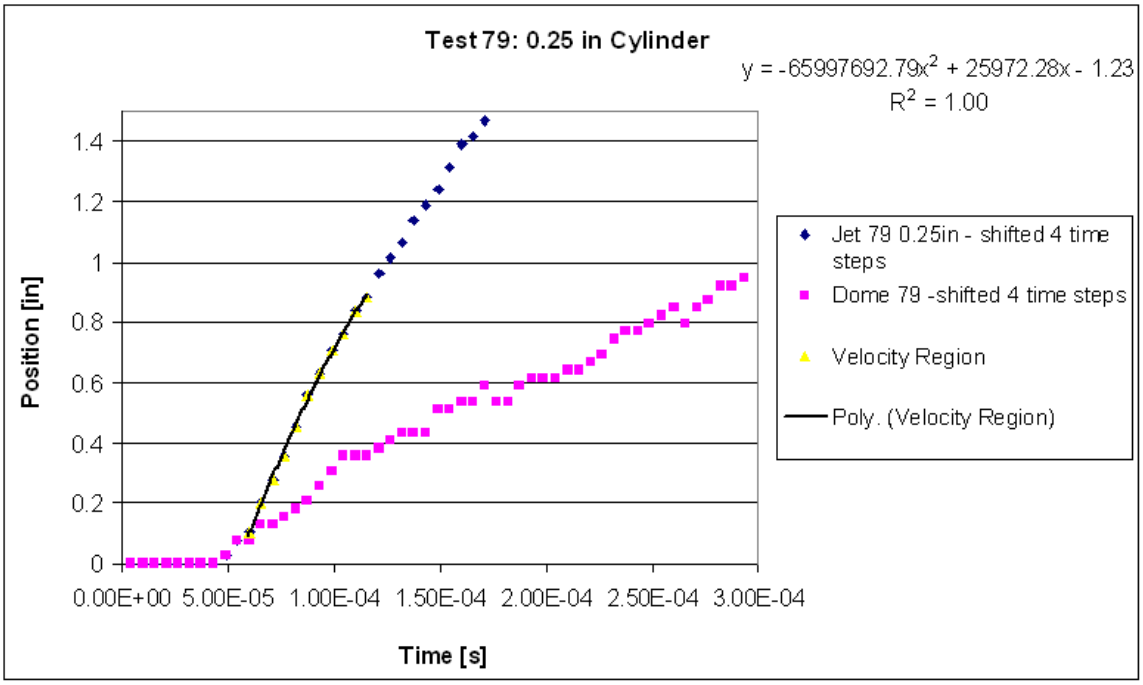
Test 79: 0.25 in Cylinder
y = -65997692.79x2 + 25972.28x - 1.23
R2 = 1.00
Position [in]
1.4
1.2
1
0.8
0.6
0.4
0.2
0
0.00E+00
5.00E-05
1.00E-04
1.50E-04
2.00E-04
2.50E-04
3.00E-04
Time [s]
Jet 79 0.25in - shifted 4 time steps
Dome 79 -shifted 4 time steps
Velocity Region
Poly. (Velocity Region)

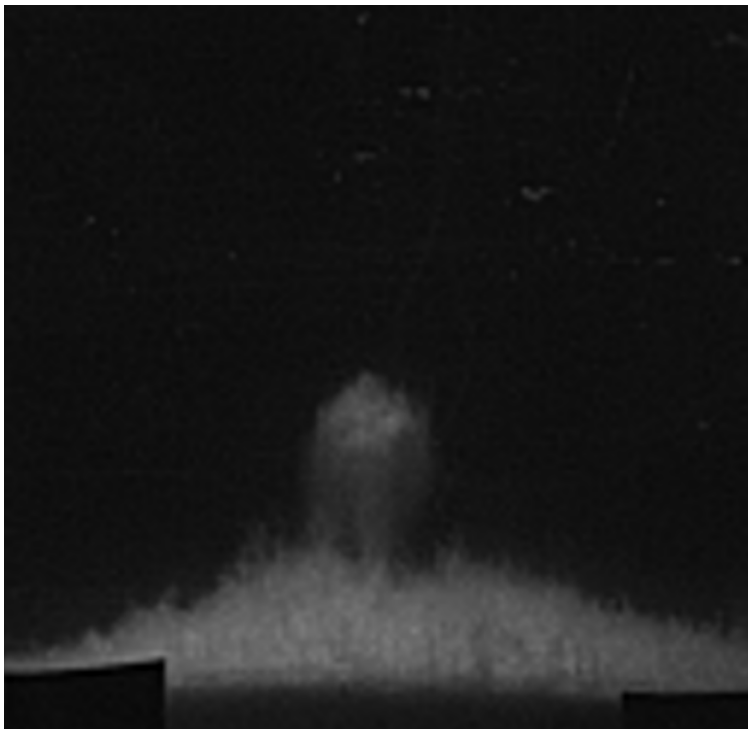

Appendix C: Results from Sieve Analysis

Berkeley Springs Sand

First Sample		1000 g		
Sieve Number	Sieve Diam(mm)	Total Weight	Percent Remaining	Percent Passing
16	1.19	0	100	0
20	0.841	0	100	0
30	0.595	316	68.4	31.6
40	0.42	411	27.3	72.7
50	0.297	180	9.3	90.7
60	0.25	52	4.1	95.9
Pan		36	4.09	95.91
Sum		995		

Second Sample		1000 g		
Sieve Number	Sieve Diam(mm)	Total Weight	Percent Remaining	Percent Passing
16	1.19	0	100	0
20	0.841	0	100	0
30	0.595	384	61.6	38.4
40	0.42	314	30.2	69.8
50	0.297	197	10.5	89.5
60	0.25	58	4.7	95.3
Pan		47	4.69	95.31
Sum		1000		

Large Grain Sand

First Sample 1000g				
Sieve Number	Sieve Diam(mm)	Total Weight	Percent Remaining	Percent Passing
16	1.19	40	96.0	4.0
20	0.841	232	72.8	27.2
30	0.595	248	48.0	52.0
40	0.42	262	21.8	78.2
50	0.297	103	11.5	88.5
60	0.25	57	5.8	94.2
Pan		50		
Sum		992		

Second Sample 1000g				
Sieve	Sieve	Total	Percent	Percent
Number	Diam(mm)	Weight	Remaining	Passing
16	1.19	58	94.2	5.8
20	0.841	227	71.5	28.5
30	0.595	233	48.2	51.8
40	0.42	214	26.8	73.2
50	0.297	183	8.5	91.5
60	0.25	59	2.6	97.4
Pan		24		
Sum		998		

References

1. Fourney, W.L., Leiste, U., Bonenberger, R., Goodings, D., *Explosive Impulse on Plates.* Fragblast, 2005. **9**(1).

2. Taylor, L.C., Fourney, W.L., Leiste, H.U., & Cheeseman, B., *Loading Mechanisms on a Target from Detonation of a Buried Charge.* Proceedings of the 24th International Symposium on Ballistics, 2008.

3. Fourney, W.L., Leiste, U., Bonenberger, R., Goodings, D., *Mechanism of Loading on Plates Due to Explosive Detonation.* Fragblast, 2005. **9**(4).

4. Palekar, A., Vorobieff, P., Truman, C. R., *Two-Dimensional Simulation of Richtmyer-Meshkov Instability.* Fluid Dynamics Research, 2004.

5. Whitlock, C., *IED attacks soaring in Afghanistan; Taliban fighters' low-tech but deadly tactic hinders U.S.*, in *The Washington Post*. 2010.

6. Benedetti, R., *Mitigation of Explosive Blast Effects on Vehicle Floorboard*, in *Mechanical Engineering*. 2008, University of Maryland: College Park.

7. Bretall, D., *Inverse Hybrid Method for Determining Explosive Loading on Plates Due to Buried Mines*, in *Mechanical Engineering*. 2007, University of Maryland: College Park.

8. Chabai, A.J., *On Scaling Dimensions of Craters Produced by Buried Explosives.* Journal of Geophysical Research, 1965. **70**(20).

9. Taylor L.C., F.W.L., Lathrop D., *Surface Instabilities from Buried Explosives*. 2009, University of Maryland College Park.

10. Teledyne RISI, I., *FS-17 Firing System*. 2008.

11. Research, P. *Data Sheet v12.1*. 2009 [cited 2010 March 29]; Available from:http://www.visionresearch.com/uploads/docs/Products/DS-WEB_v12-1.pdf.

12. *Data Sheet v12.1*. 2009 [cited 2010 March 29]; Available from: http://www.visionresearch.com/uploads/docs/Products/DS-WEB_v12-1.pdf.

13. Research, V., *25" Northstar Light with Clamp Base*.

14. Wardlaw, A., *Computational Simulations*, T. L.C., Editor. 2009. p. Computational Simulations.

15. *Sigma-Aldrich Triton X-100 Product Information*. 1999 [cited 2010 March 2010]; Product Information for Triton X-100].

16. Duncan, J., Liu, Xinan, *A Laboratory Study of Longitudinal Waves in Surfactant Films in a Water Wave Tank.* Journal of Geophysical Research, 2007. **112**.